Charge distribution and stability in electret materials

Thyssen, Anders

Publication date:
2016

Document Version
Publisher's PDF, also known as Version of record

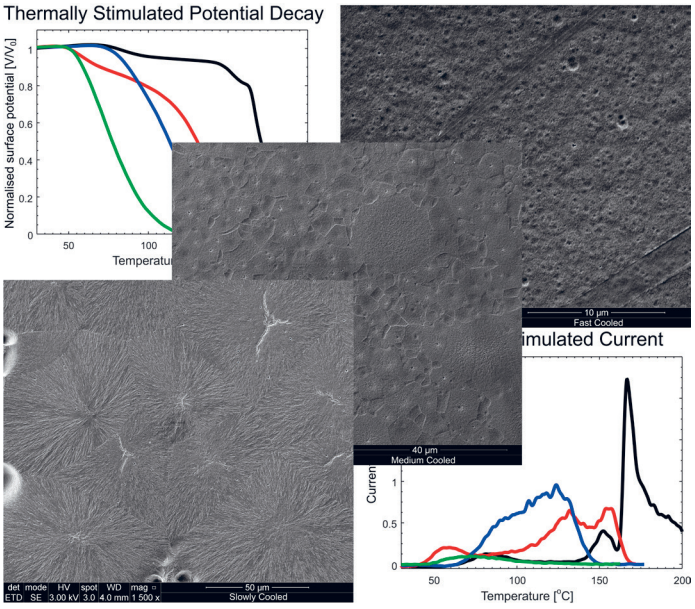

Charge Distribution and Stability in Electret Materials

Anders Thyssen

PhD Thesis January 2016

DTU Nanotech
Department of Micro- and Nanotechnology

DTU Nanotech
Department of Micro- and Nanotechnology

Charge Distribution and Stability in Electret Materials

Ph.D. Thesis

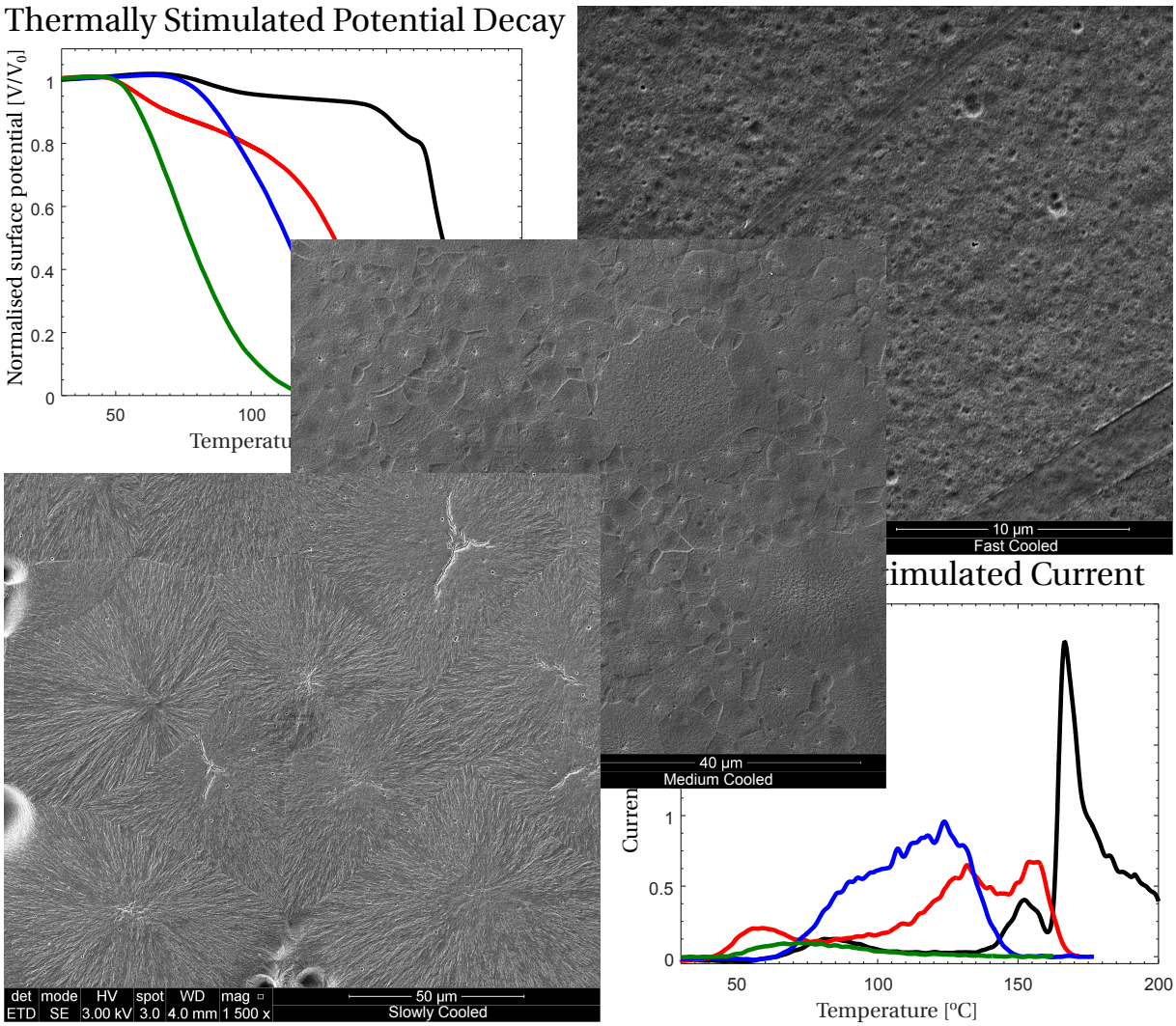

Anders Thyssen*†

Supervisors: Erik V. Thomsen*, Kristoffer Almdal* & Johan Gramtorp†

*DTU Nanotech - Department of Micro and Nanotechnology, Technical University of Denmark

†Bruel & Kjær - Transducer Departement

Janur 29th 2016

Abstract

The objective of the work presented in this Ph.D. thesis is to give a broader understanding of which key parameters influence the charge stability of polymer electrets, and how the electrical charges are distributed. This has been achieved using polypropylene as an electret polymer model system.

Theoretical considerations have been made concerning the effect, of the size of the crystalline areas known as spherulites and the degree of crystallinity, on the charge retention. The considerations showed that small spherulites and a high degree of crystallinity is favouring a high charge retention. This was also showed experimentally where the size of the spherulites was controlled through different cooling methods, and the degree of crystallinity was controlled by mixing atactic-polypropylene (a-PP) and isotactic-polypropylene (i-PP). The reason why the crystallinity have been controlled by mixing a-PP and i-PP, is because the charge retention is extremely sensitive to the sample preparation. This was seen in regard to the thermal history of the samples and the influence of micron and nano size particles in the polymer electret.

Through adding micron and nano size calcium carbonate and aluminium oxide particles in the polymer matrix is was seen that the charge retention could be enhance compared to samples with no particles. However, these results also showed that the thermal history for the samples played an equivalent importance role regarding the charge retention.

The morphology of the spherulites at the surface was visualised after a selective etch through scanning electron microscopy. The selective etch was to enhance the contrast between the amorphous and crystalline regions. Spherulites in three different size interval was seen, 50 µm to 100 µm, 3 µm to 7 µm, and 0.7 µm to 1.5 µm respectively.

By means of kinetic rate theory the discharge behaviour could be explained for polypropylene when thermally stimulated. This resulted in the determination of several activation energies, which could be used for describing the discharging seen at isothermal conditions. This theory is a powerful tool of predicting the lifetime of an electret at various thermal conditions.

Through the experimental obtained release currents, for different polypropylene samples, the critical temperature was determined from the largest current peak. If an electret is to avoid significant discharging it should be kept well below its critical temperate.

Resumé (Danish)

Målet med denne Ph.D. afhandling er at give en bredere forståelse af hvilke nøgleparametre der har indflydelse på ladnings stabiliteten for elektret polymer, og hvordan de elektriske ladninger er fordelt. Dette er blevet opnået ved anvendelse af polypropylen som et elektret polymer modelsystem.

Teoretiske overvejelser er foretaget vedrørende effekten, af størrelsen af de krystallinske områder, kendt som sfærulitter og graden af krystalliniteten, for ladnings stabiliteten. Disse overvejelser viser, at små sfærulitter og en høj grad af krystallinitet begunstiger en høj ladnings stabilitet. Dette blev også viste eksperimentelt hvor størrelsen af sfærulitter blev kontrolleret gennem forskellige kølemetoder, og graden af krystallinitet blev kontrolleret ved at blande ataktisk-polypropylen (a-PP) og isotaktisk-polypropylen (i-PP). Grunden til, at krystalliniteten blev kontrolleret ved at blande a-PP og i-PP, skyldes, at ladnings stabiliteten er yderst følsom over for hvordan prøven er forbedret. Dette blev set i forbindelse med den termiske historik for prøverne og indflydelsen fra mikro- og nanopartikler i elektret polymeren.

Gennem tilsætning af calciumcarbonat og aluminiumoxid partikler i polymer matrixen, blev det vist at ladnings stabiliteten kunne forbedres i forhold til prøver uden partikler. Men disse resultater viste også, at den termiske historik for prøverne spiller en tilsvarende stor betydning med hensyn til ladnings stabiliteten.

Morfologien af sfærulitter ved overfladen blev visualiseret, efter en selektiv ætsning, via scanning elektronmikroskopi. Den selektive ætsning var for at forbedre kontrasten mellem de amorfe og krystallinske områder. Sfærulitter i tre forskellige størrelser intervallet blev set, henholdsvis 50 µm til 100 µm, 3 µm til 7 µm, og 0,7 µm til 1,5 µm.

Ved hjælp af kinetisk rate teori kunne afladningen forklares for polypropylen prøver når de blev termisk stimuleret. Dette resulterede i bestemmelsen af flere aktiveringsenergier, som kunne anvendes til at beskrive afladning set ved isotermiske betingelser. Denne teori er et kraftfuldt værktøj til at forudsige levetiden for et elektret ved forskellige termiske forhold.

Gennem de eksperimentelle opnåede frigivelse strømme (release current), for forskellige polypropylen prøver blev den kritiske temperatur bestemt ud fra den største strøm top. Hvis et elektret materiale skal undgå væsentlig afladning bør den holdes et godt stykke under dens kritiske tempereret.

Preface

This Ph.D. thesis is submitted in partial fulfilment of the requirements for obtaining the Ph.D. degree at the Technical University of Denmark (DTU). The duration of the project has been from December 12th 2012 to January 29th 2016, including a 6 week extension due to paternity leave.

This industrial Ph.D. project has been carried out in collaboration between the Department of Micro- and Nanotechnology (DTU Nanotech) and the Company Brüel & Kjær Sound & Vibration Measurement .

The Ph.D. project has partial been founded by DTU, Brüel & Kjær and the Danish Agency for Science, Technology and Innovation (Styrelsen for Forskning og Innovation).

The supervisors of this project have from DTU been Professor Erik Vilain Thomson and Professor Kristoffer Almdal and from Brüel & Kjær Johan Gramtorp.

Anders Thyssen
Technical University of Denmark
Lyngby January 29th, 2016

Acknowledgements

First and foremost I would like to thank my supervisor Professor Erik Vilain Thomsen and co-supervisor Professor Kristoffer Almdal from DTU for their supervision and guidance during this project. Their natural enthusiasm and optimism is of tremendous value, and is passed on to everyone around them.

I world also like to thank my co-supervisor Johan Gramtorp, Jens Bendixen, Finn Kryger Nielsen and Lars Boye Rasmussen from Brüel & Kjær for all the input, ideas and constructive criticism under our weekly electret meetings.

Also a thank to the entire MEMS-AppliedSensors group at DTU Nanotech for help and assistance.

For the collaboration concerning robotic measurement of surface potential I would like to give a special thank to Claus Reckweg from Brüel and Kjær. For help in the laboratory a special thank to Lotte Nielsen from DTU Nanotech.

A great thank should be given to the enthusiastic students who worked on student projects during this project: master student Theofanis Spanos and bachelor student Mikkel Hofstedt Hansen who both have contributed to the progress and work presented in this thesis.

Last, but definitely not least, a huge thanks goes to my wife Sofie and daughter. For understanding of the many hours that have been put into this project, proofreading and for lugging dad away from the computer when time was right ☺.

Contents

Nomenclature

2D	Two Dimensional
3D	Three Dimensional
a-PP	atactic-PolyPropylene
Al_2O_3	Aluminium oxide
DSC	Differential Scanning Calorimetry
DTU	Technical University of Denmark
EVA	Ethylene Vinyl Acetate
FCC	Face Centered Cubic
FEP	Fluorinated Ethylene Propylene
i-PP	isotactic-PolyPropylene
PE	PolyEthylene
PET	PolyEthylene Terephthalate
Ph.D.	Doctor of Philosophy
PI	PolyImid
PMMA	PolyMethyl MethAcrylate
PPE	PolyPhenylene Ether, i.e. Poly(2,6-dimethyl- 1,4-phenylene ether)
PP	PolyPropylene
PS	PolyStyrene
PTFE	PolyTetraFluoroEthylene (Teflon)
PVDF	PolyVinylidene DiFluoride
PVF	PolyVinyl Fluoride
R^2	Coefficient of determination

%RH	Relative Humidity
RH	Relative Humidity
rpm	Rounds per minute
SEM	Scanning Electron Microscope
Si_3N_4	Silicon nitride
SiO_2	Silicon oxide
TSC	Thermal Simulated Current
TSPD	Thermal Stimulates Potential Decay
wt%	Percentage by weight

List of Symbols

Symbol	Description	Unit	Values
$\#_{2D}$	Refers to a 2D model	none	
$\#_{3D}$	Refers to a 3D model	none	
$A_{\perp}$	Area perpendicular to the surface	m^2	
$A_{\parallel}$	Area parallel to the surface	m^2	
A_{eff}	The effective surface area	none	
A_h	Probability coefficient of electron recombining with holes in the recombination centres	s^{-1}	
A_n	Probability coefficient of electron re-trapping in the traps	s^{-1}	
a	Side length of a unit cell	m	
$a_{e.min}$	The minimum distance between electrical charges	m	
C	Coulomb - electric charge	C	$1\mathrm{C} = 6.2415 \cdot 10^{18}$ electrical charges
D	Diameter of a spherulites	m	
$\mathbf{D}$	Electrical displacement field (vector field)	$\frac{\mathrm{C}}{\mathrm{m}^2}$	
d	Thickness	m	
d_{eff}	Effective charge distance (distance from the ground electrode to the effective plane of charges)	m	
$\mathbf{E}$	Electric field (vector field)	$\frac{\mathrm{V}}{\mathrm{m}}$	
E	Electric field (scalar)	$\frac{\mathrm{V}}{\mathrm{m}}$	
E_a	Activation energy	eV	
E_{max}	Maximum electrical field strength a material can withstand	$\frac{\mathrm{V}}{\mathrm{m}}$	

E_c	Mobility edges for the condition band	eV	
E_v	Mobility edges for the valence band	eV	
ΔH_f	Heat of fusion	$\frac{J}{kg}$	
I	Current	A	
k_b	Boltzmann constant	$\frac{eV}{K}$	$8.6173 \cdot 10^{-5}$
m_{app}	Mass of atactic-polypropylene	kg	
m_{ch}	Mass of cyclohexane	kg	
m_{ipp}	Mass of isotactic-polypropylene	kg	
m_s	Mass of sample	kg	
N	Number of available traps	none	
n	Number of electrons	none	
n_0	Number of electrons at time=0	none	
R_{ia}	Relative amount of atactic-polypropylene compared to the total amount of polymer	%	
r	Radius of a spherulite	m	
T	Absolute temperature	K	
t	Time	s	
T'	The temperature to be integrated	K	
T_e	Electrons trap	eV	
T_g	Glass transition temperature	K	
T_h	Hole trap	eV	
T_m	Melting temperature	K	
T_p	Peak temperature	K	
Q_{enc}	Enclosed free charges	C	
V	Electrical potential	V	
V_{max}	Theoretical voltage maximum	V	

Greek Symbols

Symbol	Description	Unit	Value
β	Heat rate	$\frac{\mathrm{K}}{\mathrm{s}}$	
ε_0	Vacuum permittivity	$\frac{\mathrm{F}}{\mathrm{m}}$	$8.8542 \cdot 10^{-12}$
ε_r	Relative permittivity	none	PP=2.3 [?] FEP=2.1 [?]
ΔH_f	Heat of fusion	$\frac{\mathrm{J}}{\mathrm{kg}}$	
η	Pacing factor (in percent of volume) $79\% \approx \frac{\pi}{4} \geq \eta_{2D} > 0$ $74\% \approx \frac{\pi}{3\sqrt{2}} \geq \eta_{3D} > 0$	%	
χ	Degree of crystallinity (in percent of mass)	%	
$\lambda(z)$	The relatively charges distribution	$\frac{\mathrm{C}}{\mathrm{m}}$	
ν	Attempt-to-escape frequency	s^{-1}	
ν_c	The correct values of ν (used in equation 2.31)	s^{-1}	
ρ_a	Density of amorphous regions	$\frac{\mathrm{kg}}{\mathrm{m}^3}$	
ρ_c	Density of crystalline regions	$\frac{\mathrm{kg}}{\mathrm{m}^3}$	
ρ_v	Volume charge density	$\frac{\mathrm{C}}{\mathrm{m}^3}$	
σ_{max}	Theoretical maximum surface charge density	$\frac{\mathrm{C}}{\mathrm{m}^2}$	
σ_s	Surface charge density	$\frac{\mathrm{C}}{\mathrm{m}^2}$	
$\sigma_{s_{eff}}$	Effective surface charge density	$\frac{\mathrm{C}}{\mathrm{m}^2}$	

Chapter 1

INTRODUCTION TO ELECTRETS

Electret materials has been know since at least the ancient Greece, where it was observed that by rubbing a piece of amber against fur, the amber could attract other items in close vicinity, such as feathers or bits of straw. However the word *"electret"* was not used before the late 19th century, where Oliver Heaviside coined this term. The definition of an electret is:

A dielectric material that has a quasi-permanent electric charge or dipole polarisation.

In figure 1.1 an illustration of an electret material is seen. For the understanding of the concept this electret material has both real charges, which here appear as both surface and space charges, and dipoles illustrated as the red ellipse. Normally an electret material have either real charges or dipoles. One way of utilising the electrical field, emerging from an electret material, is by having an metal film as a back electrode. In this way the potential drop over the electret can be exploit.

An electret generates internal and external electric fields, and is the electrostatic equivalent of a permanent magnet. Hence electret is formed of elektr- from *"electricity"* and -et from *"magnet"*. Electrets can be used where it is desired to utilise a high electrostatic field without

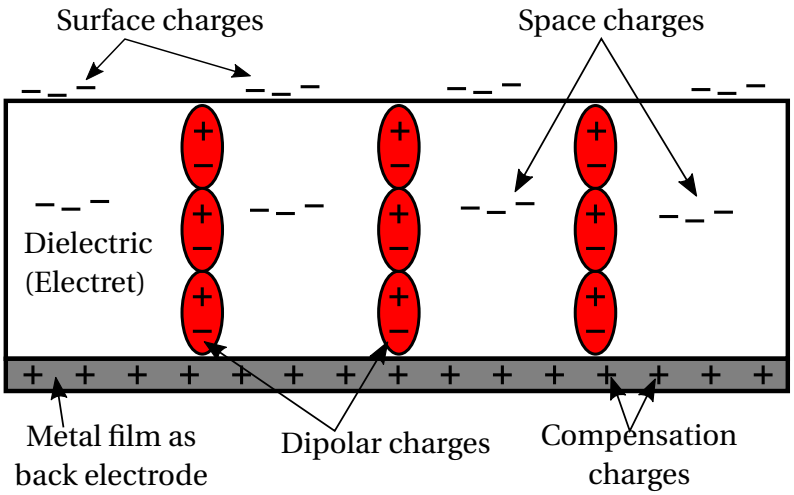

Figure 1.1: *Illustration of an electret material with both real charges and dipoles. Normally an electret contains either real charges or dipoles. The charges and dipoles in an electret generates internal and external electric fields. This makes electrets to the electrostatic equivalent of a permanent magnet.*

any external power supplies, such as batteries or high voltage sources. A few examples of places were electret has found its usefulness are electret microphones and electret headphones [**?**], electret ion chambers [**?**, **?**, **?**] for measuring radioactive gases and environmental gamma radiation, and air and gas filters for examples in respirators or large scale air cleaning devices [**?**, **?**]. Common to these mentioned application areas, is that the electret material itself plays a very critical and central role in the product, but that the product itself, except for headphones and microphones for smart-phones/tables, is aimed at a niche market. In the middle of the nineteen seventies a lot of research work [**?**, **?**], compared to the previous 30 years, was focused on polymer electrets resulting in industrial products such as high quality electret measurement microphones [**?**, **?**, **?**]. Such electret microphones are today made by Brüel & Kjær, and works as a capacitative transducer. An electret layer with a back electrode are charged to a given potential, and then placed inside a metal cylinder with a diaphragm a few µm above the charged electret layer. Thus creating a capacitor. When a sound wave is making the membrane move a change in the potential over the capacitor can be detected.

Nowadays the research activity is relatively low within the field of electrets, even though it is at a higher level than in the nineteen seventies; as measured by searchable publications, which the last couple of years have been around 300 per year compared to around 100 per year in the nineteen seventies[1]. This is also why there still are so many unexplained and not fully understood phenomenons within the field of electrets. For example, why and how does the crystallinity in a polymer affect the charge retention, where are the charges located on a molecular level or how can the discharge process be described with regard to both thermal and humidity stimulation, just to mention a few. Commonly used electret materials, in research and industry, are normally polymers or inorganic materials. This is often material described in [**?**, **?**]:

Polymers

- Fluorinated ethylene propylene (FEP)
- Polytetrafluoroethylene (PTFE)
- Polyethylene (PE)
- Polypropylene (PP)
- Polyethylene terephtalate (PET)
- Polyimid (PI)
- Polymethyl methacrylate (PMMA)
- Polyvinyl fluoride (PVF)
- Polyvinylidene fluoride (PVDF)
- Ethylene vinyl acetate (EVA)

Inorganic materials

- Silicon oxide (SiO_2)
- Silicon nitride (Si_3N_4)
- Aluminium oxide (Al_2O_3)
- Glass (SiO_2 + Na, S, Se, B, ...)

[1] These numbers are based on the search word “electret” at the DTU article database, see appendix A

where particularly the fluorinated polymers are known for their good charge stability. The charge stability of an electret is the most important property of an electret, as it is the electrical field created by the charges, that are the sole reason electret are of interest. The inorganic materials distinguish them self with often very high charge stability temperatures which the polymer electrets cannot compete with. However, the drawback for the inorganic materials is that they are very sensitive to the surrounding moisture [**?**], and that their practical stability at ambient conditions are worse than the stability obtained from most electret polymers; due to the moisture in the air. This is one of the reasons why the focus in the thesis is not on inorganic electrets but on polymer electrets.

1.1 Electret Polymer Model System

The purpose of this Ph.D. project has been to get a broader understanding of the key parameters that influence the charge stability of polymer electrets. The idea has been to use polypropylene as a model system due to the limited charge lifetime compared to other much more stable electrets, e.g. fluoropolymers. This makes it possible to study the performance of polypropylene as an electret material, in response to different processing steps, much faster than other more stable electret polymers. The background for the choice of polypropylene as model system will follow in the next paragraph. The goal is to get an understanding of how to enhance the temperature and humidity stability for polypropylene and to be able to transfer this knowledge to other electret polymers, for example Fluorinated Ethylene Propylene (FEP) which is currently used in Brüel & Kjærs microphone production.

The purpose of studying other materials than the fluoropolymers is to have a system that allows easier access to some of the phenomena we would like to study. The FEP based electret materials produced presently are well suited for the purpose they serve, even though the explanation for the attractive properties and the processing steps necessary to achieve these properties are not understood in detail. FEP is in general very sturdy, thus deterioration studies of its electret properties are very slow. The model system is a means to investigate these properties, by accelerating the ageing of the electret. In order for this to make sense, the model system must have similarities with the FEP system. FEP is a tetrafluoroethylene hexafluoropropylene copolymer which is very hydrophobic (ensures low water uptake even at high temperature), it is partially crystalline with a very high melting point (≈260 °C), and it is chemically very stable and insoluble in basically all solvents. An obvious candidate for a polymer model system would be a saturated hydrocarbon, such as polypropylene (PP) or polyethylene (PE). For both of these polymers it would be possible to have a partially crystalline material which is hydrophobic but less so than FEP, which has a lower melting point than FEP and which is still quite chemically stable but also less so than FEP. The relative permittivity (dielectric constant) is also similar between the saturated hydrocarbons and FEP. In table 1.1 relevant key parameters are shown for FEP and the two saturated hydrocarbons that, based on molecular structure, resemble FEP the most; i-PP[2] (isotactic-polypropylene) and PE respectively. What is seen in table 1.1 is that i-PP and PE resemble each other very

[2]i-PP is the type of polypropylene that is dominating in the industry and also the type of polypropylene which has the highest glass temperature and melting point.

much and that the biggest different between the two is their molecular structure. That said i-PP have a higher melting point and a higher electrical field strength than PE, both important parameters for an electret material. The electrical field strength determines the maximum theoretical potential an electret can support and the melting temperature gives a strong indication of the maximum operation temperature, an electret can keep its electrical charges

	FEP	i-PP	PE
Name	Fluorinated Ethylene Propylene	isotactic-Polypropylene	Polyethylene
Chemical formula	$(C_2F_4)_n - (C_3F_6)_m$	$(C_3H_6)_n$	$(C_2H_4)_n$
Molecular structure	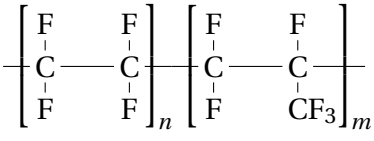	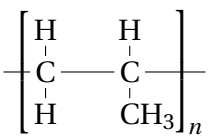	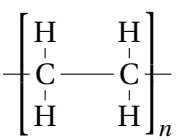
Bulk structure	Semi-crystalline	Semi-crystalline	Semi-crystalline
Polarity	non-polar	non-polar	non-polar
Density - semicrystalline, ρ_c	2120-2180 kg/m^3 [?]	900-940 kg/m^3 [?]	900-990 kg/m^3 [?]
Density - amorphous, ρ_a	-	850-870 kg/m^3 [?]	850 kg/m^3 [?]
Relative permittivity, ε_r @100Hz	2.1 [?]	2.3 [?]	2.0-2.4 [?]
Resistivity at 50% RH	$> 10^{16}\,\Omega m$ [?]	$> 10^{14}\,\Omega m$ [?]	$> 10^{15}\,\Omega m$ [?]
Electrical field strength, E_{max}	55 V/µm [?]	30 V/µm to 70 V/µm [?]	30 V/µm to 40 V/µm [?]
Glass Transition Temperature, T_g	-11 °C [?]	-20 to 0 [?,?]	-110 °C to -130 °C [?,?,?]
Transition Temperature (below T_m)	240 °C to 260 °C [?]	≈ 130 °C [?]	≈ 120 °C [?]
Melting point, T_m	255-285 °C [?]	160-170 °C [?]	115-135 °C [?,?]
Water absorption (% by mass, ASTM D570)	<0.01 % after 24 hour [?]	<0.01 % after 24 hour [?]	<0.01 % after 24 hour [?]

Table 1.1: *The table shows relevant key parameters for FEP, i-PP and PE. i-PP and PE is saturated hydrocarbons and is the polymers, based on molecular structure, that resemble FEP the most. Based on this table PP has been chosen as the polymer for the electret polymer model system. The presented parameters are a recapitulation from [?, ?, ?, ?, ?, ?, ?], it should be noted that the listed values only serves as an approximative values as the real values for a material can be influenced by manufacturing processes as well as samples preparation.*

at. Due to this and because the molecular structure of i-PP is closest to the molecular structure of FEP, i-PP has been chosen as the polymer for the electret polymer model system.

The relevance of this study is to be found in the new knowledge that will be created at DTU Nanotech and the academical society as a whole, within polymer electrets and characterisation of charged polymers. This knowledge could in the long run be used with in the field of small vibrational energy harvesting, solar cells (passivation layer) or Lab On A Chip (manipulations of particles with electrical fields), all which currently are research topics at DTU Nanotech. This study also has its relevance towards the Danish industry by raising the level of knowledge within electrets, and through that increase the efficiency of the production and the stability of electret microphones.

1.2 The Field of Electrets

Even though the applications of most electrets are niche areas, and the research within this field is low, there is still research work that is worth mention, which also have relevance for this project. Some of this work is mentioned in the following.

Investigations have been done to localise were the electrical charges are located on and in electret materials. It turns out that there is a huge difference between negative and positive corona charged FEP. The reason for this is not fully understood but Alquie C. et al. in [**?**] are suggesting that it is due to a higher mobility of holes than electrons before trapping and that negative charges in the bulk are compensating the positive charges that are initially injected on the surface. Only literature for negative corona charging is presented here, since this is the charging method used in this thesis, the reason for this is elaborated in chapter 2. Alquie C. et al. [**?**] have shown, through pressure pulse wave propagation, that negative corona charging of 50 µm thick FEP at room temperature and at potential up to −1.3 kV (corresponding to 26 MV/m) yields charges at the surface with no penetration into the volume. If this sample

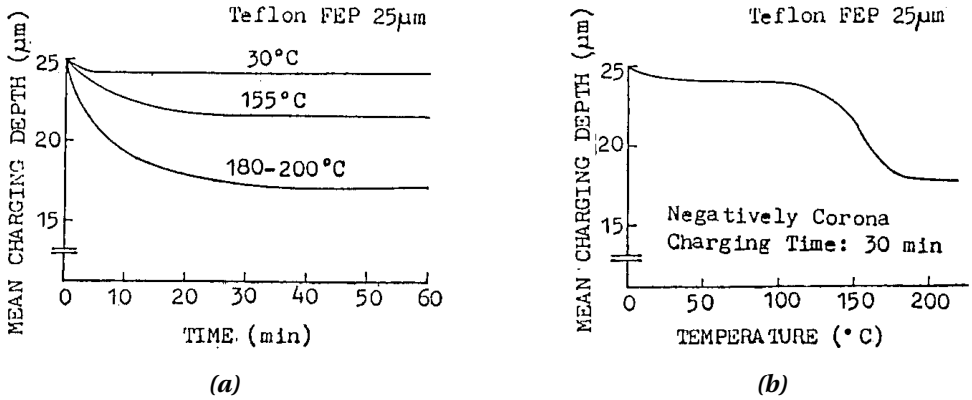

Figure 1.2: (a) *The location of charges, from negative corona charging, at different charging temperature, as a function of the charging time. The samples consist of a 25 µm thick FEP film which surface at at y=25 µm* ***(b)*** *The depth of the charges as a function of temperature, for a charging time of 30 min. Negative corona charging has been used on 25 µm thick FEP. It is seen that the temperature needs to be above 140 °C before the charges penetrates into the volume. Both figures are from [**?**].*

however, are subsequently annealed at temperatures > 120 °C it results in charge injections and volume trapping in the bulk. Meaning that the charges now have moved from being at the surface for the electret to the bulk of the electret. Sessler et. al. [**?**] have shown that if FEP (25.4 μm thick) is corona charged at room temperature with a potential of > 4 kV (corresponding to 157 MV/m) for a period of several hours, volume charges are formed in the bulk, but most of the charge are still at the surface. The bulk charges are distributed throughout the volume of the samples and they explain the bulk charges by drift of holes available in the bulk to the charged surface. T. Lu [**?**] has investigated how the charge location is affected by the corona charging temperature. What is seen in figure 1.2a is the location of the negative charges, at different charging temperature, as a function of the charging time. The surface of the FEP samples are at 25 μm on the y-axis. What is seen is that at room temperature the charges are located at the surface, with no penetration into the volume, correlating well with Alquie C. et al. in [**?**]. In figure 1.2b the depth of the charges is seen as a function of temperature, for a charging time of 30 min. What is seen is that volume penetration of negative corona charges in FEP do not happen before the temperature is above 140 °C.

Erhard et. al. have in [**?**] investigated the influence of impurities and additives in polymer electrets. They have reported that even very small amount of additives can have a significant influence on the thermal charge stability. An example of one of these studies is seen in figure 1.3a where a derivative of 1,3,5-benzenetrisamide has been added into isotactic-polypropylene. Samples containing different amount of the additive have then been charged via corona charging, and then the surface potential has been measured over a period of 24 hours at 90 °C. Figure 1.3a shows the normalised surface potentials. What is seen is that there is an optimum for the amount of this specific additive, to have an positive effect on the thermal charge stability, and that this optimum lies about 0.013 wt%. The increased thermal charge stabilities is in this case explained by the additives that act as trap centres for the electrical charges. However, when the concentration gets to high the additives begins to create rod-like nanostructures which work as discharge pathways that neutralise the initial effect. This optimal amount of additive however, only applies for this specific derivative of 1,3,5-benzenetrisamide and only for i-PP. It could also be that, it only applies for the i-PP that came from that specific manufacturer of i-PP. Erhard et. al. have in [**?**] also showed that i-PP from different manufactures performs differently at same isothermal conditions. Erhard et. al. explain these differences in the thermal charge stabilities, by different additives leftovers from the syntheses and the purification of i-PP. In figure 1.3b Erhard et. al. have mixed the polymers, PolyPhenylene Ether (PPE) and PolyStyrene (PS) to make a electret blend that have a better thermal charge stability than the two polymers have separately. The weight compositions refer to the ratio of PPE/PS. What is seen in figure 1.3b is that after 24 hours at 120 °C the blend with 75 % PPE and 25 % PS still have 74 % of its initial surface potential, contrary to pure PPE and PS which have 58 % and 0 % respectively. In figure 1.3c it is seen that the blend containing 75 % PPE and 25 % PS also was the blend with the highest density, approximatively 1.073 g/cm^3 which is higher than both PPE and PS which is 1.064 g/cm^3 and 1.043 g/cm^3 respectively. The increased stabilities is in the case explained by the a limitation of segmental motions (for the polymer chains) below T_g and thus effectively reduces the charge drift through the bulk. The take-home message from [**?**] is that the thermal charge stabilities can easily be affected by even very small amount of additives or impurities, and that a polymer blend may provide better charge stabilities than the polymers separately.

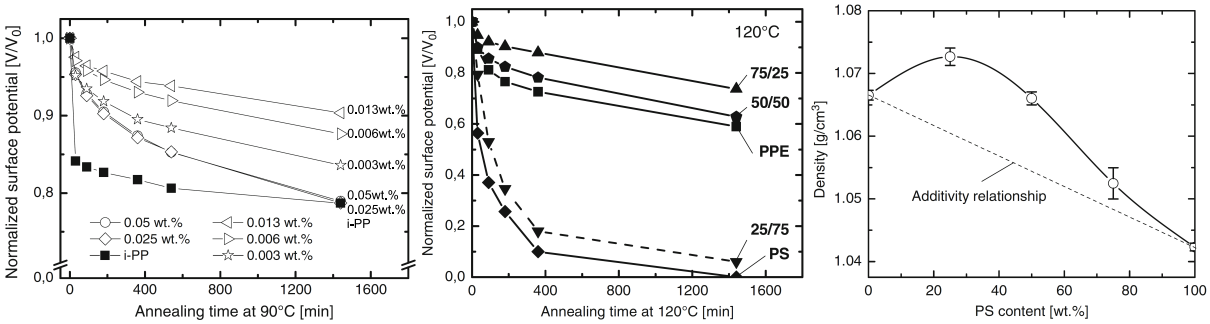

Figure 1.3: ***(a)*** *The normalised surface potential for i-PP samples with different amount of an additive derivative of 1,3,5-benzenetrisamide. The experiment has been conducted at 90 °C for 24 hours. What is seen is that there exist an optimum of adding this additive to obtain a positive effect on the thermal charge stability. The increased thermal charge stabilities is in this case explained by the additive that act as trap centres for the electrical charges.* ***(b)*** *The normalised surface potential for a polymer bled of PPE and PS, the experiment has been conducted at 120 °C for 24 hours. The weight compositions refer to the ratio of PPE/PS. What is seen is that the blend with 75 % PPE and 25 % PS outperform pure PPE and PS. The increased stabilities is in the case explained by an increased density that limits segmental motions below T_g and thus effectively reduces the charge drift through the bulk.* ***(c)*** *Shows the density of the blends used in (b). All figures are from [**?**].*

Ikezaki et. al. have in [**?**, **?**, **?**] developed a method for visualising the charged areas of spherulictic[3] PP, this was achieved in the following way. Sudan-blue, a dye that sublimes above 370 °C, was vaporized and negatively charged. The small charged particles of Sudan-blue with an average diameter of 2.7 µm were introduced to a positively charged spherulitic PP sample, resulting in the dye particles to adhere to the charged parts of the sample. Figure 1.4a shows a PP sample after it has been charged and exposed to the charged dye particles. What is seen is that the dye particles have adhered along the fibrils in the spherulites. Figure 1.4b shows a PP sample that has been charged, heated to 80 °C and then cooled to room temperature, and then exposed to the dye particles. What is seen is that the dye particles adhered only to the central parts and not to the peripheral parts of the spherulites. This indicates that the low energy traps are located at the boundaries and peripheral parts of the spherulites, and that the deeper traps sites are located at the centre of the spherulites. The dark parts seen in figure 1.4a and figure 1.4b between the spherulites is not due to particles but shadows. This work by Ikezaki et. al. indicated that a stable semi-crystalline polymer electret material, is a material that has a lot of the central part of a spherulites and less of the spherulites peripheral parts.

[3] Spherical semicrystalline regions inside non-branched linear polymers.

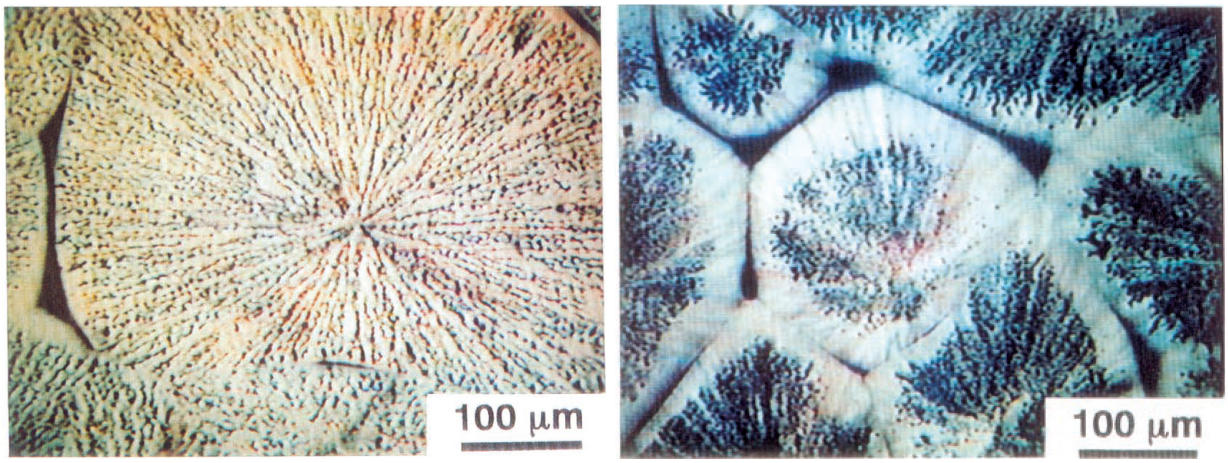

(a) *(b)*

Figure 1.4: ***(a)*** *Visualization of the charge pattern of spherulitic polypropylene before thermal cleaning. It can be seen that the dye particles have adhered along the fibrils in the spherulites* ***(b)*** *after a PP sample has been heated to 80* °C *and then cooled to room temperature. What is seen is that the dye particles adhered only to the central parts and not to the peripheral parts of the spherulites. Both images are from [**?**].*

1.3 Ideas and Hypothesis in this Thesis

Through this Ph.D. project different ideas and hypothesis has been tried, in the goal of understanding how a stable electret material looks like and, why and how the electrical charges behave when they are discharged from the electret. Some of the ideas paid off and some did not. In the following it will be briefly discussed what was tried, the ideas and hypothesis behind, what worked and what did not work. A detailed discussion of each of the paragraphs are found chapter 4 and the theory behind them in chapter 2.

Imprint Pattern In the first paragraph in section 1.2 it was stated that the electrical charges are placed on or very near the surface. From this, the idea came to increase the effective surface area. The hypothesis was that if the surface area was increased so would the number of deep traps, thus a more stable electret material. Stamps were developed, fabricated and imprinted into polypropylene samples. From the result of these experiments it was not possible to determine any improvement or deterioration in the charge stability. Unfortunately these experiments were done at a time were the importance of the samples preparation was not yet known. When the importance of the samples thermal history came clear the focus was shifted a bit and time prevented a new set of experiments where the charge stability and the effect of imprinted pattern could be investigated.

Particles Erhard et. al. have showed that additives (molecular size) could enhance the charge stability in polymer electrets. In the literature there is mixed reporting on whether particles (µm size) can do the same thing. This was tested in a master project made by Theofanis Spanos [**?**]. The particles used by Theofanis, included both micron-size and nano-size

particles. The obtained results where mixed, some of the particles seems to increase the charge stability a lot while some made the charge stability worse. In short some particles can (but not guarantee) enhance the charge stability. What also was seen, was that the sample preparation, seemed to have an equally large influence, on how the electrets charge stability ended up being, as the particles themselves. Sample preparation parameters should therefore be controlled and monitored in details.

Cooling Rate Based on previous experience, where it was seen that the sample preparation had a huge influences on the charge stability, different cooling rates from polypropylenes melt to its solid stated were investigated. Here is was seen that the charge stability were improved as the cooling rate was increased, illustrating the importance of the sample preparation. Further investigation of the samples showed that the size and number of the spherulites were different from samples that had seen different cooling rate. Increased charge stability were found to correlated with smaller spherulites and an increasing in the number of spherulites.

Crystallinity Based on the knowledge that more and smaller spherulites increases the charge stability, the influence of the samples crystallinity were investigated. This were done by mixing a-PP(atactic-polypropylene) into i-PP, the crystallinity could in this way be controlled, while keeping all other sample preparation parameters identical. The conclusion were that increased crystallinity also lead to an increasing in the charge stability.

1.4 Chapter Outline

The thesis is organised as follows. (chapter 1 is more a summary and can easily be skipped if the introduction already has been read.)

Introduction - Chapter 1 The concept and definition of an electret material is introduced as the rationale is given for choosing polypropylene as the polymer for the electret model system. Polypropylene has a limited charge lifetime compared to other much more stable electrets, e.g. fluoropolymers. This makes it possible to study the performance of polypropylene as an electret material much faster than other more stable electret polymers, and in the end transfer this knowledge to other electret material. Relevant literature for this Ph.D. project was also discussed, which has been used as a base for the ideas and hypothesis investigated and presented in the thesis.

Theory - Chapter 2 The first to be introduced is the concepts of energetic traps, known from semiconductors, that explain how the electrical charges are bound to the electret. Then classical electrodynamics is used to explain the electrical fields in and around the electrets, and how to estimate the maximum amount of charges an electret can support before voltage breakdown is reached. As literature strongly indicates that the crystalline regions in polymer electrets are of great importance when looking at charge stability theoretical reflections are done on the amount of spherulites at a polymer surface and in the near surface versus the

size of the spherulites. The last to be introduced in the theory is how to describe the thermal influence on the charges through parameter and concepts as: activation energies, attempt-to-escape frequency and re-trapping.

Experimental Techniques - Chapter 3 All the general sample preparation methods, experimental techniques and the polymers used in the experiments, are here described in details. A hole chapter has been dedicated to this, so the focus can be kept on the result in chapter 4.

Characterisation, Results and Discussion- Chapter 4 Results obtained throughout the Ph.D. project are presented here, divided into the four sections: Imprint Pattern, Particles, Cooling Rate and Crystallinity.

Conclusion - Chapter 5 A conclusion of the work and the most exciting results from in this Ph.D. thesis is given.

Outlook - Chapter 6 Finally an outlook of what could be investigated further in continuation of this Ph.D. work, but also what could be relevant to investigated for a even broader understanding of the field of electret.

Chapter 2

THEORY

In this chapter, relevant theory about polymer electrets is discussed. First to be introduced is the concepts of energetic traps, known from solid state physics, that explain how the electrical charges are bound to the electret.

Then classical electrodynamics is used to explain the electrical fields in and around the electrets, and how to estimate the maximum amount of charges an electret can support before voltage breakdown is reached.

Literature strongly indicates that the crystalline regions in polymer electrets are of great importance when looking at charge stability. In other words the physical location of the traps. Due to this, theoretical reflections are done on the amount of spherulites at a polymer surface and in the near surface versus the size of the spherulites. And how close the electrons should be too each other if they only are allowed to be in the spherulites to support a given surface potential.

To describe the thermal influence on the electrical charges in an electret, the following terms are introduced: activation energies, attempt-to-escape frequency and re-trapping of charges. This gives a theoretical explanation on how the electrical charges are discharged from an electret due to thermal stimulation.

2.1 Energy Traps

When having an electret material with real charges (surface or space charges), the charges can be thought of as being trapped in potential wells. This is illustrated in figure 2.1a with an energy diagram. Some of the traps are shallow, which corresponds to charges that are less stable, and some of the traps are deep, corresponding to charges that are very stable. It goes without saying that a good electret material has many deep traps. These traps can both be located at the surface and in the volume (space charges). The *surface traps* can be caused by, chemical impurities, specific surface defects caused by oxidation products, broken chains, adsorbed molecules or differences in short-range order of the surface and bulk. The *volume traps* can be caused by a number of structural anomalies such as impurities, defects in the monomeric units, chain irregularities or imperfections of the crystallites [**?**]. All these type of traps are rarely periodic, even if the electret should be semi-crystalline, but occur randomly

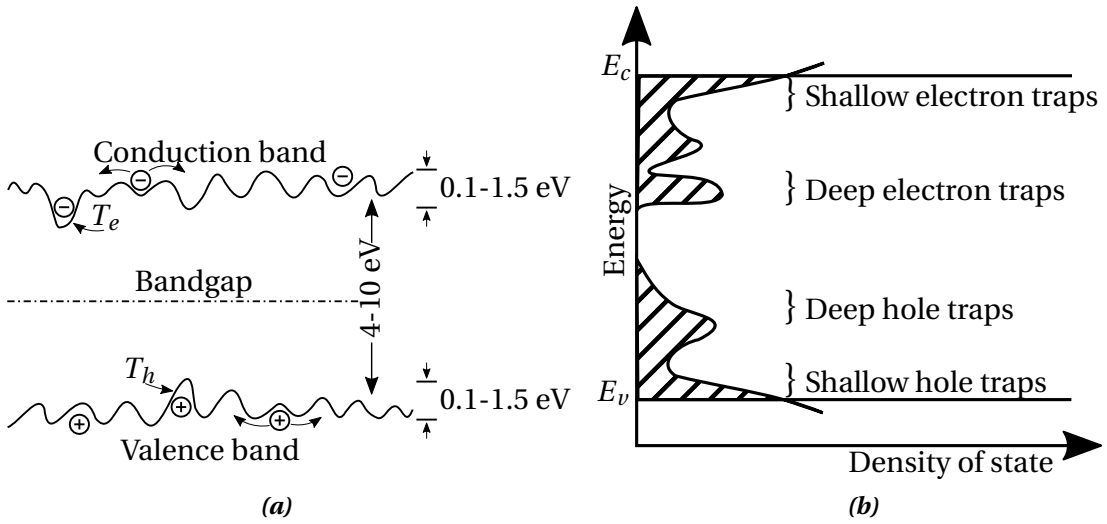

Figure 2.1: ***(a)*** *Illustration of the energy diagram for a polymer electret. The existence of the traps can be numerous and are most often randomly distributed throughout the electret. T_e electrons traps, T_h hole traps.* ***(b)*** *Illustration of a possible distribution of the density of state for a polymer electret. The shaded areas are traps, and it is seen that these are not distributed evenly over their energies. E_c and E_v indicate the mobility edges at which the mobility for the charges are increased drastically.*

throughout the electret. Also the depth of the traps can vary a lot which is illustrated in figure 2.1b, which shows a possible distribution of the *density of state* for a polymer electret. What is seen in figure 2.1b is that the traps (hatched areas) are not evenly distributed over their energies. Normally there will be many shallow traps, and then one or two peaks at higher energies. This reflects well what has been experimentally observed and is presented in chapter 4. E_c and E_v indicate the mobility edges at which the mobility for the charges are increased drastically. If a charge is entering this area it will discharge from the sample and will no longer contribute of the electrical field emerging form the electret. If the energy of a charge exceeds the depth of the trap it is in, the charge will leave the trap and begin to travel, towards either the conductive band or the valence band according the its polarity. Before the charge reaches either one of these and discharges, there is a possibility that it will be re-trapped by a trap with an energy that exceeds the energy of the charge. This is illustrated for both an electron and hole in figure 2.1a (the charges with the arrows). This phenomena of re-trapping can be used to stabilise an electret, this is done practically by heating up the electret. What happens is that the charges in the shallow traps, which energies are exceeded by the thermal energy, will either be discharged or re-trapped. Leaving back an electret, that might have fewer charges than before but, those that are left will in average be in deeper traps, and more stable than before.

2.2 Charge Density

When having a charged electret, and testing it for its stability it is often useful (but not always necessary, we will come back to this later) to know the charge density of the electrical charges. As it is the charges, which generates the electrical field around the electret, that are the sole reason electrets are of interest. However, the charges can not be measured directly, only indirectly through an electrostatic voltmeter, this is illustrated in figure 2.2. An electrostatic voltmeter detects the strength of the electrical field that is generated, above the surface, by the charges on the electret. The electrostatic voltmeter then translate this field into an electrical potential, relative to the grounded side of the electret. The grey arrows above the electret in figure 2.2 illustrate the electrical field that the electrostatic voltmeter detects. It can be shown that the electrical field above and infinite evenly charged plane is independent of the distance to that plane [**?**], which is what the electrostatic voltmeter is utilising and why the distance from the probe to the surface of the electret is of less importance. In normal use the distance from the probe to the surface of the electret is between 1 mm and 2 mm to increase the resolution of the measurement.

From the measured potential the charge density can be calculated, stating with Gauss's law [**?**].

$$Q_{enc} = \oint \mathbf{D} \cdot d\mathbf{s} \tag{2.1}$$

Equation (2.1) states that the charges, Q_{enc}, in an enclosed volume is the surface integral, $d\mathbf{s}$, over the electrical displacement field, $\mathbf{D}$. As mentioned in section 1.2, literature indicates that charges created at negative corona charging are located at the surface of the electret. In that case the displacement field is equal to the surface charge density, σ_s. In the following

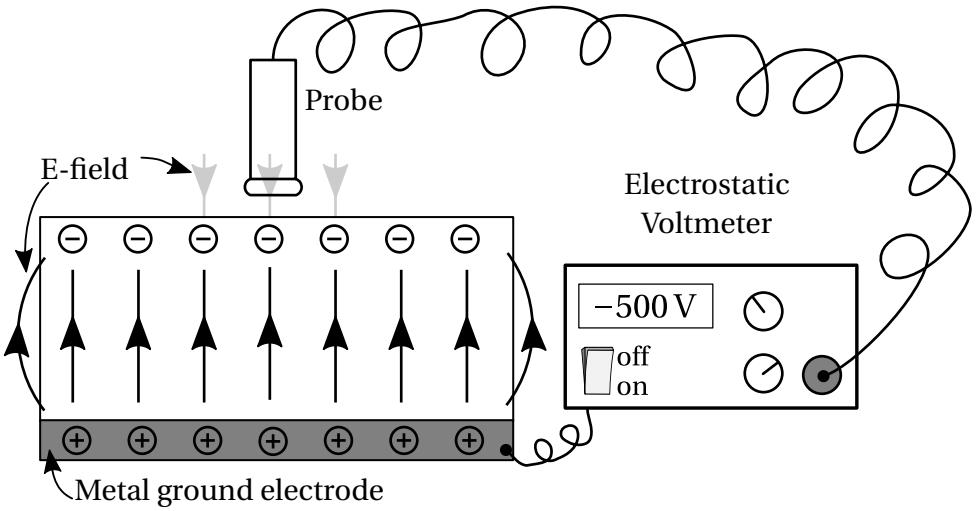

Figure 2.2: *Illustration of how the charges on and in the electret are detected through the electrical field, resulting in a surface potential measurement. The probe from the electrostatic voltmeter is placed close to the opposite side of the electret that has been grounded to the electrostatic voltmeter. The grey arrows above the electret illustrate the electrical field that the electrostatic voltmeter detects.*

the displacement field is expressed by the electrical field, **E**, the vacuum permittivity, ε_0, and the relative permittivity, ε_r:

$$\mathbf{D} = \mathbf{E}\varepsilon_0\varepsilon_r = \sigma_s \tag{2.2}$$

The electrical field can be expressed in terms of the electrical potential and the distance:

$$E = -\frac{V}{d} \tag{2.3}$$

where d is the thickness of the electret material. The surface charge density, can by combining equation (2.2) and equation (2.3), be expressed as:

$$\sigma_s = -\frac{\varepsilon_0\varepsilon_r}{d}V \tag{2.4}$$

From equation (2.4) it is possible to determine the surface charge density from the known thickness of the electret and the surface potential measured with the electrostatic voltmeter. Under the assumption that the charges are at the surface and that they are uniform distributed in the lateral dimensions.

It is however, known that all charges are not always located at the surface. If the relatively charge distribution, $\lambda(z)$, in the depth of the electret is known, the volume charge density can be determined from the measured surface potential. This is done by first determining the effective charge distance, d_{eff}, which is the distance from the grounded side of the electret and to that plane of charges that effectively will give the same surface potential as the volume charges. The effective charge distance, is to be found in the middle of the spatial distributed charges and can be calculated by solving the following expression for d_{eff}. Again it is assumed that the charge distribution in the lateral dimensions is uniform and that $\lambda(0)$ is at the grounded electrode and $\lambda(d)$ is at the surface of the electret.

$$\int_0^{d_{eff}} \lambda(z)\,dz = \frac{1}{2}\int_0^{d} \lambda(z)\,dz$$

By knowing the effective charge distance, d_{eff}, the effective surface charge density, $\sigma_{s_{eff}}$, can be determined as:

$$\sigma_{s_{eff}} = -\frac{\varepsilon_0\varepsilon_r}{d_{eff}}V \tag{2.5}$$

This is the surface charge density at the distance d_{eff} from the ground side of the electret, which will induce the same surface potential as the volume charge density; that is about to be determined. From equation (2.5) an expression for the volume charge density can be determined, as

$$\begin{aligned} \rho_v(z) &= \sigma_{s_{eff}}\lambda(z) \\ \rho_v(z) &= -\frac{\varepsilon_0\varepsilon_r}{d_{eff}}V\cdot\lambda(z) \end{aligned} \tag{2.6}$$

A thing that should be noted in equation (2.4) and equation (2.5) is that the charge densities have a linear dependence of both the thickness of the electret and the measured surface potential. This means that when comparing charge stabilities, or charge retention to use another word, from different electrets, which have the same lateral charge distribution and thickness, extra information will not be revealed by calculating the charge density. Hence plotting the electret charge stability can be done by plotting the surface potential as the qualitative unit. This is the reason it is not always necessary to know the charge density, when looking at the electret charge stability, as stated in the start of this section. One way of investigate if the lateral charge distribution is as homogeneous as wanted, is by mapping out the surface potential for the entire electret sample, and then look at the variation of the potentials.

What also can be seen from equation (2.4) and equation (2.5) is that the surface potential will drop if the charges are moved closer to the back electrode. Hence a decay in surface potential can both be due to charges leaving the electret but also charges that have moved closer to the back electrode. What also should be kept in mind when calculating the surface charge density, is that the density will be underestimated if the charges also are distributed in the volume and not only at the surface.

Electrical Field Strength

There exist a theoretical upper limit of how much an electret can be charged. And that limit depends on the electrical field strength of the electret, which can vary a lot from material to material, and even on how the material has been produced and processed. The theoretical voltage maximum, V_{max}, an electret can support, under the assumption that all the charges are uniformly distributed at the surface, is determined as:

$$V_{max} = E_{max} \cdot d \tag{2.7}$$

Were E_{max} is the maximum electrical field strength the electret material can withstand before voltage breakdown. V_{max} is also the breakdown voltage of the electret. The theoretical maximum of the surface charge density, σ_{max}, can be determined as:

$$\sigma_{max} = -\varepsilon_0 \varepsilon_r E_{max} \tag{2.8}$$

It can be practical to know the maximum surface potential the electret can be charged too. Not only to avoid damaging the electret but also to know if the reached surface potential is due to the theoretical maximum or if it is due to other properties of the electret; e.g. no available trap sites. In table 2.1 the electrical field strength and the relative permittivity are seen for different polymer electrets. What is seen is that the variation between different polymers electrical field strength and the relative permittivity is notable. However, within the normally used electret thicknesses (10µm - 100µm) and the normally used surface potential (a few volt to 1.000 volt) the upper limit for the surface potential is rarely caused by the electrical field strength. As also mentioned in the introduction the electrical field strength and the relative permittivity for FEP and PP are similar.

Polymer	Electrical Field Strength, E_{max}	Relative permittivity, ε_r @100 Hz
FEP	55 V/µm [?]	2.1 [?]
PTFE	48 V/µm [?]	2.1 [?]
PP	30 V/µm to 70 V/µm [?]	2.3 [?]
PE	30 V/µm to 40 V/µm [?]	2.0-2.4 [?]
PVDF	18 V/µm [?]	8.4 [?] (@1 MHz)
PVF	20 V/µm [?]	8 [?] (@1 kHz)

Table 2.1: *The electrical field strength and the relative permittivity for different electret polymers.*

2.3 Spherulites

As briefly mentioned in section 1.1, there is literature [**?**, **?**, **?**] which indicates that the crystalline regions in polymer electrets are of great importance when looking at thermal charge stability. It was also stated in section 1.2 that the electrical charges are located at the surface of the electret. When a polymer-melt cools and solidifies, an amorphous surface is usually formed, although its bulk phase may be semicrystalline. Fractions not accommodated in the crystalline structure are rejected to the surface. However, if the polymer is cooled and solidified against a nucleated surface, various degrees of crystallinity can be obtained [**?**].

Both Polypropylene (PP) and Fluorinated Ethylene Propylene (FEP) can form spherulites upon crystallisation [**?**, **?**, **?**, **?**]. However, both polymers can also form other kinds of crystalline areas such as randomly arranged lamella, rod-like and transcrystalline surfaces. The type of crystals formed depend on the way the polymer has been processed. FEP will normally form spherulites upon cooling from its melt but, is the cooling rate sufficiently low rod-like crystals, similar to those seen in PolyTeraFluoroEthylene (PTFE), will be formed.

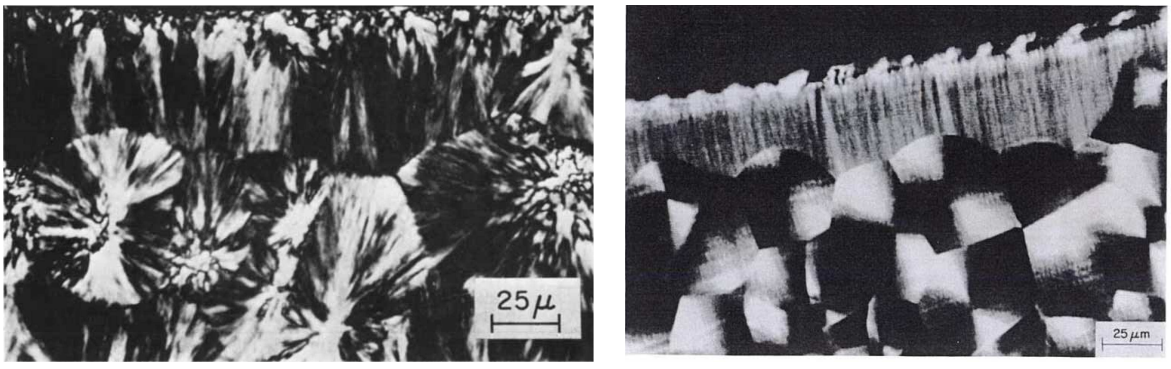

(a) ***(b)***

Figure 2.3: (a) *A cross-section of a PP sample where a transcrystalline surface has been formed moulded against PET. This happens when the polymer melt is in contact with a surface that nucleates massive numbers of crystals, which are so crowded that they are forced to grow perpendicular to the surface. Beneath the transcrystalline surface spherulites are seen. Image is from [**?**]. **(b)** A cross-section of a polyethylene sample where a transcrystalline surface easier can be seen than in (a). The polyethylene sample has been moulded against aluminium foil. Image is from [**?**] (reprinted from [**?**]).*

If the cooling rate from a FEP melt, is sufficiently high randomly arranged lamella will be formed [**?**, **?**]. PP will also normally form spherulites, but is the surface, upon cooling from its melted state, in contact with for example PTFE, PolyEthylene Terephthalate (PET) or gold [**?**, **?**] a transcrystalline surfaces will be formed [**?**, **?**, **?**, **?**]. This phenomenon is seen in figure 2.3a which shows a cross-section of a PP sample where a transcrystalline surface has been formed moulded against PET. This happens when the polymer melt is in contact with a surface that nucleates massive numbers of crystals, which are so crowded that they are forced to grow perpendicular to the surface. The thickness of transcrystalline surface is usually 10 µm to 100 µm thick. A high cooling rate however, will counteract this phenomena toward a surface with spherulites. This phenomenon is also known from polyethylene which is easily seen in figure 2.3b.

As already mentioned, the crystal formation can be controlled by the amount of nucleation sites present. These sites can be chemical impurities, particles, structural defects along the polymer chain or structural disturbances at the surface. The cooling rate may, however, play an equally important role as the nucleation sites. In general a fast cooling rate will result in small crystals and a lower crystallinity of the polymer than a slow cooling rate which, will result in fewer but larger crystals, and with a higher sample crystallinity. The question is what is the most beneficial for a stable electret material. Is it an electret with few large crystals and a higher crystallinity or an electret with many small crystals and a lower crystallinity? Is the literature discussed in section 1.2 correct, it would be beneficially with as many spherulites centres as possible, as this is the location of the deep traps. However, when talking about spherulite centres in practice, these are not a mathematical point at the spherulites but an area around the centre. How big this area is and how this area is favoured by the size of a spherulite is unknown. In the following subsection considerations concerning the above will be discussed.

2.3.1 Surface and Volume Considerations

In this subsection considerations about the number and the area/volume of spherulites at the surface and near surface versus the size of the spherulites, will be discussed. Considerations about the number of electrical charges will also be discussed, this includes how close, and how many charges there should be on/in the spherulites to sustain a given surface potential, and how close the charges can be to one another based on theoretical assumptions. This is done to create an overview on how the size and number of the spherulites can effect the charge stability.

Before these calculations can be performed assumptions have to be made, these are listed below with comments:

- The spherulites are treated as perfect circles (2D-model) or perfect spheres (3D-model)
  - Even though most spherulites are not actually spheric, this assumption is fair to use as it is the centre of the spherulites which primarily is of interested.
- All the spherulites have the same size and are packed as a Face Centered Cubic (FCC) unit cell; see figure 2.4a.

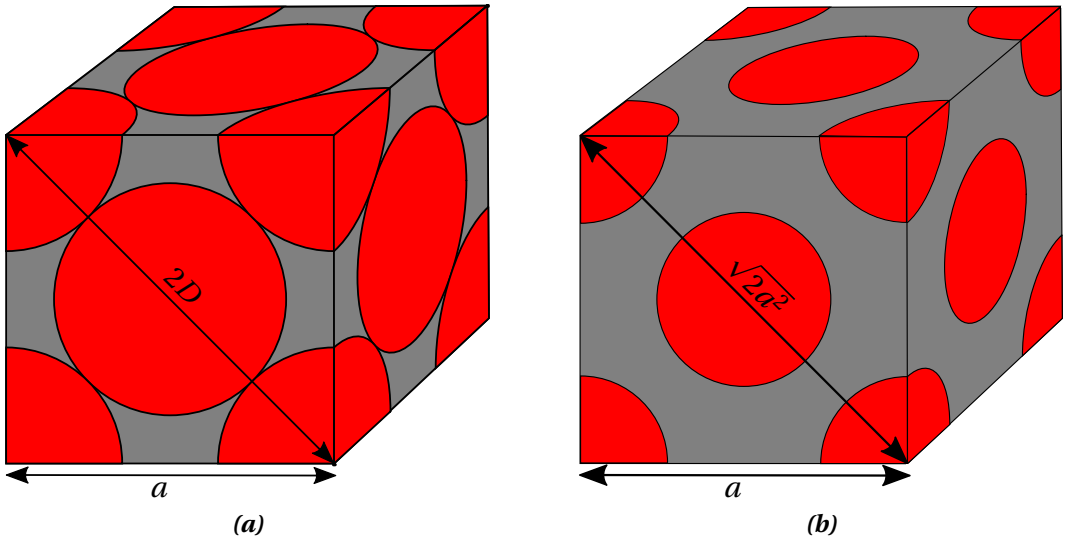

Figure 2.4: *Illustration of FCC unit cells which are used in the calculations concerning the surface and volume considerations of spherulites.* ***(a)*** *A FCC unit cell where the spherulites are packed at closely as they can; packing factor is here* $\approx 74\,\%$ *.* ***(b)*** *A FCC unit cell where the distance between the spherulites are increased so that the packing factor can be controlled from 0 % to 74 %.*

  - Of course all the spherulites are not of the same size, but this assumption is made so that the spherulites can be places in a simple unit cell, which will simplify the calculations.

- The spherulites are 100 % crystalline and the crystallinity of the sample is controlled through the distance between the spherulites within the FCC unit cell; see figure 2.4b.
  - In reality the spherulites are not 100 % crystalline but a mixture of randomly arranged molecular chains (amorphous regions) and structured molecular chains (crystal regions). This assumption however, allows the calculations to accommodate different crystallinity, and it counteracts the assumption of equally large spherulites, made in the previous assumption.

- In the 3D model we assume that the charges are evenly distributed in the spherulites first 5 µm from the surface.
  - As previously mentioned (section 1.2) the charges from negative corona charging, at room temperature, are located at the surface, but can be forced into the bulk under either an extreme large electrical field or at high temperature. The 3D model is thought to clarify the effect on the number and the volume of the spherulites as the size of the spherulites are changed. From literature based on FEP, at temperature above 140 °C [**?**] the electrical charges penetrates between 3 µm to 7 µm into the bulk; is it from here that the depth of 5 µm comes.

Electrical Charges

How close can electrical charges be to each other if they are evenly distributed (square grid) on the surface (2D-model)? Based on equation (2.8) which yields:

$$\sigma_{max} = -\varepsilon_0 \varepsilon_r E_{max}$$

The minimum distance, $a_{e.min\_2D}$, between the electrical charge can be determined as:

$$a_{e.min\_2D} = \sqrt{\left| \frac{1}{C} \cdot \frac{-1}{\varepsilon_0 \varepsilon_r E_{max}} \right|} \tag{2.9}$$

where C is the number of electrical charges in a Coulomb. For polypropylene, based on values in table 2.1, the theoretical minimum distance would be between:

$$a_{e.min\_2D}\,(\mathrm{PP}) = 11\ \mathrm{nm} \text{ and } 16\ \mathrm{nm}$$

If the same were to be calculated for charges that were to be evenly distributed in the first 5 µm of the surface $\left(1\,\mathrm{m} \cdot 1\,\mathrm{m} \cdot 5\,\mu\mathrm{m} = 5 \cdot 10^{-6}\,\mathrm{m}^3\right)$ the minimum distance, $a_{e.min\_3D}$, would depend of the thickness of the sample. Be combining equation (2.7) and equation (2.8) $a_{e.min\_3D}$ can be determined as:

$$a_{e.min\_3D}\left(\mathrm{PP}_{\mathrm{d}\mu\mathrm{m}}\right) = \sqrt[3]{\left| \frac{1}{C} \cdot \frac{-5 \cdot 10^{-6}}{\varepsilon_0 \varepsilon_r E_{max}} \cdot \frac{d_{eff}}{d} \right|} \tag{2.10}$$

where $d_{eff} = d - \frac{5\,\mu\mathrm{m}}{2}$ as the charges are evenly distributed in the first 5 µm of the surface. For polypropylene thicknesses of 10 µm, 30 µm, 50 µm and 100 µm the minimum distance between the charges would be:

$$\begin{aligned}
a_{e.min_3D}\left(\mathrm{PP}_{10\mu\mathrm{m}}\right) &= 75\ \mathrm{nm} \text{ and } 99\ \mathrm{nm} \\
a_{e.min_3D}\left(\mathrm{PP}_{30\mu\mathrm{m}}\right) &= 80\ \mathrm{nm} \text{ and } 106\ \mathrm{nm} \\
a_{e.min_3D}\left(\mathrm{PP}_{50\mu\mathrm{m}}\right) &= 81\ \mathrm{nm} \text{ and } 108\ \mathrm{nm} \\
a_{e.min_3D}\left(\mathrm{PP}_{100\mu\mathrm{m}}\right) &= 82\ \mathrm{nm} \text{ and } 109\ \mathrm{nm}
\end{aligned}$$

Now that the minimum distances between the charges are known, it is time to look at how close to that limit a normal use of electret is. A typical electret thickness is between 10 µm to 100 µm, which normally has a surface potential between a few volts to a few thousand volts. Figure 2.5 shows, for polypropylene, what the maximum distance between charges can be for conditions mentioned above, and under the assumption that the electrical charges freely can choose where they want to be at the surface (2D) or in the first 5 µm of the surface (3D). What is seen in figure 2.5, is that a typical use of electret only will give challenges, for the distance between the charges, around and above thousand volt. Thus, if operating with a thickness around 30 µm to 50 µm and at a surface potential of a few hundred volts, then there should be more than enough space for the charges. One thing that should be kept in mind though, is the assumption that the charges freely can choose where they want to be (corresponding to a crystallinity of 100 %), this is most likely not true, which makes it relevant to look at the area and volume the spherulites occupy in an electret. This will be addressed in the next sub-subsection. As a consequence of equation (2.4) the distance between the

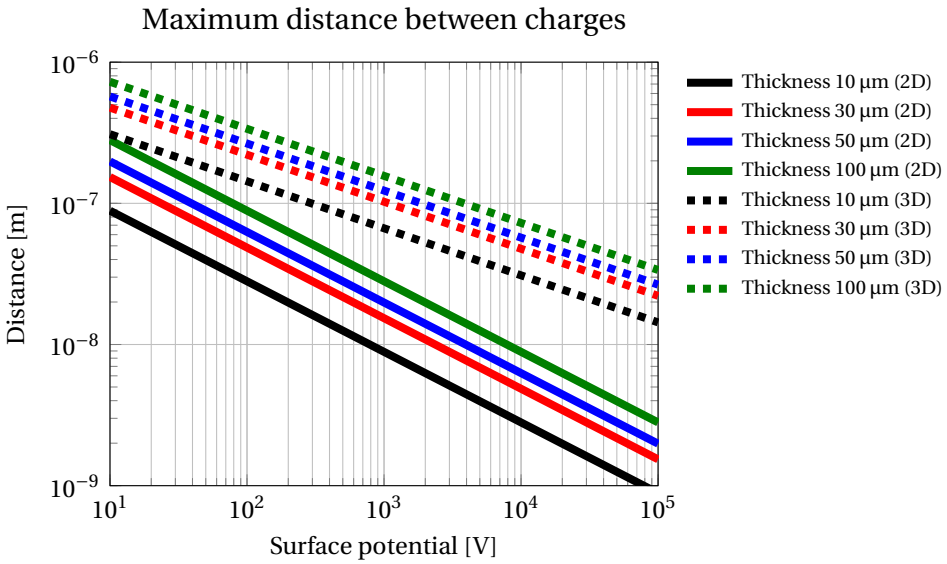

Figure 2.5: *Shows the maximum distance between charges in polypropylene as a function of surface potential. Roughly speaking, surface potentials that are durable for the 2D-model (solid lines) is were the distance between the charges are more than 10 nm. Similar for 3D-model (dash lines) the distance between the charges have to be more than 100 nm. (In the calculation for the 3D-model the thickness of the electret should of course not be used but the distance from the grounded side of the electret to the plane of the effective surface carhge density; in this case it is 2.5 µm under the surface!)*

charges become larger as the thickness of the electret is increased. This is because when the thickness is increased a lower surface charge density is needed to sustain the same surface potential.

Spherulites Density

To be able to find the area and the volume of the spherulites, and calculate how close the charges are to each other, the size of the unit cells seen in figure 2.4 must be known. As well as the packing factor, and the total number of spherulites at the surface and in the first 5 µm of the surface. The packing factor is the ratio between 'the area/volume of the spherulites' and 'the area/volume of the unit cell'.

The side length, a, of a FCC unit cell, as seen in figure 2.4a, can be expressed by the diameter, D, of the spherulites:

$$a = \sqrt{2}D$$

2D-model - Spherulites per surface unit

The packing factor in 2D, η_{2D}, with 2 spherulites per unit cell, can be expressed as:

$$\eta_{2D} = \frac{2 \cdot \left(\frac{D}{2}\right)^2 \pi}{a^2} = \frac{\pi}{4} \approx 79\,\% \tag{2.11}$$

Where ≈ 79 % is the maximum packing factor that can be obtained for a 2D FCC unit cell. If the spherulites do not touch each other, as in figure 2.4b and the packing factor is known then the side length can be expressed, by rewriting equation (2.11), as:

$$a_{2D} = D \cdot \sqrt{\frac{\pi}{2\eta_{2D}}} \tag{2.12}$$

Equation (2.12) is only valid in the interval of η_{2D}; $\frac{\pi}{4} \geq \eta_{2D} > 0$.

Is the density of the crystalline and amorphous regions the same, then the packing factor would be the same as the crystallinity. However, this is rarely the case which means that an adjustment of the crystallinity has to be made. It can be shown that the general relationship between the packing factor and the crystallinity, χ, is:

$$\eta = \frac{\chi\rho_a}{\chi\rho_a - \chi\rho_c + \rho_c} \tag{2.13}$$

Were ρ_a and ρ_c are the density of the amorphous and the crystalline regions respectively. The number of spherulites at the surface can then be determined as:

$$\frac{\text{No. of spherulites}}{1\text{m}^2} = \frac{2}{a_{2D}^2} = \frac{4\eta_{2D}}{\pi D^2} = \frac{4}{\pi D^2}\frac{\chi\rho_a}{\chi\rho_a - \chi\rho_c + \rho_c} \tag{2.14}$$

Equation (2.14) is plotted in figure 2.6a and will be commented in the end of next paragraph.

3D-model - Spherulites per volume unit

The packing factor in 3D, η_{3D}, with 4 spherulites per unit cell, can be expressed as:

$$\eta_{3D} = \frac{4 \cdot \frac{4}{3}\left(\frac{D}{2}\right)^3 \pi}{a^3} = \frac{\pi}{3\sqrt{2}} \approx 74\,\% \tag{2.15}$$

Where ≈ 74 % is the maximum packing factor that can be obtained for a FCC unit cell. As for the 2D-model the side length in the 3D-model can also be expressed in terms of the packing factor and the diameter of the spherulites, by rewriting equation (2.15), as:

$$a_{3D} = D \cdot \sqrt[3]{\frac{2}{3}\frac{\pi}{\eta_{3D}}} \tag{2.16}$$

Equation (2.16) is only valid in the interval of η_{3D}; $\frac{\pi}{3\sqrt{2}} \geq \eta_{3D} > 0$.

The number of spherulites in the first 5 µm of the surface can then be determined as:

$$\frac{\text{No. of spherulites}}{1\text{m}^2 \text{ x } 5\mu\text{m}} = \left(1 \cdot 1 \cdot \left(5 \cdot 10^{-6}\right)\right) \cdot \frac{4}{a_{3D}^3} = \frac{3\eta_{3D}}{\pi D^3} \cdot 10^{-5} = \frac{3 \cdot 10^{-5}}{\pi D^3}\frac{\chi\rho_a}{\chi\rho_a - \chi\rho_c + \rho_c} \tag{2.17}$$

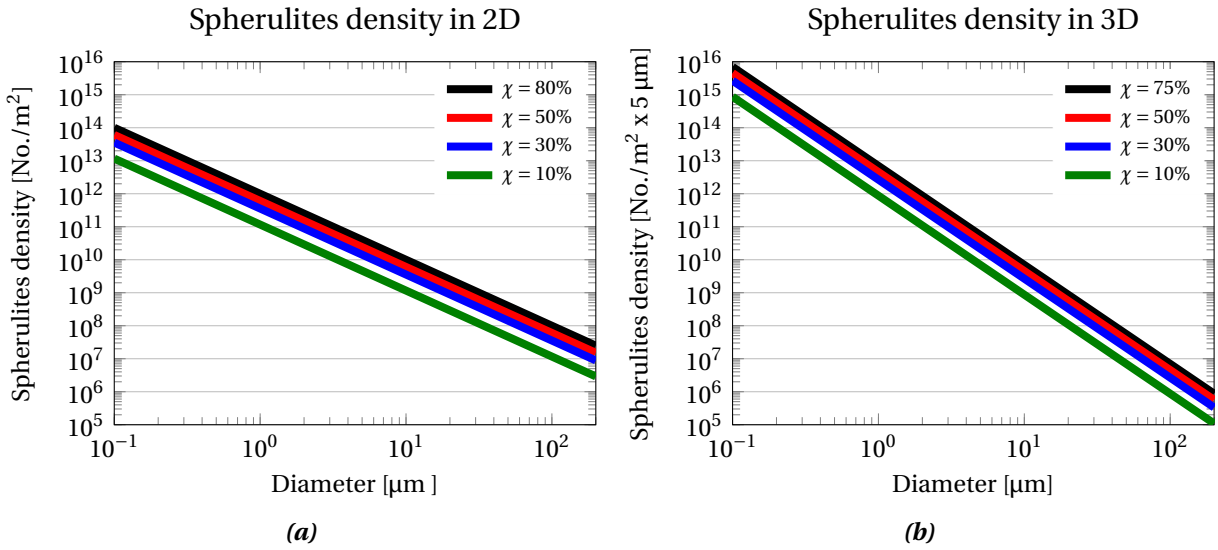

Figure 2.6: *Shows for the 2D-model* ***(a)*** *and the 3D-model* ***(b)*** *the density of the spherulites at the surface and at the top surface respectively, as a function of the spherulites diameter. The spherulite density for the 2D-model is inverse proportional to the square of the spherulite diameter and the spherulite density for the 3D-model is inverse proportional to the cubic of the spherulite diameter. The densities used to calculate the packing factors were:* $\rho_c = 940\,\mathrm{kg/m^3}$ *and* $\rho_a = 850\,\mathrm{kg/m^3}$*, see table 1.1 on page 4.*

In figure 2.6a and figure 2.6b the spherulites densities are seen for the 2D-model and the 3D-model respectively. What can be seen is that the number of accessible (for the charges) spherulites is much more influenced by the diameter of the spherulites than the crystallinity. This is due the linear dependence of the crystallinity, compared to the inverse squared and inverse cubic dependence of the spherulites diameter for the 2D-model and the 3D-model respectively; see equation (2.14) and (2.17). From a practical perspective, it is also easier to change the size of the spherulites with an order of magnitude than the crystallinity.

The interesting thing is how close the charges should be if they only are allowed to be on (2D-model) or in (3D-model) the spherulites. The total surface area of the spherulites in the 2D-model, only depend on the packing factor, η, as the area of a circle is proportional to the square of the diameter, and the number of the spherulites is proportional to the inverse square of the diameter. Similar for the 3D-model, the total volume is also only dependent of the packing factor. Thus the maximum distance between charges on and in the spherulites is a parallel shift of the curves in figure 2.5, corresponding to the packing factor given by equation (2.11) and equation (2.15)[1]. Figure 2.7a and figure 2.7b shows a modified versions of figure 2.5.

What is seen in figure 2.7a and figure 2.7b is the maximum possible distance between charges (for polypropylene), where the charges have been evenly distributed, on/in the electrets to support the given surface potential. Two thickness's with three different crystalliniteis is seen, for both the 2D-model and the 3D-model. The curves corresponding to 100 % crystallinity (solid curves) are the same curves as in figure 2.5, the charges can here use the whole

[1]The modification of the curves should be done to the area or volume of which the charges should be distributed on or in.

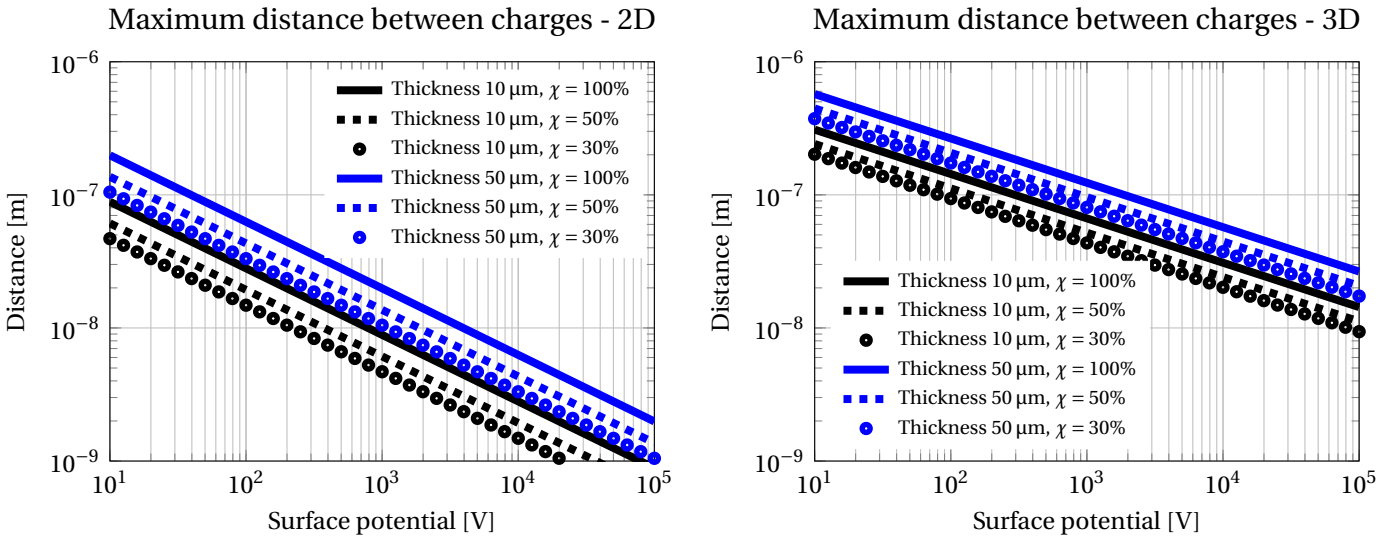

Figure 2.7: *Shows the maximum possible distance between charges for an electret with different thickness's and crystallinity as a function of the surface potential.* ***(a)*** *2D-model* ***(b)*** *3D-model. What is seen, is that as the degree of crystallinity get lower, the distance between the charges are diminishing, for the electret to sustains the same surface potential.*

surface or the whole volume in the first 5 µm from the surface. Basically what figure 2.7a and figure 2.7b tells is that the maximum distance between charges is reduces with a factor of:

$$\text{Reduces factor}_{2D} = \frac{1}{\sqrt{\eta_{2D}}} \approx \frac{1}{\sqrt{\chi}} \qquad \text{Reduces factor}_{3D} = \frac{1}{\sqrt[3]{\eta_{3D}}} \approx \frac{1}{\sqrt[3]{\chi}}$$

for the 2D-model and the 3D-model respectively, compared to figure 2.5. It makes good sense that as the degree of crystallinity gets smaller, the charges have to move closer to each other to sustain the same surface potential. It is expected that this will have an influence on the charge stability, and that it will be notable even though the "Reduces factors" indicates that the influence will be the square-root or cubic-root of the crystallinity. As for figure 2.5 the maximum distance between the charges is also in figure 2.7a and figure 2.7b increased with the thickness of the electret.

Having figure 2.6a to figure 2.7b in mind, it is now possible to design an experiment that will determine whether it is the number of spherulites or the accessible area/volume of the spherulites that have the large influence on the charge stability.

- If it is the number of spherulites that is the critical parameter for the charge stability, an electret with many small spherulites would significantly outperform an electret with fewer larger spherulites; both having the same crystallinity.
- If it is the accessible area/volume of the spherulites that is the critical parameter for the charge stability, an electret with high crystallinity will outperform an electret with low or zero crystallinity, regardless the size of the spherulites.

2.4 Activation Energy

A good way of understanding the charge behaviour of different electret materials and their ability to retain electrical charges, is the activation energy of the potential traps in the materials. The activation energy is a measure on how stable the charges are on/in the electret, the higher the activation energy the more stable the charges are. By thermal stimulating the charges, the depth of the traps can be reviled. In the following the electrical charges will be mentioned as electrons, as this thesis only addresses negative charged electrets. The behaviour of traps in a positive charged electret is however, the same. Two cases will be addressed in this section; one where it is assumed that re-trapping does not occur, and one where re-trapping is occurring. For a more detailed derivation of the mathematics in the following subsections see Appendix B.

2.4.1 Absent Re-trapping

Constant Temperature

The first case to be addressed is where re-trapping is absent, which means that an electron that has escape its trap will go directly to the conductive band, and no longer contribute to the electrical field in and around the electret. For electrets only containing traps of one depth E_a and at any time these contain a total of n electrons, the charges released form the electret, which can be interpreted as a current, is represented by the following equation [**?**, **?**]:

$$I = -\frac{dn}{dt} = n\nu \exp\left(\frac{-E_a}{k_b T}\right) \tag{2.18}$$

where $\nu \exp(-E_a/k_b T)$ is the probability per unit time that an electron escape its trap. ν is the rate constant with the unit $\sec^{-1}$ and can be interpreted as an attempt-to-escape frequency; from now on just escape frequency. This parameter is proportional to the frequency between the collisions of the electron and the material phonons. Typically the values of ν is between $10^{12}\,\mathrm{s}^{-1}$ and $10^{14}\,\mathrm{s}^{-1}$ [**?**]. k_b is the Boltzmann constant and T is the absolute temperature in Kelvin. The solution to equation (2.18) at a constant temperature is given by:

$$I(t) = n_0 \exp\left(-t\nu \exp\left(\frac{-E_a}{k_b T}\right)\right) \cdot \nu \exp\left(\frac{-E_a}{k_b T}\right) \tag{2.19}$$

where n_0 is the total number of electrons at time, t=0. Equation (2.19) tells us, which make good sense, that if the temperature is increased the discharging of the electret charges will increase exponential. However, an increasing in the activation energy, or a decreasing in the escape frequency will counteract this. What also can be seen from equation (2.19) is that, the discharging is diminishing with time, meaning that the loss of charges are largest at first.

Increasing Temperature

If the temperature is not kept constant but increased linear with time, the solution to equation (2.18) is given by:

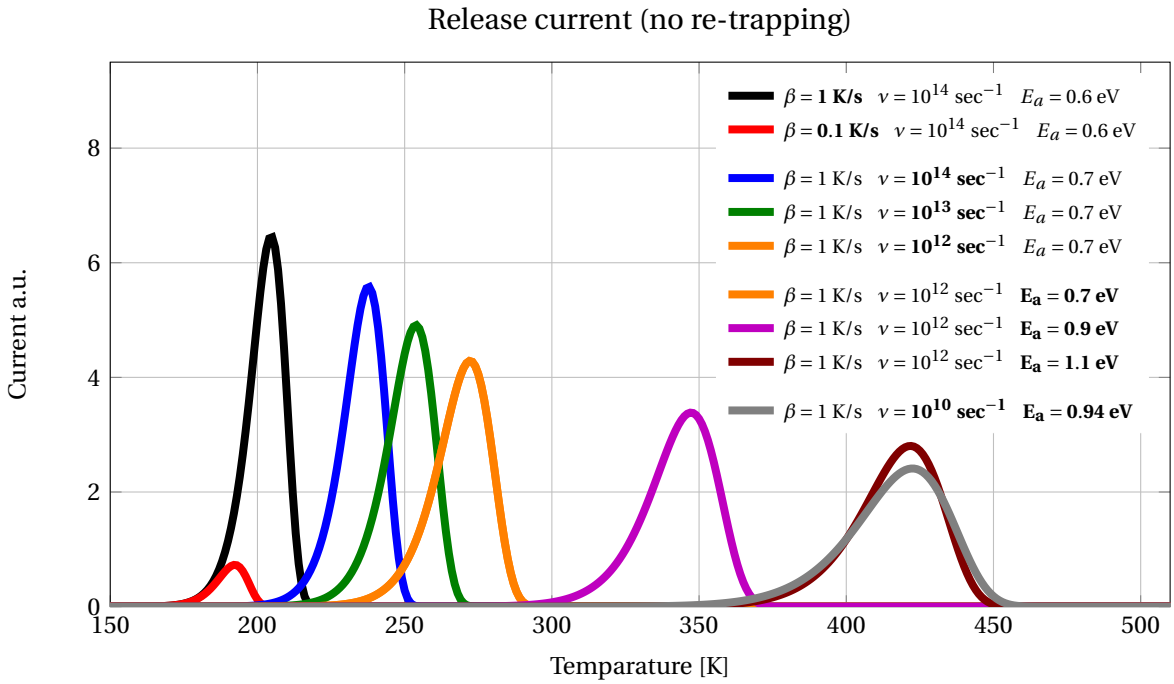

Figure 2.8: *Thermally stimulated current of an electret with a single trap depth. The curves are theoretical, assuming re-trapping to be absent. n_0 has been kept constant for all curves.*

$$I(T) = n_0 \exp\left(-\frac{\nu}{\beta}\int_0^T \exp\left(\frac{-E_a}{k_b T'}\right) dT'\right) \cdot \nu \exp\left(\frac{-E_a}{k_b T}\right) \tag{2.20}$$

Where β is the heat rate and T' is the temperature to be integrated. Equation (2.20) is a peak function, meaning that a maximum current is occurring at a given temperature. The temperature at which this peak occur depends on a combination of E_a, ν and β. Figure 2.8 shows how this dependency is, and can be summarised as:

1. For given values of n_0, β and ν the temperature at which the current is at its maximum is proportional to E_a. The absolute temperature shift for a given change in the activation energy depends on β and ν, hence it is only possible to state a general rule as: increasing activation energy = increasing the temperature of the current peak (see **orange**, **purple** and **brown** curve in figure 2.8).

2. For given values of n_0 and E_a the temperature of maximum current varies with ν/β. The absolute temperature shift for a given change in ν/β depends on the activation energies, hence it is only possible to state a general rule as: decreasing in the ratio ν/β = increasing the temperature of the current peak. However, as a rule of thumb a decreasing of two orders of magnitude in ν/β correspond to a change in the activation energy of 0.1 eV (see **blue**, **green** and **orange** curve in figure 2.8).

3. The area under the curves divided by β is equal to n_0; the number of electrons trapped at T=0. n_0 do not affect the shape of the curve only the hight (see **black** and **red** curves in figure 2.8).

ν, the escape frequency, and E_a, the activation energy are strongly correlated. Meaning that when these parameters are increased, they will shift the position of the current peak in opposite directions. Thus it is necessary to have a reasonable assumption of ν, or even fix it to a specific value, to get a reasonably estimating of the activation energy. This effect of ν and E_a working in opposite direction is seen in figure 2.8 by the **brown** and **grey** curves. Here it is seen that two very different values of ν and E_a can give almost the same release current.

Extracting the Activation Energy

The curves seen in figure 2.8 can be obtained practically from a charged electret material by a technique called Thermally Simulated Current (TSC) or by recalculating the results from Thermally Stimulated Potential Decay (TSPD), for now it is not important to know how these techniques are carried out, and TSPD will be discussed in Chapter 3. What is important to know is how to extract the activation energy or activation energies from a curve as those seen in figure 2.8. If equation (2.20) is differentiated with respect to the temperature and solve for equal to zero, the relationship between the peak temperature, T_p and the activation energy is as following (as mentioned earlier, for a more detailed derivation of the mathematics in this subsection see Appendix B):

$$\frac{E_a}{k_b T_p} = \ln\left(\frac{T_p \nu}{\beta}\right) + \ln\left(\frac{T_p k_b}{E_a}\right) \tag{2.21}$$

When plotting the activation energy as a function of the peak temperature as given in equation (2.21), an almost perfect linear relation is obtained. This is due to the logarithm terms which do not change much as the temperature is increased. The slope of the relation, given in equation (2.21), is primarily dominated by $\ln(\nu/\beta)$ and it turns out that equation (2.21) can be simplified even more. Within the intervals $10^{12} < \nu/\beta < 10^{16}$ (which most electrets fits within) and $273 < T_p < 773$ (°K), the relation between E_a and T_p is given to an accuracy of $\pm 0.5\,\%$[2] by:

$$\frac{E_a}{k_b T_p} \approx \ln\left(\frac{T_p \nu}{\beta}\right) - 3.52 \tag{2.22}$$

In the above the activation energy have been determined from the temperature peak from the released current, it is a fast and easy way but, the weakness is the unknown escape frequency; unless that have been fixed to a certain value of course. Another way of determining the activation energy is by a mathematical fit of equation (2.20) to the obtained released current. Where ν has been expressed by the peak temperature, T_p:

$$\nu = \exp\left(\frac{E_a}{k_b T_p}\right) \cdot \frac{\beta E_a}{k_b T_p^2}$$

which can be deduced from equation (2.21). The thermally stimulated current from an electret sample with a linear increased temperature, were re-trapping is assumed absent, can then be described by:

[2] Underestimating E_a for ν/β ratios below $2 \cdot 10^{13}$ and overestimating E_a for ν/β ratios above $6 \cdot 10^{13}$

$$I(T) = n_0 \exp\left(-\exp\left(\frac{E_a}{k_b T_p}\right) \cdot \frac{E_a}{k_b T_p^2} \int_0^T \exp\left(\frac{-E_a}{k_b T'}\right) dT'\right) \cdot \frac{\beta E_a}{k_b T_p^2} \exp\left(\frac{E_a}{k_b T_p}\right) \exp\left(\frac{-E_a}{k_b T}\right) \quad (2.23)$$

A full fit with equation (2.23) can be done by a fitting routine, which can run many iteration in a short amount of time. This is a bit more comprehensive method than just using the peak temperature and equation (2.22), but in addition to finding E_a, values for ν can also be determined, which definitely is this method strength. In the next subsection re-trapping is assumed to occur which have a large influence on how the charges are released. This is easily seen on shape of the curve for the released current.

2.4.2 When Re-trapping Occurs

The above theoretical development rests on the assumption that re-trapping, is a negligible process. It is essential however, to consider the modification of this theory when an electron escaping from its trap has a probability of being re-trapped. Instead of recombining with an opposite charged charge. Consider an electret containing a total number of electron traps, N, of which n are filled by electrons at any instant. Then there will be $(N-n)$ empty traps and n empty recombination centres previously vacated by the trapped electrons (the number of electrons in the conduction band at any instant is assumed to be small compared to n). The probability that an escaping electron will recombine with an empty recombination centre and not be re-trapped is given by [**?**, **?**]:

$$\frac{A_h n}{A_n (N-n) + A_h n} \quad (2.24)$$

where A_h is the probability coefficient of an electron recombining with a hole in a recombination centre and A_n is the probability coefficient of an electron being re-trapped. The charges released form an electret, where re-trapping is occurring, is given by combining equation (2.24) with equation (2.18), and can be represented by the following equation:

$$I = -\frac{dn}{dt} = \frac{n^2}{\frac{A_n}{A_h}(N-n) + n} \nu \exp\left(\frac{-E_a}{k_b T}\right) \quad (2.25)$$

For the case where $A_n / A_h = 1$ (corresponding to an equal probability for electrons being re-trapped or recombined) a simple solutions exist for equation (2.25) for constant temperature and for a linearly increased temperature. These are given by equation (2.26) and equation (2.27) respectively:

$$I(t) = \frac{n_0^2 \nu}{N} \exp\left(\frac{-E}{k_b T}\right) \left(1 + \frac{n_0 \nu}{N} \exp\left(\frac{-E}{k_b T}\right) t\right)^{-2} \quad (2.26)$$

$$I(T) = \frac{n_0^2 \nu}{N} \exp\left(\frac{-E}{k_b T}\right) \left(1 + \frac{n_0 \nu}{N\beta} \int_0^T \exp\left(\frac{-E}{k_b T'}\right) dT'\right)^{-2} \quad (2.27)$$

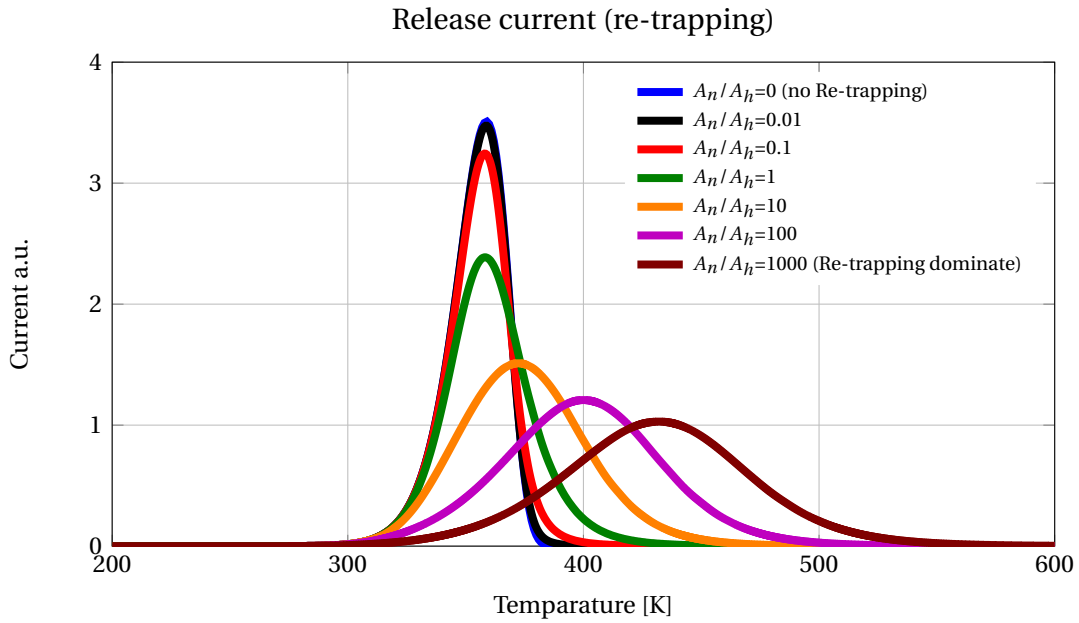

Figure 2.9: *Thermally stimulated current of an electret with a single trap depth. The curves are theoretical, where the re-trapping is varied, through the ratio of A_n/A_h. For all curves the following values have been used: $E_a = 1.0\,eV$, $\nu = 10^{13}\,sec^{-1}$, $\beta = 1\,K/min$ and $N = n_0 = 100$.*

For the case where $A_n/A_h \neq \{0,1\}$ an numerical approach is needed. In figure 2.9 equation (2.25) is plotted as a function of temperature for different values of A_n/A_h. The blue curve in figure 2.9 (behind the black curve) is identical to the blue curve in figure (2.8). What is seen in figure 2.9 is that as the values of A_n/A_h is increased, the curves are going towards a more symmetrical shape and that the width of the curves are increased, meaning that the electrons are released at higher temperature. For values of $A_n/A_h > 1$ the peak temperature is also shifted towards higher temperature, this correspond well to the fact that re-trapping now has become the dominating effect for the transport of the electrons, and thus the later temperature release of the electrons.

There is evidence from previous studies, on luminescent materials which to a degree behave as an electret, regarding charge release, that the two probabilities, A_n and A_h, in equation (2.25) are about equal [**?**, p. 405]. For now this is also assumed to be true for electrets. This means that the charges released from electrets can be described by equation (2.26) and equation (2.27). The ratio between the number of traps, N, and the number of filled traps (electrons), n, also influences the releases current. This is illustrated in figure (2.10), where the amount of electrons have been kept constant will the number of available traps have been increased from the lowest amount possible (n_0) to a hundred times of the initial electrons. What is seen in figure (2.10) is that, if the ratio N/n_0 is increased the peak temperature increases as well. This seems reasonable as the electrons in the high N/n_0 ratio have many more traps to be re-trapped in than the electrons in the electrets with few traps.

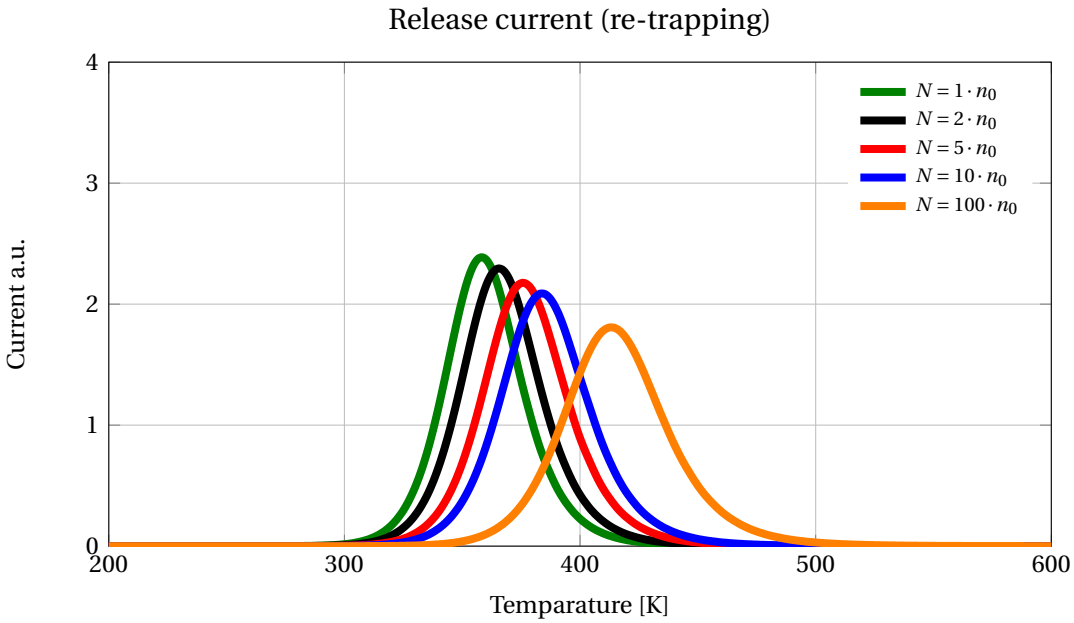

Figure 2.10: *Thermally stimulated current of an electret with a single trap depth. The curves are theoretical, where the ratio between the number of traps, N, and the number of filled traps at $T = 0$ (n_0) are varied. For all curves the following values have been used: $E_a = 1.0\,eV$, $\nu = 10^{13}\,sec^{-1}$, $\beta = 1\,K/min$, $A_n/A_h = 1$ and $n_0 = 100$.*

Extracting the Activation Energy

As for the none re-trapping case the activation energy can also be determined from the peak temperature for the case where re-trapping is occurring. This can be done by the relation: (remember that it is still assumed that $A_n/A_h = 1$)

$$\frac{E_a}{k_b T_p} = \ln\left(\frac{2k_b T_p}{E_a}\right) - \ln\left(\frac{N\beta}{n_0 \nu T_p} + \frac{1}{T_p}\int_0^{T_p} \exp\left(\frac{-E_a}{k_b T'}\right) dT'\right) \tag{2.28}$$

As seen equation (2.28) is not as simple as its corresponding equation where re-trapping was absent; equation (2.21) on page 26. However equation (2.28) can also be approximated and within the intervals $10^{12} < n_0\nu/\beta N < 10^{16}$ and $273 < T_p < 773$ (°K), the relation between E_a and T_p is given to an accuracy of $\pm 0.5\,\%$[3] by: (again see Appendix B for a detailed derivation)

$$\frac{E_a}{k_b T_p} \approx \ln\left(\frac{n_0 \nu T_p}{N\beta}\right) - 3.47 \tag{2.29}$$

As in the case were re-trapping where absent, it is also possible to obtain a more general expression for ν, which can be deduced from equation (2.28):

$$\nu = \left(\frac{2n_0 k_b T_p^2}{E_a N\beta}\exp\left(\frac{-E_a}{k_b T_p}\right) - \frac{n_0}{N\beta}\int_0^{T_p} \exp\left(\frac{-E_a}{k_b T'}\right) dT'\right)^{-1} \tag{2.30}$$

[3] Underestimating E_a for $n_0\nu/\beta N$ ratios below $2\cdot 10^{13}$ and overestimating E_a for $n_0\nu/\beta N$ ratios above $7\cdot 10^{13}$

Equation (2.30) can in combination with equation (2.27) be used in a fitting routine to remove ν as a variable. This can make the fitting routine significantly easier as ν and E_a is correlated. Unfortunately this simplification in a fitting routing is only possible when $A_n/A_h = 1$. As stated in the start of this subsection if $A_n/A_h \neq \{0,1\}$ an purely numerical approach is needed, to describe the behaviour of the charges when thermally stimulated.

Uncertainty of E_a with fixed ν

As previously stated E_a and ν is strongly correlated. In practice ν will need to be fixed, normally in the interval $10^{12}\,s^{-1}$ to $10^{14}\,s^{-1}$ [**?**], to get a meaningful estimate of the activation energy. However, when fixing ν, an uncertainty to the activation energy is also introduced, which comes from the possibility of a wrong guess on ν.

To give an example: If ν is fixed to $\nu = 10^{13}$ and it turns out that this guess is wrong by a order of magnitude (to either side), equation (2.29) can be used to show that the error made on the activation energy, depends on T_p and the correct value of the attempt-to-escape frequency, ν_c by:

$$Error\ on\ E_a = k_b T_p \ln\left(\frac{\nu}{\nu_c}\right) \tag{2.31}$$

This means that the error, under the above mentioned assumptions, for the activation energy which gives a current peak at 80 °C is 0.07 eV and 0.08 eV if the current peak is located at 130 °C. By solving equation (2.25) numerically, as a function of temperature instead of time, it can be shown that the error stated in equation (2.31) only weekly depends on the ratio of A_n/A_h, the heating rate, the number of available traps relative to the number of electrons at $T = 0$ and the initial guess of ν. Thus equation (2.31) can be used as a role of thumb for the uncertainty on the activation energy when ν has been fixed. A current peak at 80 °C and 130 °C correspond to an activation energy of 1.0467 eV and 1.1219 eV respectively; using $\nu = 10^{13}$, $A_n/A_h = 1$, $N = n_0$, $\beta = 7.5\,K/min$.

2.5 Summary

In this chapter the concept of trap sites were introduced, which is where the electrical charges are bound to the electret. The trap sites can be thought of as energetic potential wells, known from solid state physics, where shallow traps corresponds to charges that are less stable, and deep traps corresponds to charges that are very stable.

With simple electrodynamics it is possible to calculate the surface charge density and if the relatively charge distribution in the depth is known the volume charge density can be calculated as well. When comparing charge stabilities from different electrets, which have the same lateral charge distribution and thickness, extra information will not be revealed by calculating the charge density. Hence plotting the electret charge stability can be done so by plotting the surface potential as the qualitative unit. What also was seen from the electrodynamic was that the surface potential will drop if the charges are moved closer to the back electrode. Hence a decay in surface potential can both be due to charges leaving the electret but also charges that have moved closer to the back electrode.

Theoretical considerations was discussed about the number of spherulites at the surface and near surface as a function of the size of the spherulites and the degree of crystallinity. As well as how close the electrical charges should be to each other to sustain a given surface potential, where it was assumed that the electrical charges only would be in the crystalline regions. From the discussion of the theoretical considerations is was possible to state the following:

- If it is the number of spherulites that is the critical parameter for the charge stability, an electret with many small spherulites would significantly outperform an electret with fewer larger spherulites; both having the same crystallinity.
- If it is the accessible area/volume of the spherulites that is the critical parameter for the charge stability, an electret with high crystallinity will outperform an electret with low or zero crystallinity, regardless the size of the spherulites.

The behaviour of the electrical charges when thermally stimulated was explained though terms as activation energies, attempt-to-escape frequency and re-trapping. With these terms it is possible to explain the behaviour of the electrical charges on/in an electret when exposed to isothermal conditions our to an linear increased temperature.

Chapter 3

EXPERIMENTAL TECHNIQUES

This chapter is dedicated to the general sample preparation methods, experimental techniques and the polymers that have been use throughout this thesis. In the next chapter, "Characterisation, Results and Discussion", results will be presented from various experiments and analysis techniques, that have been testing the charge stability and mechanical properties of polypropylene. The thought behind and the carrying out of the experiments, sample preparation and the analysis techniques are here elaborated and will therefore not be discussed when the results are presented. In the next chapter it is assumed that the reader is familiar with the following techniques and concepts. Specific details and smaller variations between the different experiments will still be stated together with the results.

To get an overall idea of which preparation methods and experimental techniques used and how they are connected to each other, a brief description of an electret "life" is given in the following: An electret sample, used for characterisation, consist of a **support structure** with a **spin coated** electret layer on top. For the spin coating process **polymer solutions** have been developed. After spin coating, the polymer layer is **levelled in a press** to ensure a smooth and consistent surface, both for the individual sample but also among the different samples in the specific experiment. When a smooth electret sample has been achieved, it is **corona charged** to a certain surface potential. Characterisation of the electrets charge stability, can be done in several ways: **isothermal potential decay**, **humidity potential decay** and **thermally stimulated potential decay**. After the charge stability has been investigated, some of the electret samples have been exposed to destructive characterisation. This includes determination of the samples crystallinity through **differential scanning calorimetry**, and **selective etch of the electret material** for use to **visualisation of the crystalline regions** in a scanning electron microscope.

3.1 Polymers under Investigation

Isotactic-polypropylene In section 1.1 it was decided that isotactic-polypropylene (i-PP) should be the polymer for the electret polymer model system. The used i-PP had a weight average molecular weight of 250,000 g/mol, a number average molecular weight of 67,000 g/mol and came as beads. The supplier for the i-PP was Sigma-Aldrich, see Appendix C for product specification. The i-PP beads are seen in figure 3.1a.

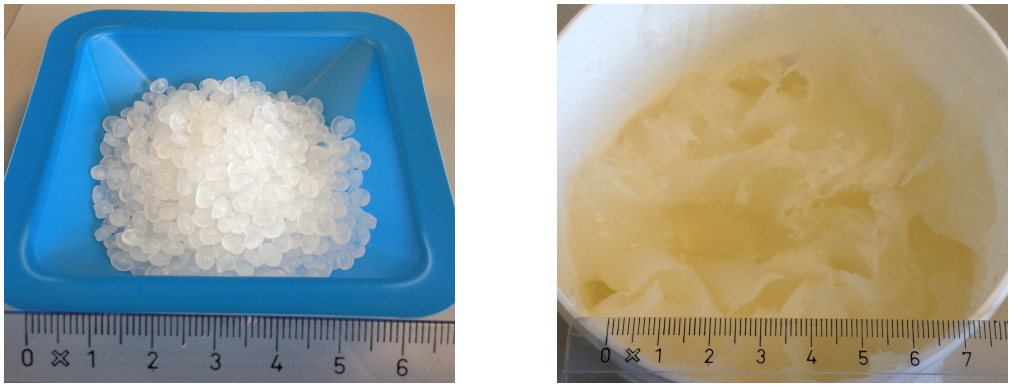

(a) *(b)*

Figure 3.1: ***(a)*** *Picture of i-PP beads.* ***(b)*** *Pictures of a-PP waxy gel. Both scales are in cm.*

Atactic-polypropylene In the experiments, where the crystallinity were controlled (see section 4.4), atactic-polypropylene (a-PP) was used. The weight average molecular weight for the a-PP was 12,000 g/mol and came as a waxy gel. The supplier for the a-PP was Goodfellow, see Appendix D for product specification. The a-PP waxy gel is seen in figure 3.1b.

3.2 Support Structures

For studying polypropylenes electret properties, the polymers were spin coated on a support structure. The support structure consist of a single side polished, 10 cm in diameter, highly doped silicon wafer with a 100 nm thick layer of titanium on the front side. The titanium provides good electrical conductivity throughout the support structure and ensures the adhesion of polypropylene to the front side. A highly doped silicon wafer as a support structure has been chosen due to its very low electrical resistivity, which is below 0.025 Ω·cm, and flatness.

3.3 Polymer Solutions

Before the polymer, that is to be investigated, can be spin coated on the support structure, a solution with the polymer has to be made. The different types of polymer solutions that have been used, are all mentioned in this section. Common to all of them is that the recipes used for mixing the solutions have been developed within this project, as the requirement to the solutions were that they could be spin coated at room temperature (the solutions were allowed to be warm), and that a sufficient layer could be achieved within 1 or 2 spin coatings.

Isotactic-polypropylene After an iterative process where multiple solvents (see table 3.1) were investigated for how well they could hold 1 wt% (percentage by weight) of i-PP in solution at 90 °C, 70 °C, 60 °C and 50 °C after the solution had been heated to 120 °C for 18 hours, only two candidates were left at 70 °C; tetra-chloro-ethylene and cyclohexane. And only

Solvent	Boiling point	Cas. No.
1,1,1,2-Tetrachloroethane	130 °C	630-20-6
2,2,4-Trimethylpentane(Iso-Octane)	99 °C	540-84-1
a,a,a-TriCholoToluene	220 °C	98-07-7
Cyclohexane	80 °C	110-82-7
Cyclohexanone	155 °C	108-94-1
Decahydronaphthalene	188 °C	91-17-8
Di-Phenyl-Ether	259 °C	101-84-8
m-DiChloroBenzene	174 °C	541-73-1
o-DiChloroBenzene	180 °C	95-50-1
o-Xylene	144 °C	95-47-6
p-Xylene	138 °C	106-42-3
TetraChloroEthylene	121 °C	127-18-4
Toluene	111 °C	108-88-3

Table 3.1: *The solvents under investigation for bringing i-PP into solution. Cyclohexane was the only solvent, without discolouring the solutions, that could hold i-PP in solution at 70 °C after the solution had been heated to 120 °C (in a closed dram glass under pressure).*

cyclohexane could hold 1 wt% of i-PP in solution at 50 °C. The solution with tetra-chloro-ethylene (at 70 °C) had been discoloured, which made cyclohexane the obvious solvent to continue working with. The solutions were heated in a closed dram glass under pressure. The 120 °C was first and foremost chosen as an upper safety temperature, but the high temperature was also helping the i-PP to go into solution faster than it would have done, at a lower temperature. The 90 °C was chosen as the upper temperature for investigation of i-PP solubility under the assumption that this temperature would be close to the upper limit of how warm an solution can be spin coated at room temperature. To spin coat a solution above 90 °C would ideally require a heating system to keep the media, which the solution are to be spin coated on, at elevated temperature while spin coating, to diminish the risk of to soon precipitation of the solute, and large changes in the solutions viscosity will spin coating. The solvents that were investigated are listed in table 3.1.

Another iterative process was initiated, where the amount of i-PP that could be brought into solution by cyclohexane was investigated. It turned out that a cyclohexane solution with 25 wt% of i-PP could be brought into solution after approximatively 18 hours at 120 °C; the solution was as thick as syrup though. However, this temperature is well above cyclohexane boiling point and at 70 °C after 3 hours, solutions above 12 wt% of i-PP were beginning to precipitate i-PP. This effect is see in figure 3.2a. Common to all of the solutions, both at 120 °C and at 70 °C, were that as the concentration of i-PP increased so did the viscosity.

Based on the observations, solubility and viscosity, it was decided to use the 10 wt% solution for the spin coating step. However, the 10 wt% solution does solidify at room temperature, this is shown in figure 3.2b, and due to this the solution had to be warm when spin coated. A solidified solution can be reused after reheating it to 120 °C for a couple of minutes, and then cooled below cyclohexane boiling point.

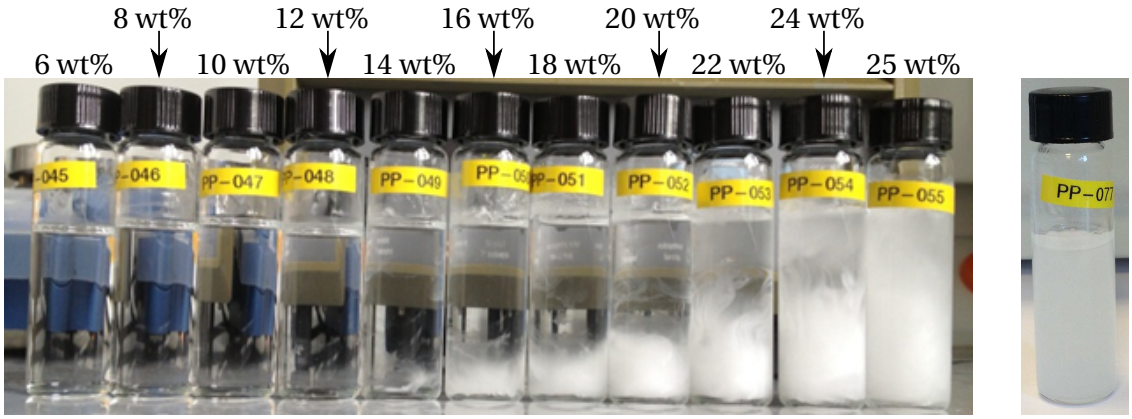

Figure 3.2: ***(a)*** *Cyclohexane solution with different concentration of i-PP at 70 °C. The picture shows the solutions 3 hours after they have been cooled from 120 °C to 70 °C. As seen the solutions with 14 wt% of i-PP is beginning to precipitate i-PP at the bottom of the solution.* ***(b)*** *A cyclohexane solution with 10 wt% of i-PP at room temperature, seen as it has solidified.*

Isotactic-polypropylene with atactic-polypropylene For the experiment where the crystallinity was controlled through adding atactic-polypropylene (a-PP) in the i-PP solution, a new recipe for a mixed solution had to be developed. This was necessary as the solubility of a-PP in cyclohexane is very different than for i-PP. After an iterative process it was found that the ratio between cyclohexane and a-PP should be 40 wt%/60 wt% respectively to gain the same viscosity, approximatively, as for the cyclohexane/i-PP solution with the ratio of 90 wt%/10 wt%. Both types of solutions had been heated to 120 °C until the polymers went into solution, and then cooled to approximative 70 °C before comparison. On the basis of a known quantity (by weight) of i-PP, m_{ipp}, and a wanted relative amount of a-PP compared to the total amount of polymer, R_{ia}, a formula that gives the amount of a-PP, m_{app}, and the amount of cyclohexane, m_{ch}, can be stated as:

$$m_{app} = \frac{m_{ipp} \cdot R_{ia}}{1 - R_{ia}} \tag{3.1}$$

$$m_{ch} = \frac{m_{ipp}}{10\%}(1 - 10\%) + \frac{m_{app}}{60\%}(1 - 60\%) = 9m_{ipp} + \frac{2}{3}\frac{m_{ipp} \cdot R_{ia}}{1 - R_{ia}} \tag{3.2}$$

Equation (3.1) and equation (3.2) were used when mixing solutions with both i-PP and a-PP.

Atactic-polypropylene For the solutions that only contain a-PP, the ratio between cyclohexane and a-PP were changed to 60 wt%/40 wt% respectively; as opposed to the ratio 40 wt%/60 wt% in the previous paragraph. This was done because it was possible to make a suspension between cyclohexane and a-PP that could be spin coated without any previous thermal treatment, which made the spinning process simpler. This suspension[1] was milky as opposed to the solutions which were transparent.

[1] If the a-PP suspension is heated to above 100 °C it will also become transparent however, upon cooling to room temperature it will solidifies.

Summary of Solutions Throughout the experiments presented in this thesis four different types of solutions have been used. If excluding the cyclohexane their content of polymer is:

1. 100 % i-PP
2. 67 % i-PP with 33 % a-PP
3. 33 % i-PP with 67 % a-PP
4. 100 % a-PP

The mixing and preparation of the three first solutions were practically done in the following way:

Step 1) The desired amount of i-PP and a-PP were weighed on a µ-scale weight and put into a dram glass with a cap. The needed amount of cyclohexane was then added, also weighed on a µ-scale weight.

Step 2) The cap is tighten and the dram glass was heated to 120 °C in a block heater, see figure 3.3a. The i-PP is the last to be dissolve and is so after approximatively 18 hours.

Step 3) The temperature on the block heater was lowered to the desired temperature, 78 °C which will be elaborated in the next section. After approximatively 30 min the temperature has been reached and the spin coating process can start.

The mixing and preparation of the fourth solution was practically done in the following way: The desired amount of i-PP was weighed on a µ-scale weight and put into a dram glass with a cap. The needed amount of cyclohexane was then added, also weighed on a µ-scale weight. The cap was tighten and after 30 min at room temperature, the a-PP and cyclohexane had formed a suspension, ready to be spin coated.

3.4 Spin Coating

As mentioned in the previous section, four different solutions were used for spin coating. The three solutions with i-PP were prior to spin coating heated to 120 °C for a minimum of 18 hours. Approximatively 30 min before spin coating the block heater, seen in figure 3.3a with all of the solutions, was set to 78 °C. This temperature is just below cyclohexane boiling point, and was chosen from empirical knowledge, regarding the change in viscosity. When the solutions have reached 78 °C there is a window of approximative 1 hour where the spin coating should be carried out, before the viscosity has changed so much in the solutions that it will begin to affect the thickness of the spin coated layer. Carrying out the practical part of the spin coating is done as follows:

Step 1) A support structure (Silicon-wafer with titanium) is placed on the spin coater as in figure 3.3b. The lid is closed and the first of two step of the spin-program is started. The wafer is now spinning at 250 rounds per minute (rpm)

Step 2) The 78 °C warm solution is, in a quick motion, poured through an opening in the spin coater lid onto the centre of the wafer, and when the solution reaches the edge of the

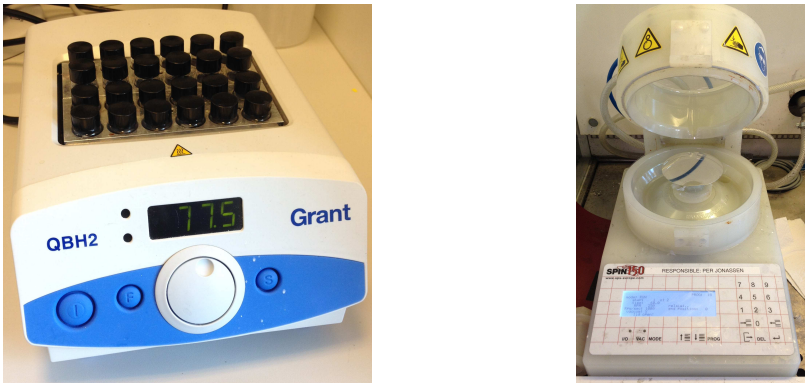

(a) *(b)*

Figure 3.3: ***(a)*** *The block heater used for warming the solutions, and keeping the solution warm until used for spin coating* ***(b)*** *The spin coater used for spinning the polymer on the support structures (Silicon-wafer with titanium).*

(a) *(b)* *(c)*

Figure 3.4: ***(a)*** *Wafer right after spin coating. The white layer is the polymer, and the colour is partially due to the porous structure of the polymer (entrapped air) and small residuals of cyclohexane.* ***(b)*** *Wafer after a thermal treatment at* 180 °C *for 2 min. This is to remove the last traces of cyclohexane and the entrapped air.* ***(c)*** *The wafer after levelling in an press at* 180 °C *for 5 min at 8 kN.*

wafer step two of the spin-program is started. The second step of the spin-program is individual for the different solutions to ensure the same thickness. The thickness that is aimed for is 30 µm. The details of the second step for the spin-programs will be discussed at the end of this section.

Step 3) When the second step is finished, the edge of the wafer is cleaned for excess polymer, which has been precipitated on the wafer, and its edges, after the evaporation of cyclohexane under the second step of the spin coating. The excess polymer is vary fragile and can easily be remove with the fingers (in a glove). The wafer now looks like the picture in figure 3.4a. The white layer is the polymer, and the colour is partially due to the porous structure of the polymer (entrapped air) and small residuals of cyclohexane.

Step 4) The wafer is placed in a preheated oven at 180 °C for 2 min. This is to remove the last traces of cyclohexane and the entrapped air. The thin polymer layer is completely melted in this process. The wafer now looks like the picture in figure 3.4b. The used oven was a Memmert model UFE 400.

Solution	Step 1	Step 2	No. of runs (separated by thermal treatment)
100 % i-PP	250 rpm	500 rpm @ 60 s	2
67 % i-PP with 33 % a-PP	until solutions	500 rpm @ 60 s	2
33 % i-PP with 67 % a-PP	reaches the	500 rpm @ 60 s	1
100 % a-PP	wafer edge	1500 rpm @ 60 s	1

Table 3.2: *The four spinning programs that has been empirical tuned to each solution, so that the end result, after levelling, were approximatively a 30 µm thick polymer layer.*

Step 5) Some of the solutions need to be spin coated twice on the support structure to achieve a final thickness of 30 µm after the levelling step; which will be discussed in the next section. If the wafer needs to be spin coated twice, step 1 to 4 should be repeated. As seen in figure 3.4b the surface of the polypropylene is not particularly smooth. This is solved in an levelling step which, as just mentioned, will be discussed in the next section. The results after the levelling process however, can be seen in figure 3.4c.

As mentioned in step 2 the details of the different spinning programs will now be elaborated, and are listed in table 3.2. The steps in the four programs have been empirically tuned to each solution, so that the end result, after levelling, was approximatively a 30 µm thick polymer layer.

3.5 Sample Levelling

After the wafers have been spin coated with a polymer layer, the surfaces are very undulated and rough. To get more identical wafers the surface was levelled in a press at 180 °C. The press a P/O/weber model PW10H and is seen in figure 3.5a. The pressing was done in the following way:

Step 1) The lower and upper hotplate in the press are set to 180 °C 30 min before use. This is 10 °C to 20 °C above the melting point of polypropylenes.

Step 2) A sandwich structure with the wafer that is to be pressed is made. The sandwich structure, is illustrated in figure 3.5b and consisted of a: aluminium foil - a soft silicone rubber sheet (thickness 2 mm) - aluminium foil - wafer with polymer - silver coated silicon wafer (silver side towards polymer surface) - aluminium foil - a soft silicone rubber sheet - aluminium foil. After an iterative process, it was found that a silver coated wafer was a non-adherent surface for polypropylene, and at the same time spherulites were created at the polypropylene surface. The silicone rubber sheets (2 mm thick) are used to ensure an even distribution of the pressure. The aluminium foils are used partly to protect the press and rubber sheets from melted polypropylene and partly to ensure an easy disassembly of the sandwich structure.

Step 3) The sandwich structure is placed in the press at 8 kN for 5 min at 180 °C. A COMSOL multiphysics (Version 4.4) [**?**] simulation has shown that the core temperature of the sandwich structure will reach 180 °C after 4 min.

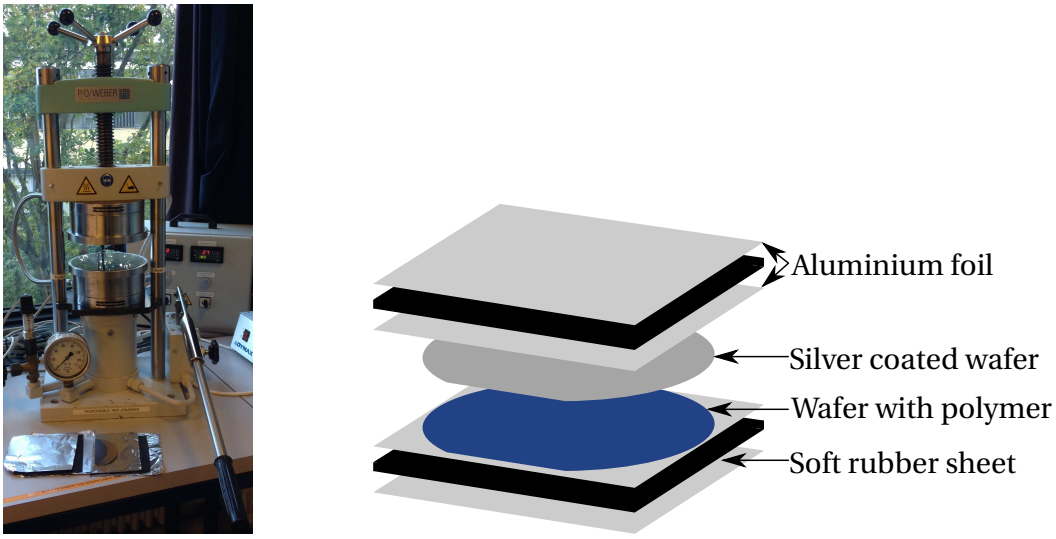

Figure 3.5: ***(a)*** *The press used for levelling the polymer surface on the support structure. The pressing is conducted at 180 °C for 5 min at a pressure of 8 kN.* ***(b)*** *Illustration of the sandwich structure, that was pressed in the press seen in (a).*

Step 4) After 5 min the sandwich structure is removed from the press. The two wafers are quickly removed from the sandwich structure and according to the different experiment, the wafers have seen different cooling methods. Through the cooling methods, the size of the spherulites could be controlled. The different cooling methods for the different experiments will be discussed in the next chapter, where they belong. A pressed wafer with polypropylene is seen in figure 3.4c.

After step 4 the levelling is finished and the samples are now to be considered as an electret sample, ready to be corona charged. Corona charging is discussed in the next section.

3.6 Corona Charging and Surface Potential Measurement

The electret samples are all charged in a corona charging setup [**?**, **?**, **?**]. The corona charging has been chosen as the charging method due to its simplicity and short charging time. For other charging methods see reference [**?**, Ch. 2]. The corona charging setup used in the thesis was build to charge the electret samples to a negative potential. This is due to the fact that negatively charged electrets are more stable than positively charged electrets [**?**]. Figure 3.6a shows an illustration of how the corona charging works. The working principle is that a high potential, in the order of several kV, is put between the needle and the conducted grid. Due to an extremely high electrical field at the tip of the needle, electrons are pulled out of the needle and is ionising the air near the needle. This negative ions are forced downwards, by the electrical field, to the conductive grid. The ions that do not hit the grid are further forced down onto the electret sample, by a potential from the grid to the sample. As more and more ions reach the surface of the electret sample, the effective potential from the grid to the sample is diminishing; due to the electrical field from the ions. When the effective

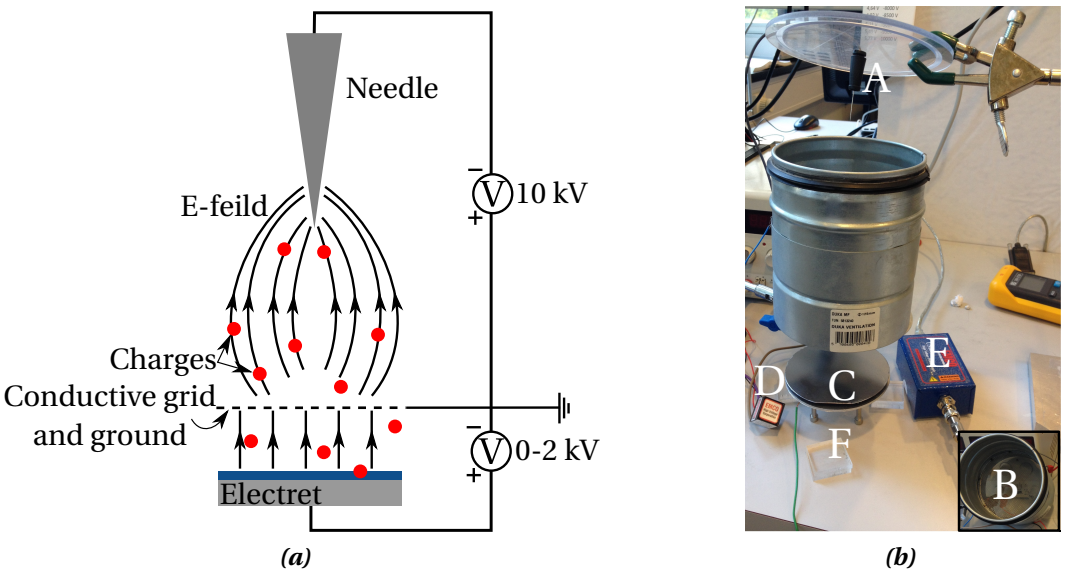

Figure 3.6: ***(a)*** *Illustration of a corona charging setup.* ***(b)*** *The used corona setup lifted apart for view of the different components. A=needle, B=Conductive grid, inside cylinder, C=Sample holder and sample, D=EMCO high voltage component "Q101N", supports the 10 kV potential drop, E=EMCO USB high voltage power supply "USB20P", support the potential drop from grid to sample, F=Spacer for the grid cylinder to ensure 3 mm spacing from grid to the sample.*

potential is zero, no more ions will reach the surface, and the charging of the electret sample stops. The negative ions that still are being generated are lead away by the grounded grid. In this way it is possible to control the amount of charges that reach the electret sample, and through that the surface potential. The conductive grid also makes sure that the samples are homogeneously charged. If the grid was not there the centre of the electret samples would have a higher charge density than the edges. In figure 3.6b a picture of the used corona charging setup is seen. Se figure text for components. The predominant ions created at ambient pressure are CO_3^-, all ions created can be "escorted" by one or more water molecules when forced towards the electret. For further reading about this subject and a more theoretical explanation of the ions created please refer to [**?**, **?**, **?**].

The electret samples in this thesis have been corona charged in the following way: The distance from the needle to the grid was 3 cm and the distance from the grid to the sample was 3 mm. The potential from the needle to the grid was fixed at -10 kV using an EMCO high voltage component "Q101N". The potential from the grid to the sample could be controlled from 0 V to 2000 V using an EMCO USB high voltage power supply "USB20P". All samples were charged to -500 V and left at ambient conditions for a minimum of 12 hours before being used in any experiments. This was done because the interest in this thesis has been the long time stability of the electrets and in this way the short time decay is excluded from the experiments. Depending of the quality of the electret, the decay in the first 12 hours are normally between 3 % to 15 %. The black curve in figure 3.7a show a typical surface potential decay the hours after being charged to -500 V. The red curve in figure 3.7a shows the potential decay the last hour, e.g. the potential decay from the second to the third hour was 2.5 V, and the potential decay from the third to the fourth hour was 1.4 V. As seen, almost no decay is occurring after 12 hours. The small decay that still occurs can be neglected as the following experiments will remove several times more charges than the "natural" decay at room

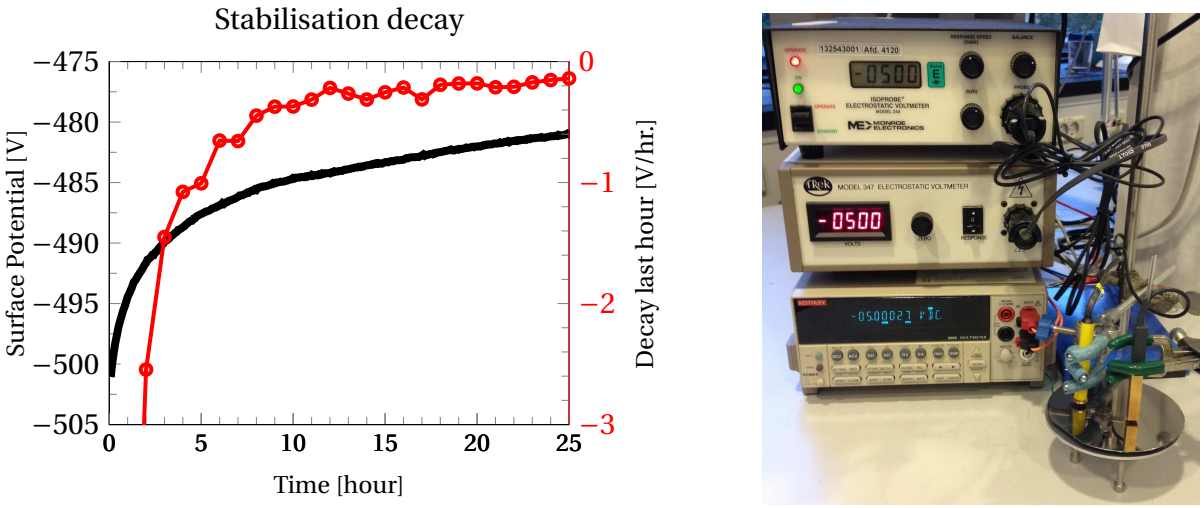

(a) *(b)*

Figure 3.7: ***(a)*** *A normal surface potential decay the hours after being charged. As seen almost no decay is occurring after 12 hours. The red curve shows the decay that has occurred the previous hour. The data is from a 30 µm thick polypropylene sample.* ***(b)*** *The two electrostatic voltmeters used in this thesis. From the top Isoprobe 244A with probe 1017AE(yellow) and Trek 347 with probe 6000B-7C(brown). At the bottom a Keithley 2000 multimeter is seen, which together with a Matlab script was used for data acquisition.*

temperature will due in a week.

The surface potentials have been measured with an electrostatic voltmeter located 1 mm to 2 mm above the surface of the samples. As mention in section 2.2 on page 13, what an electrostatic voltmeter detect is the electrical field from the electret material, and then translates this field into a surface potential. For a more detailed and theoretical explanation on how an electrostatic voltmeter works please refer to the literature [**?**]. Two electrostatic voltmeters have been used which both were reading the same values: Isoprobe 244A with probe 1017AE and Trek 347 with probe 6000B-7C; both seen in figure 3.7b.

3.7 Isothermal Potential Decay

The idea behind the isothermal potential decay is to study the long time stability by accelerating the ageing of the electret. In this way the charge stability, for an electret, can be estimate many years ahead by looking at the potential decay at an elevated temperature for a short amount of time; typically 24 hours. In this period of time the surface potential is measured several times. In addition to comparing the charge stability for different electret materials at elevated temperature it will also be possible to use the theory presented in section 2.4 on page 24. This was the theory about the activation energy, and from this theory it will be possible to describe the potential decay, at this constant temperature over time. And from there it will then be possible to estimate how the potential decay, seen at the elevated temperature, would have been at a different temperature, for example at room temperature.

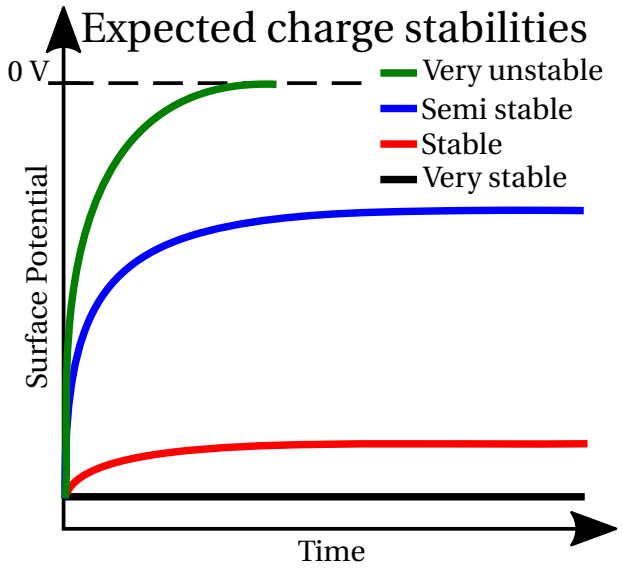

Figure 3.8: *Illustration of how the expected potential decay would be, for different electret materials, in an isothermal potential decay experiment. Note that the electrets have been negatively charged.*

The isothermal potential decay experiments in this thesis was conducted at 90 °C and at 120 °C, both for a period of time between 24 hours and 25 hours. This was done practically by placing the charged electret samples in a preheated oven and at each measurement all samples were taken out of the oven and returned when all the measurements had been performed. In this way, it was ensured that all electret samples, in the same set of experiments, had the same thermal history.

Figure 3.8 shows an illustration of how the expected potential decay would be, for different electret materials, in an isothermal potential decay experiment. An extremely stable electret material will not lose any charges over time and is illustrated as the black curve in figure 3.8. A very unstable electret material will lose all of its charges in a relative short amount of time, this is illustrated with the green curve. The red and blue curves represent stable and semi stable electret material, they will loose some of their charges at first and then stabilise at a lower surface potential, where the residual potential drop can be negligible.

3.8 Humidity Stimulated Potential Decay

The idea behind the humidity induced potential decay is to study how high humidity influence the charge stability. A high thermal charge stability does not necessarily mean that the humid stability is high as well. As for the isothermal potential decay experiments the surface potential of the electret samples has to be measured several times during the experiment.

The humidity induced potential decay experiments in this thesis were conducted at 50 °C and 90 %RH for a period of between 24 hours and 25 hours. This was done practically by placing the electret samples in the preheated climate chamber. The climate chamber used was

a Vötsch VC 4060. When the electret samples reached the same temperature as the chamber, to prevent condensation of water, the humidity was ramped up to 90 %RH; in approximatively 20 min. Before the surface potential of the electret samples could be measured the humidity was lowered to below 30 %RH before the door to the climate chamber was opened. Again this was done to prevent condensation of water. When all the samples had been measured they were put back into the preheated climate chamber, and the cycle started all over. The previous stated times, 24 hours and 25 hours, is the time where the electret samples are at 90 %RH at 50 °C.

The expected decay behaviour for a humidity induced potential decay experiment is similar to that of an isothermal potential decay experiment. See figure 3.8. However the mechanism of the decay is of course very different.

3.9 Thermally stimulated Potential Decay

The idea behind thermally stimulated potential decay is to study and determine the depth of the energetic traps, where the charges are located, and the attempt-to-escape frequency. This is done by linear heating the electret sample while measuring the decay in the surface potential. It is necessary to know the depth of the traps and the attempt-to-escape frequency, if the behaviour of the charges, when thermally stimulated, are to be explained. The theory described in section 2.4 on page 24, explain this.

The thermally stimulated potential decay experiments were conducted using a programmable hotplate, EchoTherm Model HS60 from Torrey Pines Scientific, and both of the electrostatic voltmeters mentioned in section 3.6. Figure 3.9a shows the used setup. In this way two measurements could be obtained from the same sample. It is not possible to perform this kind of experiment twice on the same sample, as the temperature is going above the melting point of the polymer, and thereby changing the crystallinity of the electret. This experiment is therefore to be considered destructive. The samples were placed on a 6 mm thick aluminium block, with a built in temperature probe in the centre of the block. The signal from the temperature probe was fed back to the hotplate, in this way the heat rate could be controlled. The surface potential was measured continuously throughout the experiment with the aluminium block as electrical ground.

Figure 3.9b shows an illustration of how the expected potential decay would be, for different electret materials in a thermally stimulated potential decay experiment. The black curve illustrates a very stable electret. What is seen is that the charges are stable all the way up to the melting point of the electret. At the melting point molecular motion of the chains is occurring, and empirically this will discharge the electret completely. The green curve shows a very unstable electret material where a completely discharging of the electret is occurring not much higher than room temperature. The red and blue curves shown a more realistic discharging of a stable and semi stable electret, than the black curve. The blue curve in figure 3.9b is special, in the sense that the curve has a very distinctive shoulder, indicating that there exist more than one type of traps in that electret. This could be two traps but also more which then would overlap each other.

By differentiating the curves, seen in figure 3.9b, with respect to the temperature, the release current as a function of the temperature can be obtained. Graphical examples of this can

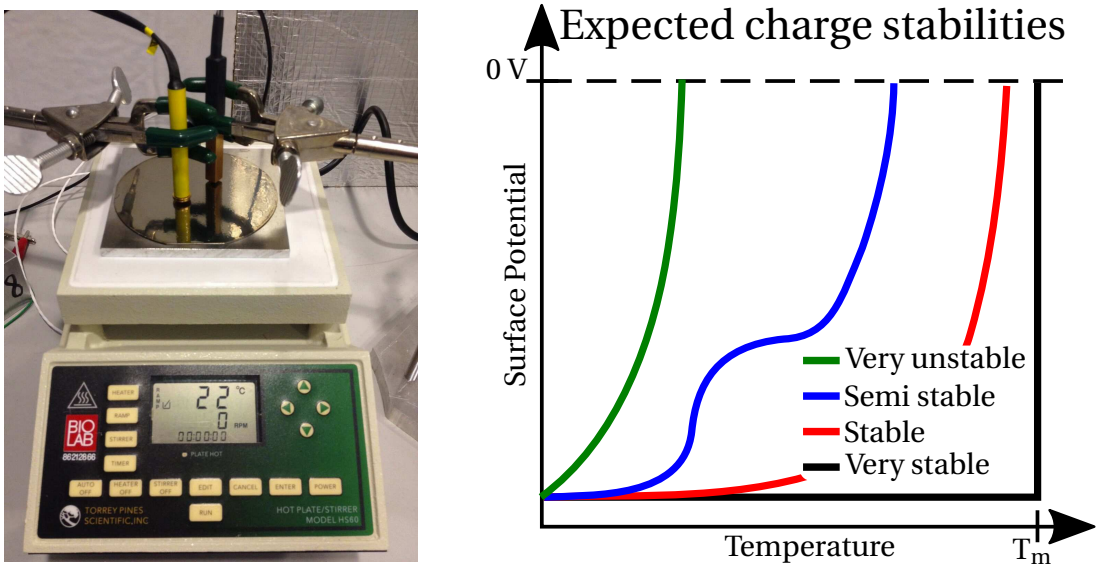

(a) ***(b)***

Figure 3.9: ***(a)*** *Thermally stimulated potential decay setup.* ***(b)*** *Illustration of how the expected potential decay would be, for different electret materials, in a thermally stimulated potential decay experiment. Note that the electrets have been negatively charged. T_m is the melting temperature of the electret material.*

be seen in section 2.4 figure 2.8 on page 25; is was the figure which showed the theoretical thermal release current. By applying the theory, discussed in section 2.4, on the differentiated curves the activation energy (or energies) and the attempt-to-escape frequency can be obtained. To obtain the release current in the unit A/m^2 the differentiation should be done in the following way:

$$I(T) = \frac{\varepsilon_0 \varepsilon_r}{d_{eff}} \beta \frac{dV(T)}{dT}$$

were ε_0 is the the vacuum permittivity, ε_r the relative permittivity and β the heat rate. d_{eff} is the effective charge distance, which is the same as d, the thickness of the electret, if all the charges are located at the surface of the electret. $V(T)$ is the measured surface potential as a function of temperature.

3.10 Differential Scanning Calorimetry

As mentioned in the previous chapters, the crystallinity of the electret will have an influence on the charge stability. The crystallinity can be determined by the thermoanalytical technique, Differential Scanning Calorimeter (DSC). What happens in DSC is that the amount of heat required to increase the temperature of a sample and reference is measured as a function of temperature. Both the sample and reference are maintained at nearly the same temperature throughout the experiment. Normally the reference sample is an empty capsule, identical to the capsule which the "sample of interest" is in. In this way only the heat

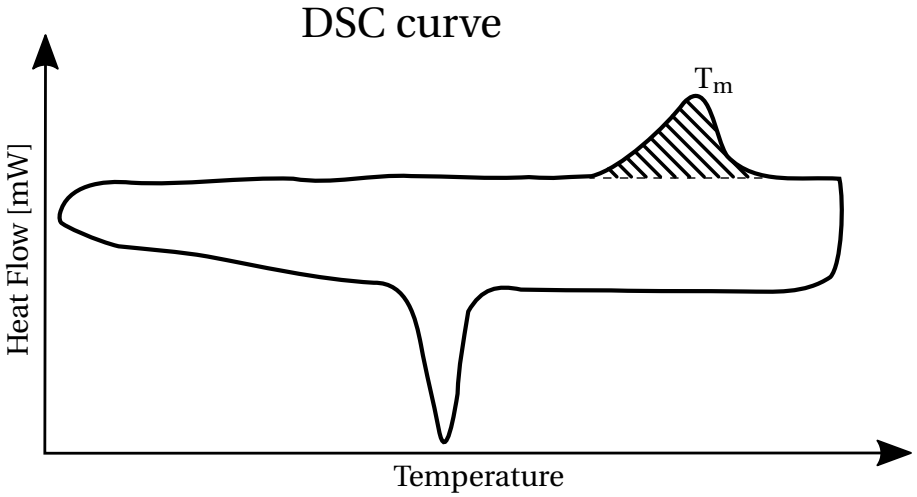

Figure 3.10: *A typical heat flow scan from a DSC analysis. The samples crystallinity can be determined from the melting energy, which can be determined from area under the hatched peak, in the time domain.*

required to increase the temperature for the sample are obtain. DSC can also measure the emission of heat upon cooling. Figure 3.10 shows an illustration of a typical DSC curve for polypropylene. The upper curve is obtained upon heating and the lower curve is obtained upon cooling. The peak seen at heating occurs at the melting point of the polymer, and the valley seen at cooling occurs at the crystallisation temperature. And yes, the melting temperature and the crystallisation temperature are not always the same. The area under the heating peak (hatched area), in the time domain, is the energy used to melt the crystals in the polymer. If the heat of fusion, ΔH_f, for the polymer is known the crystallinity, χ, of the sample can be determined by:

$$\chi = \frac{E_h}{m_s}\frac{1}{\Delta H_f}$$

were E_h is the energy corresponding to the scatted area under the heating peak seen in figure 3.10, and m_s is the weight of the sample. Values for polypropylenes heat of fusion has been reported varying from 60 J/g to 260 J/g [**?**, p. 63]. The large difference can partly be explained by different experimental methods and partly be the configuration of the crystals; folding length, molecular weight, defect and deformation of crystals. For absolute and highly precise determination of the crystallinity this would be a problem, since determining the heat of fusion, is not a trivial thing to do. If the purpose of determining the crystallinity to a wide extent only is to compare the crystallinity between different samples, the exact value of the heat of fusion is less important. The used value for polypropylenes heat of fusion, has in this thesis been 165 J/g [**?**, p. 63].

The crystallinity of the electret samples was practically determined with data obtained with a DSC 4000 from Perkin Elmer. Approximatively 10 mg of polypropylene was removed from the support structure, and put into a DSC capsule, for each analysis. The heating rate was 20 °C/min and the crystallinity was determined from the first cycle. As polymer was removed from the support structure, this analysis technique is destructive.

3.11 Visualisation of Spherulites

For visualisation of the spherulites at the electret surface, optical microscopy and Scanning Electron Microscopy (SEM) were used. The optical microscope could be used to visualise spherulites larger than approximatively 10 µm. Simple putting the samples under the optical microscope did this.

Visualisation of the spherulites in the SEM was a bit trickier. It turns out that the contrast between the crystalline and amorphous regions were to small to be visualised in a SEM. Both in an Environment SEM and with approximatively 3 nm of evaporated gold on the polymer surface; to make the sample electrically conductive. The solution to this problem was found with a selective etch of polypropylene [**?**, **?**]; at room temperature. With the selective etch the amorphous regions in polypropylene are etched a bit faster than the crystalline regions. The difference in etch rate is not large, though large enough for enhancing the contrast in the SEM between the amorphous and crystalline regions. The selective etch was done in a $KMnO_4/H_2SO_4/H_3PO_4$ mixture[2] in the weight ratio 1:22:11 respectively. It turns out that the optimal etch time differs from sample type to sample type, so the etch time had to be tuned for the different sample types, that were to be investigated in the SEM. Before the selective etch, the support structure, with the electret material, was diced out in 10 mm x 10 mm pieces, so op to seven of them could fit in the used SEM; which was a FEI Quanta FEG 200 SEM. After the etch the samples were first washed in hydrogen peroxide (H_2O_2), to neutralise the potassium permanganate, and then in demineralised water. Before the samples were put in the SEM, 3 nm of gold was sputtered on the surface for electric conductivity.

After visualisation of the spherulites, in either the optical microscope or the SEM, the spherulite density at the surface and the mean size of the spherulites were determined with the program ImageJ 1.48v [**?**].

ATTENTION: When mixing the chemicals for the selective etch it is very important that the mixture is not put in a bottle with a closed cap. Gases are produced, even though no bubbles are seen, the built up pressure over night can result in an mechanical explosion!

3.12 Summary

The general sample preparation methods, experimental techniques and the polymers that have been use throughout this thesis have in this chapter been described in detailed. This has been done so that the focus in the next chapter can be kept on the results.

In headlines, what has been covered in this chapter is as follows:

- Two different polymers have been used; isotactic-polypropylene and atactic- polypropylene.
- A 4” silicon support structure with evaporated Ti on the top, has been used a support structure for the polypropylene electret layer.

[2] Potassium permanganate / Sulfuric acid (99%) and Phosphoric acid (85%)

- 3 different polymer solutions and one polymer suspension have been developed for spin coating, of the polypropylene layer, onto the support structure.
- After tuning the spin coating process, for the 3 polymer solutions and the polymer suspension, to a polymer thickness of around of 30 µm, the samples were levelled in a press. This was done to ensure a smooth and consistent surface, both for the individual sample but also among the different samples in the specific experiment.
- A corona charging setup was build where the samples were charged to -500 V. Two electrostatic voltmeters were used to measure the surface potential. It was seen that the potential decay was most pronounced the 12 first hours, after which the decay that still occurs can be neglected as the following experiments will remove several times more charges than the "natural" decay at room temperature will due in a week.
- Isothermal potential decay, humidity potential decay and thermally stimulated potential decay were all introduced and explained. The goal of these three types of experiments is to stress and test the electrets charge stability and get an understanding of how the discharge mechanisms behaves.
- The crystallinity of a polymer sample can through differential scanning calorimetry be determined.
- Through a selective etch of polypropylene, which enhance the contras between the amorphous and crystalline regions, the spherulites can be visualised in an scanning electron microscope.

In the next chapter results from the experiments which purpose have been to investigate the charge retention of polypropylene will be presented.

Chapter 4

CHARACTERISATION, RESULTS AND DISCUSSION

In this chapter the results from the experiments are presented, for which the purpose has been to investigate the charge retention of polypropylene. Polypropylene has been used as an electret model system to establish a broader understanding of which key parameters influence the charge retention of polymer electrets. As mentioned in section 1.1, the idea has been to use polypropylene as a model system due to the limited charge lifetime compared to other much more stable electrets, e.g. fluoropolymers. This makes it possible to study the performance of polypropylene as an electret material much faster than other more stable electret polymers.

In the previous chapter, the general sample preparation and experimental techniques were described in detail, and it is expected that the reader is familiar with these. Specific details and smaller variations between the different experiments will be stated together with the results.

In the course of this Ph.D. project, I have supervised bachelor student Mikkel Hofstedt Hansen and master student Theofanis Spanos. Results from their projects are presented in section 4.1 and section 4.2 respectively.

Parts of the performed research have been presented at conferences and published in scientific Journals. The publications are included in Appendix H.

4.1 Imprint Pattern

The literature study presented in section 1.2 clearly indicated that the charges, from corona charging, are located at the surface of the electret. The phenomenon that supports this claim has been observed when a moist cloth or running water briefly came in contact with a charged electret material. If this happens, a complete discharge of the area that was in contact with the cloth or water, was seen.

In a combination of the literature and these observations it is reasonable to believe that the charge retention is correlated with the effective surface area. The thought behind this is that the amount of accessible deep traps, for the charges, are increased with an increased surface

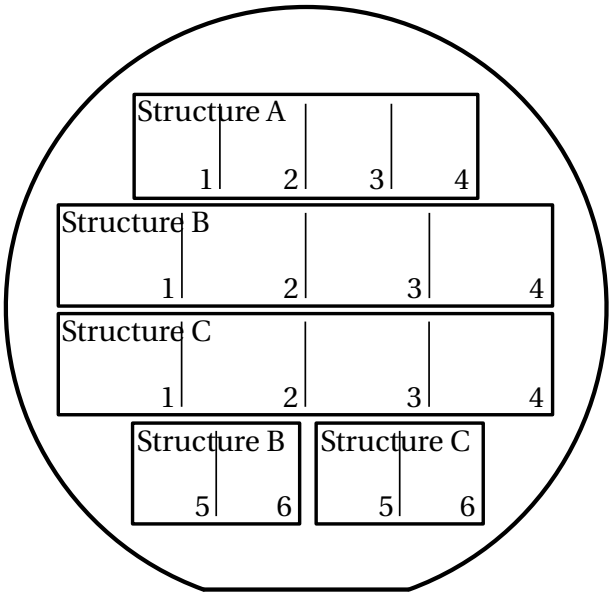

Figure 4.1: *Illustration of the 16 individually areas on the stamps made by Mikkel Hofstedt Hansen in [**?**]. The stamps were 10 cm in diameter.*

area. One way of increasing the effective surface area is by imprinting the surface with a pattern. The effective surface area is hereby increased corresponding to the the side walls of the pattern. The effective surface area, A_{eff}, can be expressed as:

$$A_{eff} = \frac{A_{\perp} + A_{\parallel}}{A_{\parallel}} = 1 + \frac{A_{\perp}}{A_{\parallel}}$$

where $A_{\parallel}$ is the area parallel to the surface and $A_{\perp}$ is the area perpendicular to the surface. The stamps used in these experiments were fabricated in a bachelor project, by Mikkel Hofstedt Hansen [**?**], using semiconductor fabrication methods. For details on the fabrication please refer to Mikkels bachelor thesis [**?**]. The output of Mikkels project was three different nickel stamps, each with 16 individual areas; see figure 4.1. Each stamp contains three different structures which fill the 16 individual areas by different unit cells seen in figure 4.2. The differences between the areas (in figure 4.1) with the same structures is the length, c, of the unit cells. The differences between the three stamps is the size of the structures (length of b), seen in figure 4.2. The reason for changing the lengths, b and, c in figure 4.2 were to control the effective surface area. The reason behind the different structure was to investigate any structural influences. With values of b stretching from 1.5 µm to 21 µm and values of c stretching from 1.5 µm to 100 µm, an A_{eff} between 1 and 11 where obtained with a stamp protrusion height of 15 µm.

The stamp imprints in these experiments were done on levelled samples at 120 °C in the same way as the levelling step described in section 3.5. The silver coated wafer was just replaced with the stamp. The imprint temperature of 120 °C was chosen as this temperature yield the best imprint result.

As the experiments with the imprinted surfaces, were the first real experiments that were made in this project additional samples to the imprinted ones, were included to this series of experiments. Those were, samples that had not been levelled so the surface was rough and

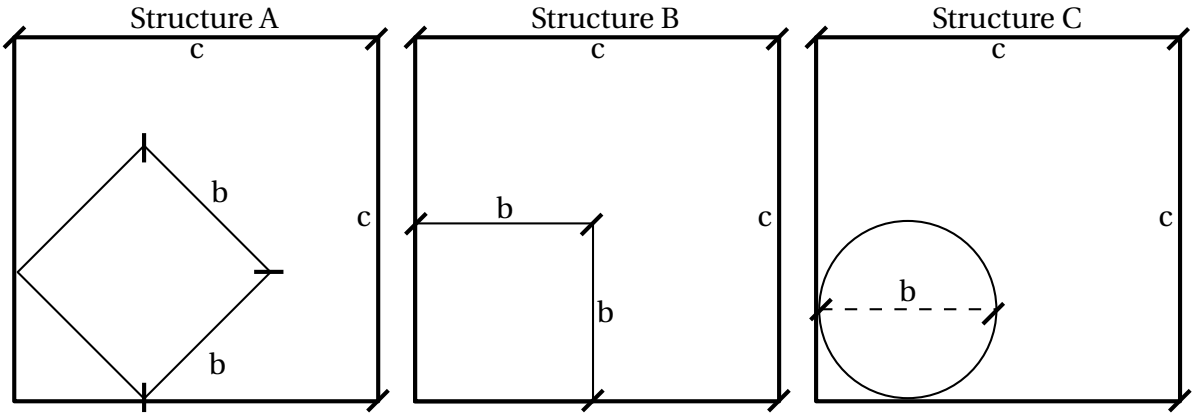

***(a)** Diamond structure* ***(b)** Square structure* ***(c)** Circular structure*

Figure 4.2: *The three different structures that are filling the 16 areas on the stamp, seen in 4.1.*

undulated, samples that had been levelled so the surface was smooth and homogeneous (also used a reference samples to the imprinted samples), and samples that had been levelled where the cooling rate after the levelling step was significantly lower than for all other samples. At this point in time, the importance of sample preparation was not yet known so the cooling time was not measured precisely. The samples that were cooled "normally" after the levelling, were cooled from 180 °C to room temperature in less than one minute, the samples where the cooling rate was "slow", were cooled from 180 °C to room temperature in approximatively 5 minutes. The samples that were not levelled were also cooled from 180 °C to room temperature in less than one minute. No particular attention was given to the cooling after the imprint step at 120 °C, as the recrystallization temperature for isotactic polypropylene, coming from room temperature, is well above 120 °C [**?**]. The data presented in the following, is for the samples without imprint, the average measurement from two samples each measured at five different location on the sample; centre, north, east, south and west. For the samples with imprint, the presented data is the average from two different samples but from identical areas; see the 16 different areas in figure 4.1.

For the three sample types, levelled surface, rough surface and levelled surface which had been slowly cooled, two isothermal- and one humidity induced potential decay experiments were conducted; at 90 °C, 120 °C and at 50 °C with 90 %RH respectively. The results from these experiments can be seen in figure 4.3. Figure 4.3a, figure 4.3c and figure 4.3e shows the potential decay in absolute values, while figure 4.3b, figure 4.3d and figure 4.3f shows the normalised potential decay, with respect to the start of the experiment. The reason the potential decay is shown both in absolute values and as normalised values is that the two types of plots give different information. The plot with the absolutes values shows the absolute performances with different starting point, while the plot with the normalised values shows the performances relative to one another. In some cases a misleading conclusion can be drawn if only looking at one of these graphs. As stated in section 3.6 all the samples have been charged to -500 V and then left for a minimum of 12 hours to stabilise. This is the reason the samples do not have the exact same surface potential at the start of the experiment.

The surface potential after 24 hours at the 90 °C experiment, for the sample type 'levelled surface', in figure 4.3b, is 85 % of its initial surface potential. And for the sample type 'levelled

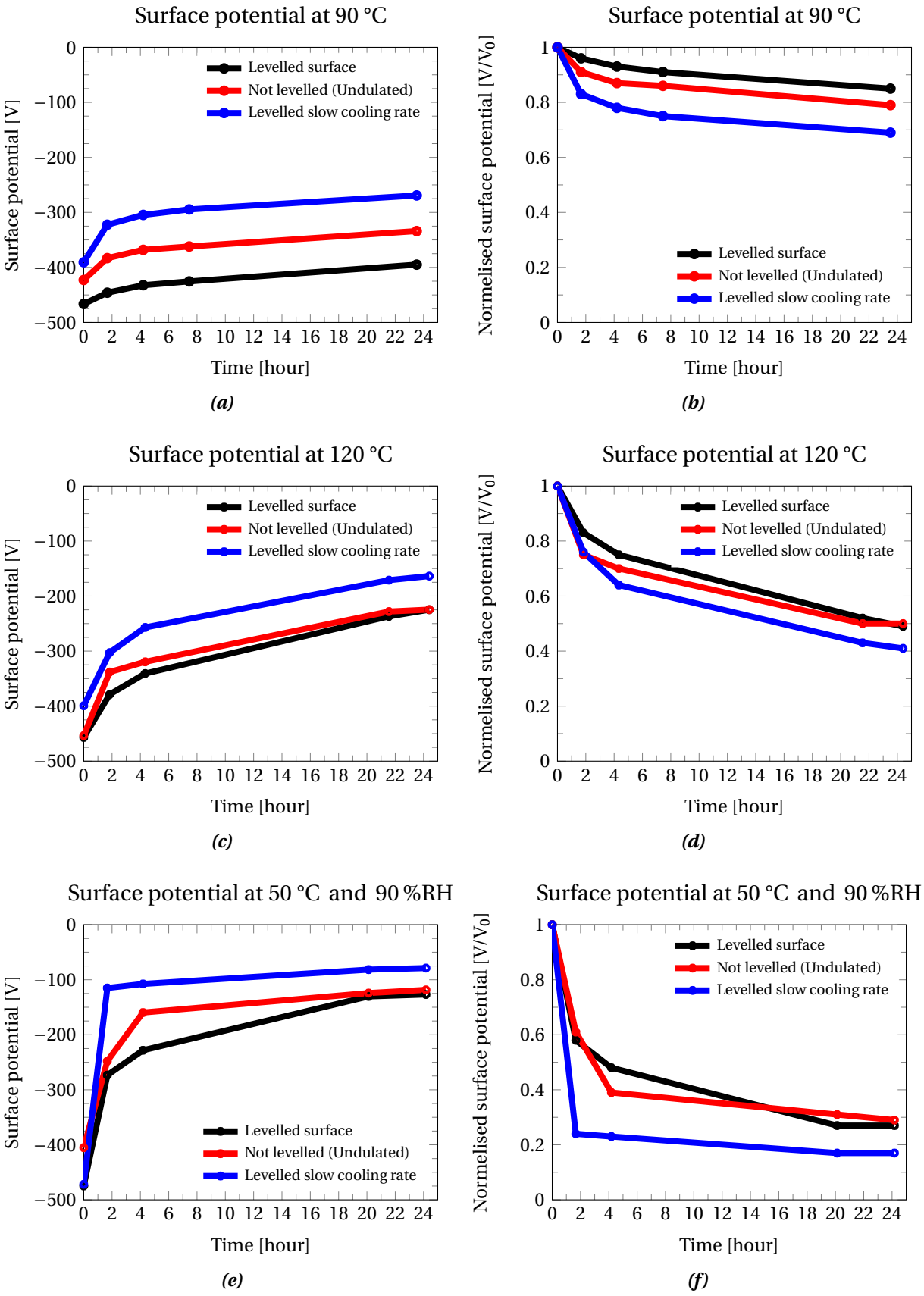

Figure 4.3: *The surface potential decay for the samples with a levelled surface (black curves), samples that have not been levelled (red curves), and samples which have experienced a slow cooling rate after the levelling step (blue curves). The graphs to the left shows the potential decay in absolute values and the graphs to the right shows the potential decay in normalised values, with respect to the start of the experiment.*

surface which had been slowly cooled' it is 69 %. The corresponding values for the 120 °C experiment, seen in figure 4.3d, is 49 % and 41 % for the sample type 'levelled surface' and the sample type 'levelled surface which had been slowly cooled' respectively. For the experiment at 50 °C with 90 %RH, seen in figure 4.3f, the numbers are 27 % and 17 % respectively. From figure 4.3 it can be said in general terms, that the samples with levelled surfaces have a bit higher charge retention than samples with surfaces that have not been levelled. Samples for which the surface have been levelled, and been slowly cooled, after the levelling step, performed the worst. Thus it can be said, regarding charge retention, that:

$$\underbrace{\text{Levelled surface} > \text{not levelled surface} > \text{levelled surface which had been slowly cooled}}_{\text{charges stability}}$$

For the samples with the imprinted structures, two isothermal- and one humidity induced potential decay experiments were conducted; also at 90 °C, 120 °C and at 50 °C with 90 %RH respectively. The normalised surface potential, after 24 hours plotted against the effective surface area can be seen in figure 4.4, while the absolute values can be found in appendix E figure E.1; due to no extra information, in this case, is revealed by looking at these absolute values. In figure 4.4a and figure 4.4b no correlation between the increased effective surface area and charge retention can be seen. The normalised surface potentials in figure 4.4a and figure 4.4b have approximatively the same values, after 24 hours, as the levelled samples in figure 4.3b and figure 4.3d respectively. If anything can be said from figure 4.4a and figure 4.4b it is that the large structure (blue symbols, large b-value in figure 4.2), seems to perform a bit worse than the smaller structure.

Figure 4.4c shows the normalised surface potential, after 24 hours plotted against the effective surface area, for the humidity induced potential decay experiment. The effect of the increased effective area is here a bit more blurred. It seems that there exist and optimum around an $A_{eff} = 2$ however, the polypropylene on these samples did not adherence as good to the support structures as for the isothermal experiments, which is a significant source of error. It is suspected that the high humidity was the reason for the bad adherence. Due to this no data, in figure 4.4c, are represented for the 6 µm structures.

Based on the observation from the experiments presented in this section, it can be concluded that the preparation of the electret samples is of greater importance than changing the effective surface area; which effect, in these experiments, were absent. For this reason it was decided to investigate the effect of different cooling profiles, after the levelling step, with respect to the charge retention. Results from these experiments is discussed in section 4.3. In the next section results from the master project made by Theofanis Spanos, about particle enhanced electret, is discussed.

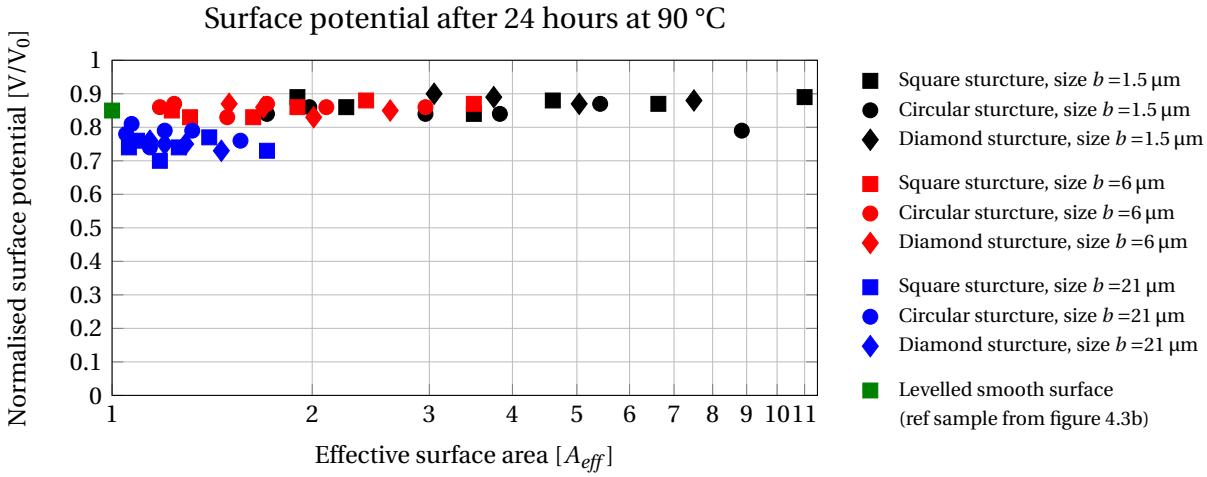

(a)

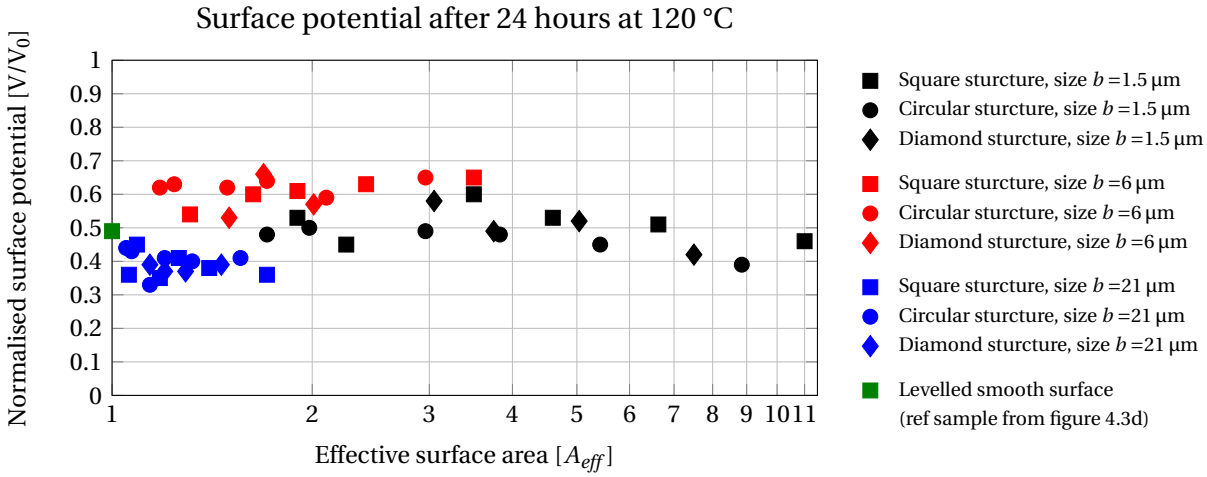

(b)

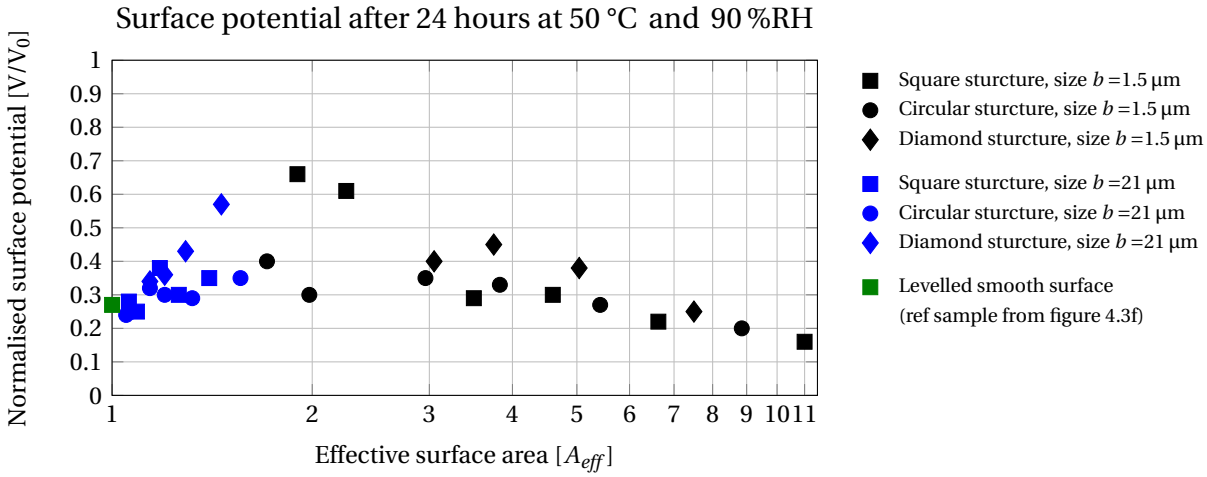

(c)

Figure 4.4: *The normalised surface potential, for the humidity induced potential decay experiment, after 24 hours. Corresponding graphs with absolute values can been found in appendix E figure E.1 on page 98.*

4.2 Particles

In a master project made by Theofanis Spanos [**?**] it was investigated how the charge retention were effected by introducing, micron-size and nano-size, particles to the polypropylene solution prior to the spin coating step. In this way the particles were trapped in the polymer matrix, and were effecting the internal structure and crystallinity of the electret samples. The idea behind these experiments was that small size particles would form trap centres for the electrical charges and effect the crystallinity which also would effect the charge retention. This was based on literature disclosed in [**?**]. The particles Theofanis used are listed in table 4.1.

The results obtained by Theofanis, are shown in figure 4.5. Here the surface potential decay for isothermal experiments, at 90 °C and 120 °C are shown [**?**]. After introducing the particles to the polypropylene solutions, some of the samples bond extremely strong to the wafer it was levelled against. Since this problem has not been observed before, this effect was attributed to the introduction of particles. For the sample to be as identical to each other as possible none of the samples were levelled. The particle concentrations in the samples, which results are presented in figure 4.5, are the optimal concentrations that was seen in all of the particle experiments. The particle concentrations used in [**?**] were for Al_2O_3-micron-particles and $CaCO_3$: 0.1 wt%, 0.5 wt%, 1 wt%, 3 wt% and 10 wt%. The corresponding concentrations for Al_2O_3-nano-particles and SiO_2, were: 0.1 wt%, 0.5 wt% and 1 wt%. All the "wt%" is in respect to the amount of polypropylene in the solutions, that were used for spin coating.

What is seen in figure 4.5a and figure 4.5b is the absolute values and the normalised values respectively, for the 90 °C isothermal surface potential decay. What is seen in figure 4.5a is that, with the right amount, all types of particle tried, exempt for SiO_2, can improve the charge retention for polypropylene. What is also seen, by the purple curve (slowly cooled sample with Al_2O_3-nanoparticles), in figure 4.5a is that a wrong cooling profile after the levelling step can disrupt the positive effect that particles can have. This is seen as the slowly cooled Al_2O_3-nanoparticles sample, at room temperature, has lost around 150 V after charging; resulting in a surface potential at t=0 at around -350 V. The performance however, for the slowly cooled sample with Al_2O_3-nanoparticles, is only bad when looking at absolute values. If looking at the relative potential decay, in figure 4.5b, this sample is one of the best at keeping its charge. This example clearly illustrates the importance of looking at both the absolute values and the normalised values. The slowly cooled sample with Al_2O_3-nanoparticles in figure 4.5a and figure 4.5b indicate that the particles can help stabilise the charge, while the cooling profile, in this case, seems to have an influence on how many deep traps that are accessible for the charges. In figure 4.5b, which shows the normalised surface potential for

Particles	**Size**	**Product specification**
Aluminium oxide (Al_2O_3) (micron-particle)	$\leq 10\,\mu m$	See Appendix F
Aluminium oxide (Al_2O_3) (nano-particle)	$< 50\,nm$	
Silicon oxide (SiO_2)	10 nm to 20 nm	
Calcium carbonate ($CaCO_3$)	$\leq 30\,\mu m$	

Table 4.1: *The particle used in Theofanis master project [**?**].*

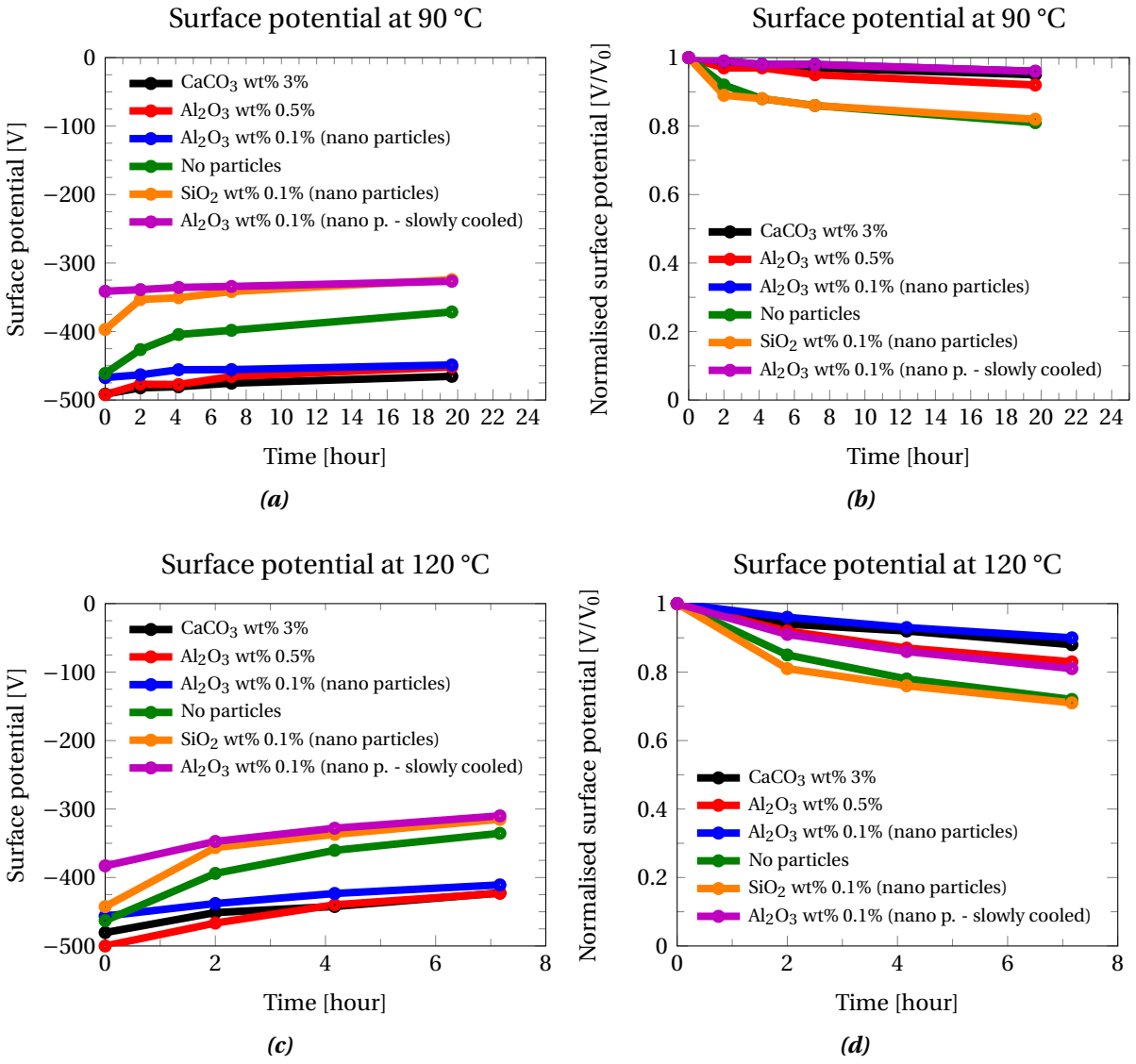

Figure 4.5: *Shows the surface potential decay for samples where different particles in different sizes have been introduced to the polymer matrix. What is seen is that with the right amount, all types of particle tried, exempt for SiO_2, can improve the charge retention for polypropylene.*

the experiment at 90 °C it is seen that the sample with no particles (green curve), after 24 hours has 81 % of its initial potential. For the samples with $CaCO_3$-, and Al_2O_3-particles the corresponding numbers are between 92 % to 96 %.

Figure 4.5c and figure 4.5d shows the surface potential decay for the 120 °C isothermal surface potential decay experiment; be aware of the shorter time scale for this experiment. In short these graphs tells the same story as the graphs in figure 4.5a and figure 4.5b. The normalised surface potential for the sample with no particles (for the experiment at 120 °C) is after 7 hours 72 %. For the samples with $CaCO_3$-, and Al_2O_3-particles the corresponding numbers are between 81 % to 90 %.

No reliable results were obtained for humidity experiments, thus non of them are shown here.

In short, some particles can enhance the charge stability. What was also seen from the particles experiments, was that the sample preparation, seemed to have an equally large influence, on the electret charge retention, as the particles themselves. Sample preparation parameters should therefore be controlled and monitored in details. In the next section the cooling rate influence on the charge retention, from polypropylenes melt to its solid state, is investigate. It turns out that the size and numbers of the spherulites play a huge role in this regard.

4.3 Cooling Rate

In the previous sections strong indications have been seen that, sample preparation has a huge influence regarding polypropylenes charge retention. Due to this the influence of the cooling rate from polypropylenes melt to its solid state has been investigated. The thought behind this is that the size and number of the spherulites are affected by the cooling rate. A slow cooling rate should give few and large spherulites and a fast cooling rate should give many and small spherulites. The degree of crystallinity is also thought to be affected, giving the samples which sees the slowest cooling rate, the highest degree of crystallinity.

Three different cooling methods were used, designated: *'slowly cooled'*, *'medium cooled'*, and *'fast cooled'*. The cooling step was introduced right after the levelling step (see section 3.5 on page 39), while the samples still had a temperature of 180 °C.

Slowly cooled: The samples that were slowly cooled, were cooled from 180 °C to room temperature in 5 min. This was done by leaving the sample inside the sandwich structure, used in the levelling step, on a table next to the press. After 5 min. when the sandwich structure had cooled down the sample was removed and ready to be charged in the corona setup.

Medium cooled: The samples that were medium cooled, were cooled from 180 °C to room temperature in approximately 10 sec. This was done by quickly removing the pressed sample from the sandwich structure and in a smooth and slow motion dragging the sample over a room temperate marble table. The samples were only touched at the edges in this process.

Fast cooled: The samples was cooled from from 180 °C to room temperature in approximately 1 sec. This was achieved by quickly removing the pressed sample from the sandwich structure and throwing the samples in a bucked with ice water. The samples were only touched at the edges in this process.

Before the charge retention for the different samples types are revealed, characteristic properties of the samples will first be discussed, a summary of the following can be seen in table 4.2 on the following page. After the cooling step a clear difference between the different samples types could easily be seen by visual inspection. The samples that had been slowly cooled were grey in a foggy and blurry way, while the samples that had been medium cooled were semi-transparent. The samples that had been cooled the fastest were clear and fully transparent. The crystallinity for the different sample types, were obtained by differential scanning calorimetry (see section 3.10 on page 45), and were for the slowly cooled, medium cooled and fast cooled samples, 61 %, 54 % and 51 % respectively. As expected, the highest degree of crystallinity was found for the samples that had been slowly cooled, and the lowest degree of crystallinity was found at the samples that had been cooled the fastest.

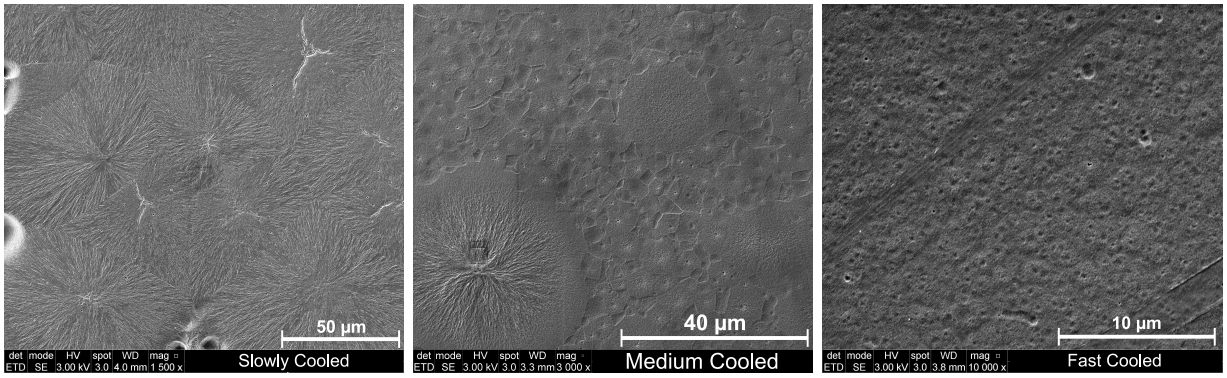

(a) *Slowly cooled* ***(b)*** *Medium cooled* ***(c)*** *Fast cooled*

Figure 4.6: *SEM images of the spherulites from the three different cooled samples types. As the cooling rate is increased the size of the spherulites is drastically reduced.*

	Slowly cooled	**Medium cooled**	**Fast cooled**
Cooling time, from 180 °C to room temperature	5 min	10 s	1 s
Transparency	Foggy/blurry	Semi-transparent	Transparent
Degree of crystallinity, χ	61 %	54 %	51 %
Diameter of spherulites	50 µm to 100 µm	3 µm to 7 µm*	0.7 µm to 1.5 µm
Average spherulite area	2950 µm^2	23 µm^2	1 µm^2
Number† of spherulites pr. cm^2	$8 \cdot 10^3$ to $30 \cdot 10^3$	$1 \cdot 10^6$ to $7 \cdot 10^6$	$28 \cdot 10^6$ to $129 \cdot 10^6$
Number† of spherulites pr. cm^3 (in the first 5 µm from the surface)	6 to 46	$15 \cdot 10^3$ to $186 \cdot 10^3$	$1 \cdot 10^6$ to $14 \cdot 10^6$

Table 4.2: *List the difference between the three sample types. *a few spherulites up to 45 µm is seen. † based on equation (2.14) and equation (2.17).*

The spherulites from the different samples types were visualised in a SEM after a selective etch (see section 3.11 on page 47) and can be seen in figure 4.6. Figure 4.6a shows the spherulites from the slowly cooled samples. Here the diameter of the spherulites is between 50 µm to 100 µm and with an average area of 2950 µm^2. By equation (2.14) and equation (2.17) on page 21 the number of spherulites per cm^2 and per cm^3(in the first 5 µm from the surface) can be determined. The number of spherulites per cm^2 is in the range of $8 \cdot 10^3$ to $30 \cdot 10^3$ and the number of spherulites per cm^3 is in the range of 6 to 46. All these numbers are first really interesting when comparing them with the corresponding numbers from the two other sample types. As mentioned earlier, all of these numbers are summarised in table 4.2. Figure 4.6b shows the spherulites from the medium cooled samples, and the diameter of the spherulites are here between 3 µm to 7 µm and with an average area of 23 µm^2. What also can be seen in figure 4.6b is that there are a few spherulites which have diameters that are significantly larger than 7 µm, up to 45 µm have been seen. However, the majority of the

spherulites (in area and number) are dominated by the 3 µm to 7 µm spherulites. The number of spherulites for the medium cooled samples per cm^2 is in the range of $1{\cdot}10^6$ to $7{\cdot}10^6$ and the number of spherulites per cm^3 is in the range of $15{\cdot}10^3$ to $186{\cdot}10^3$. Figure 4.6c shows the spherulites for the fast cooled samples. The spherulites are here harder to see than in figure 4.6a and figure 4.6b, but the structures that look like craters are the centres of the spherulites. The diameter of these spherulites are roughly between 0.7 µm to 1.5 µm with an average area of 1 μm^2. These small spherulites result in a huge number of spherulites per cm^2 and cm^3 which are in the range of $28 \cdot 10^6$ to $129 \cdot 10^6$ and $1 \cdot 10^6$ to $14 \cdot 10^6$ respectively. When looking at table 4.2 it is clear that there is a huge difference between the different sample types. The largest difference is seen for the size of the spherulites, which also affects the average area of the spherulites and the number of spherulites at the surface and near surface. However, a notable difference in the degree of the crystallinity is also seen. All these differences also manifest themselves in the experiments that shows the charge retention.

Figure 4.7 shows the results from the isothermal experiments at 90 °C and 120 °C and the humidity included potential decay at 50 °C and 90 %RH. Figure 4.7a, figure 4.7c and figure 4.7e shows the absolute values and figure 4.7b, figure 4.7d and figure 4.7f shows the normalised values. The general trend is that the fast cooled samples show the best charge retention, this is easiest seen in figure 4.7c and figure 4.7d, which shows the results from the isothermal experiment at 120 °C. In figure 4.7e and figure 4.7f, which shows the results from the humidity induced experiment it is seen that, the fast and medium cooled samples are equally good, outperforming the slowly cooled samples which, across all experiments, showed the worst charge retention. In figure 4.7b it is seen that the surface potential after 25 hours, for the 90 °C experiment, is 84 % and 70 % of the initial surface potential for the fast cooled and the slowly cooled samples respectively. These numbers is for the 120 °C experiments (see figure 4.7d) 56 % and 26 %; again for the fast cooled and the slowly cooled samples respectively. The corresponding values from the humidity induced potential decay (see figure 4.7f) is 38 % and 24 % of the initial surface potential. From the results in figure 4.7, it can be said that the faster polypropylene has been cooled from its melted state, the better charge retention is achieved.

Figure 4.8 shows the normalised surface potential after 25 hours across the different sample types, for the two isothermal, and the humidity induced potential decay experiments. Here the relation between the experiments normalised surface potential and the number of spherulites, the average area of the spherulites, and the degree of crystallinity (χ) are seen. What is seen in figure 4.8 is that the samples charge retention is higher for samples with small in size and in number many spherulites. However, when looking at the degree of crystallinity, it looks like the charge retention also is favoured by a low degree of crystallinity. This is however not the case, which will be shown in the next section, where the effect of the crystallinity is investigated. The increased charge retention, that is observed with smaller and several more spherulites, is occurring in spite of the decrease in the degree of crystallinity.

Figure 4.9a shows the normalised thermally stimulated potential decay, which is the potential decay as a function of a linear increased temperature; see section 3.9 for experimental procedure. The used heating rate was 3 K/min. Figure 4.9b shows the corresponding thermally stimulated current (released current), from which the activation energies of the traps, the electrons are located in, in theory could be determined. However, as the current peaks in figure 4.9b are all in the melting interval of polypropylene, no activation energies can be determined. The melting interval has been determined for all sample types by DSC to

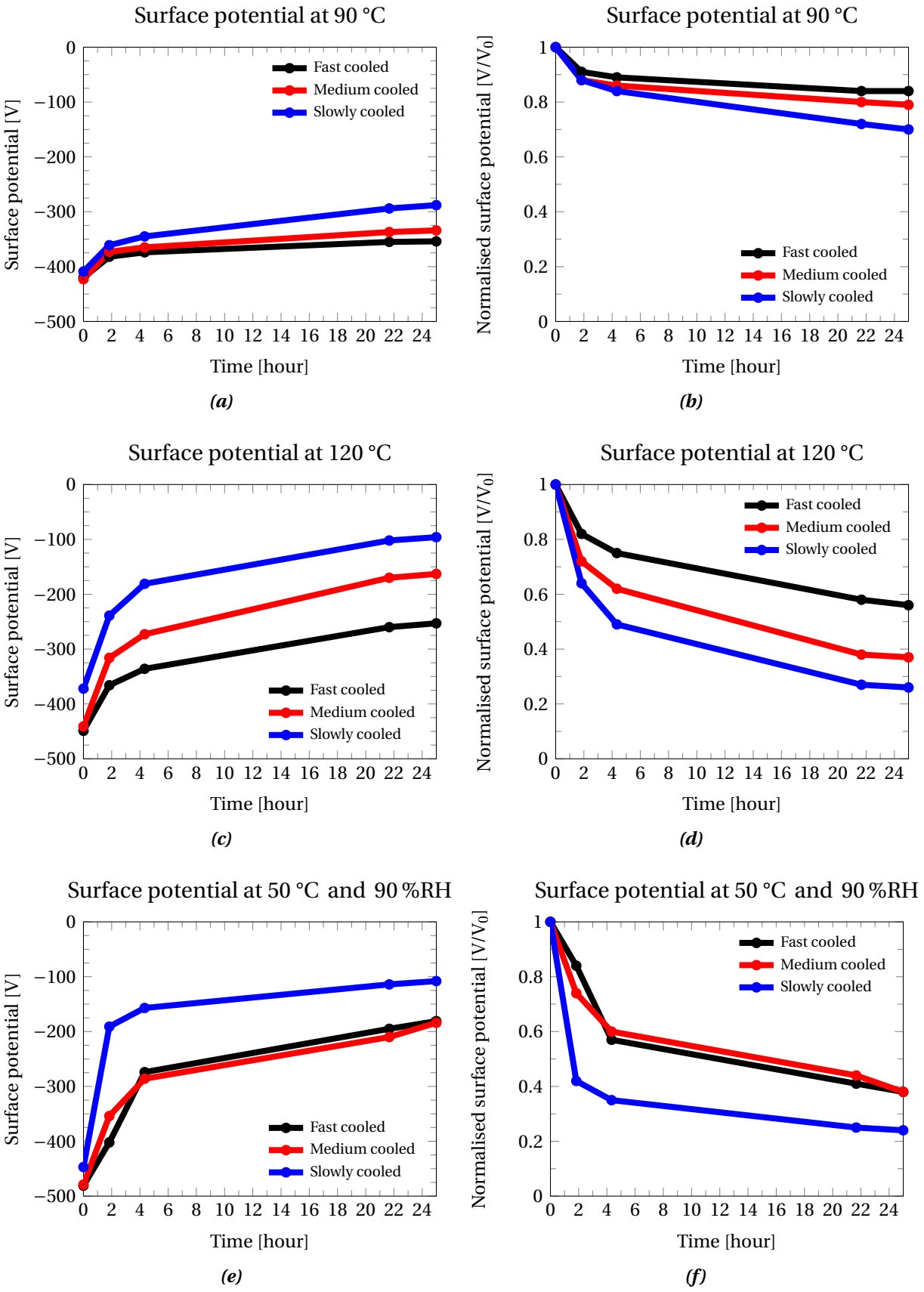

Figure 4.7: *The surface potential decay for samples that have been exposed to different cooling rates from polypropylenes melted state to its solid state. The graphs to the left show the potential decay in absolute values and the graphs to the right show the potential decay in normalised values, with respect to the start of the experiment.*

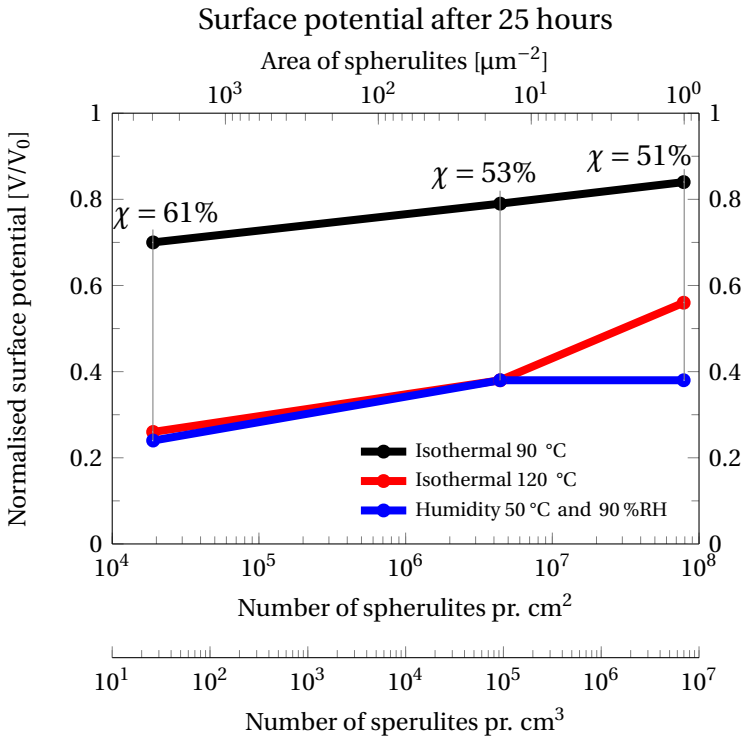

Figure 4.8: *Shows the normalised surface potential after 25 hours across the different samples types, for the two isothermal, and the humidity induced potential decay experiments. What is seen is that the charge retention is increasing with an increased number of small spherulites in spite of the decreased degree of crystallinity.*

be in the interval between 150 °C and 180 °C. The theory concerning the activation energy, covered in chapter 2, only apply for materials where the phase state is preserved, and not materials that are in their melted state. What can be seen in figure 4.9a though, and clearly, is that the samples that have been cooled the fasted (smallest spherulites) have a higher charge retention than samples that have been medium cooled and slowly cooled. This is in good agreement with the previous discussion in the section. In figure 4.9b it is seen that the current peak for the slowly cooled sample is at 151 °C while the largest current peak for the fast cooled sample is at 171 °C.

Another interesting thing seen in figure 4.9a is that it seems that the surface potential is increasing with increased temperature, this is very distinct for the fast cooled sample (black curve). What is happening is not, due to an increased number of charges at the surface but a combined effect of thermal expansion of the polypropylene layer and a decrease in polypropylenes dielectric constant, which is known to depend non-linearly on temperature [**?**, **?**, **?**]; this effect is largest above 100 °C. The linear thermal expansion coefficient (thermal expansion in one dimension) for polypropylene is also known to depend non-linear on the temperature unless the sample is 100 % crystalline [**?**]. As both the thermal expansion and the change in the dielectric constant are non-linear, with respect to temperature, and unknown for the samples types used in these experiments, it has not been possible to make a correction of these effects when calculating the thermally stimulated current in figure 4.9b. However, it is not expected and highly unlikely that these effects will change the shape of the release currents, seen in figure 4.9b, but more the absolute values. The fact that these mentioned effects can be seen indicated a high charge retention of the samples.

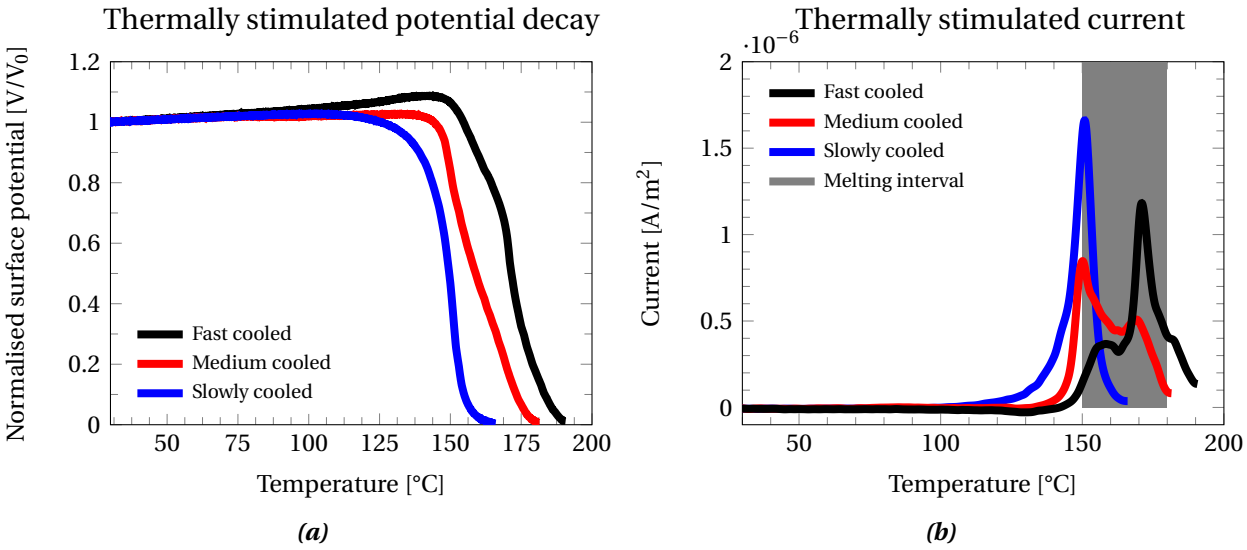

Figure 4.9: ***(a)*** *Thermally stimulated potential decay for the three different sample types. Heat rate was 3 K/min. The cause for the increasing in the potential prior to the large potential decay (most clearly for the black curve) is due to thermal expansion of the polypropylene layer and the change in the dielectric constant, with both depend non-linear of the temperature.* ***(b)*** *The thermally stimulated current calculated from the thermally stimulated potential decay.*

In this section the effect from the variation of the size of the spherulites and the number of spherulites on the charge retention in polypropylene has been investigated. This could however, not be done with an identical degree of crystallinity throughout all samples. In the next section the effect of the degree of crystallinity related to the charge retention will by addressed.

4.4 Crystallinity

In the previous section it has been established that the preparation of a polypropylene sample is of pronounced importance for the charge retention. However, so far the isolated effect of the degree of crystallinity has not yet been investigated, which will be addressed in this section.

Changing the degree of crystallinity in polypropylene can be achieved in several ways. This could be by different cooling rates from polypropylenes melted state to its solid state, the introduction of nucleation agents in the polypropylene melt or by mixing atactic-polypropylene (a-PP) with isotactic-polypropylene (i-PP). The later approach has been used to control the degree of crystallinity, as this method allowed all other process parameters to be kept identical. In this way the only difference between the samples would be the degree of crystallinity, thus the change in charge retention would be caused solely by the difference in the degree of crystallinity. As stated in section 3.3 on page 34 four different solutions were used for spin coating. The polymer content of the four solutions, as well as their calculated crystallinity and measured thicknesses are listed in table 4.3. As described in section 3.10 on page 45 the crystallinity has been determined by a differential scanning calorimeter. The thickness

Sample type	Crystallinity	Height
100 % i-PP	47 %	27 µm
67 % i-PP with 33 % a-PP	39 %	32 µm
33 % i-PP with 67 % a-PP	22 %	30 µm
100 % a-PP	7 %	25 µm

Table 4.3: *Crystallinity and thickness of the polypropylene layer for the four different sample types.*

of the samples has either been determined by a stylus profiler or by an optical microscope using confocal and interferometric techniques. The reason why the heights are not more identical than they are, is due to the slightly different viscosity between the four solutions and the different spin coating programs; which were mentioned in section 3.4 on page 37. Difference in height has not been an issue in the previous presented results as the solution used for those experiments all have been identical, as well as the spin coating program. All the figures in this section, which shows the absolute surface potential has been corrected to the surface potential the sample types would have had, if the same amount of charges had been on a 30 µm thick electret layer, instead of the actual thickness of the sample; as state in table 4.3. This has been done for a more fair comparison of the different sample types, as it is the amount of charges that is of interest and not the surface potential; when looking at the charge retention of an electret. The samples in this section have been fast cooled after the levelling step, as described in the previous section. This means that the fast cooled samples in the previous section is comparable with the samples in this section.

Figure 4.10 shows the surface potential decay for four reference samples at room temperature for the four different samples type, for a period of 294 days. Figure 4.10a shows the corrected absolute values and figure 4.10b shows the equivalent normalised values. The values has been normalised to t=0. As also stated in section 3.6 on page 40, the surface potential decay is most pronounced in the first 12 hours after being charged. Which is the time prior to time equals 0 in figure 4.10. After this the different sample types are fairly stable at room temperature. The average potential loss from day 5 to day 291 is 0.10 V, 0.46 V and 0.84 V for the samples consisting of 100 % i-PP, $^{2}/_{3}$*i-PP and* $^{1}/_{3}$*a-PP* and $^{1}/_{3}$*i-PP and* $^{2}/_{3}$*a-PP* respectively. The sample that consist of 100 % a-PP (green curve) has such a bad charge retention that it loosed half of its initial charges in the first couple of minutes between being charged to -500 V and to the surface potential could be measured and about 90 % within the first 12 hours. For comparison, the three other samples had after 12 hour lost 2 %, 11 % and 13 % of their initial charges, for the samples consisting of 100 % i-PP, $^{2}/_{3}$*i-PP and* $^{1}/_{3}$*a-PP* and $^{1}/_{3}$*i-PP and* $^{2}/_{3}$*a-PP* respectively. So the low surface potential, seen for the sample consisting of 100 % a-PP, is a consequence of bad electret properties and not a conscious choice. From figure 4.10b is seems that the sample consisting of $^{1}/_{3}$*i-PP and* $^{2}/_{3}$*a-PP* (blue curve), the first 5 days, has a better charge retention than the sample consisting of $^{2}/_{3}$*i-PP and* $^{1}/_{3}$*a-PP* (red curve). This goes against what is expected as the sample with $^{2}/_{3}$i-PP has a 17 percentage point higher crystallinity than the sample with only $^{1}/_{3}$i-PP, going from a crystallinity of 39 % to 22 % respectively. The reversed and expected tendency is however, seen after 291 days (and most likely before) and in the following experiments. The reason for this unexpected behaviour the first 5 days, seen in figure 4.10, is unknown. However, the overall tendency, that the charge retention is favoured by high crystallinity, is seen.

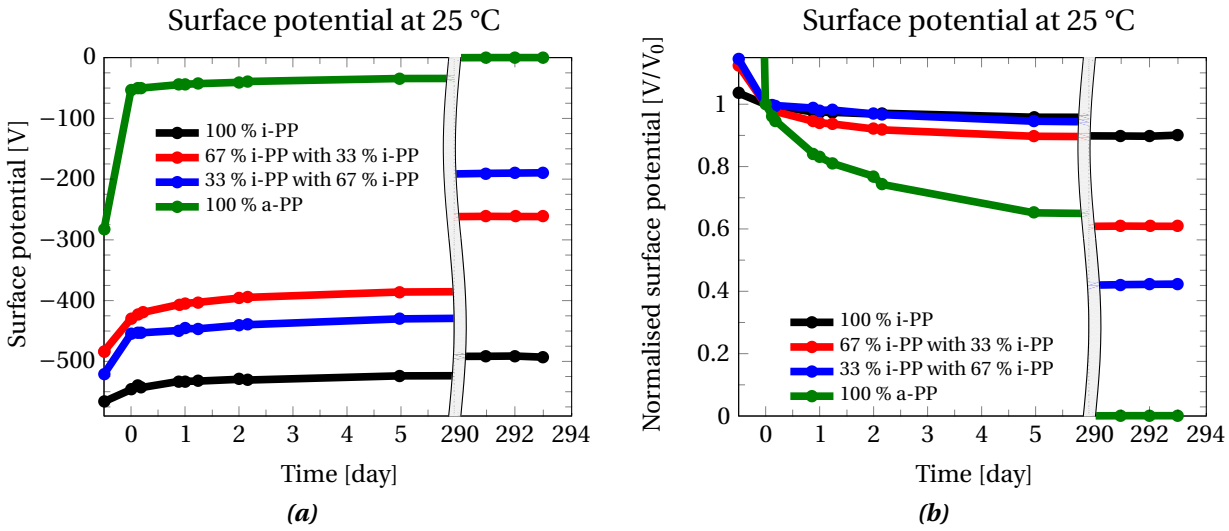

Figure 4.10: *The surface potential decay for four reference samples at room temperature for the four different sample types listed in table 4.3. An overall tendency, that the charge retention is favoured by high crystallinity, is seen. The values in (b) have been normalised to t=0.*

Figure 4.11 shows the results from the isothermal experiments at 90 °C and 120 °C and the humidity included potential decay at 50 °C and 90 %RH. Figure 4.11a, figure 4.11c and figure 4.11e shows the corrected absolute values and figure 4.11b, figure 4.11d and figure 4.11f shows the equivalent normalised values. The tendency is quite clear when looking at figure 4.11, that as the amount of i-PP, in the samples, is decreasing so are the charges retention. This tendency is however, most pronounced in the isothermal experiments at 90 °C and 120 °C. From figure 4.11b, which shows the normalised surface potential for the 90 °C experiment, is it seen that after 24 hour the sample that contain 100 % i-PP has 75 % of its initial potential while its closest competitor, sample $^{2}/_{3}$*i-PP and* $^{1}/_{3}$*a-PP*, only has 24 % of its initial potential. The corresponding numbers for the 120 °C, seen in figure 4.11d, is 36 % and 0 % respectively. Similar numbers for the experiment at 50 °C and 90 %RH, is 51 % and 43 % respectively. Also in figure 4.11 the very bad charge retention for the samples consisting of 100 % a-PP (green curves) is seen.

Figure 4.12 shows the normalised surface potential after 24 hours versus the crystallinity, for the results presented in figure 4.10, figure 4.11, and for the fast cooled samples in the previous section; which crystallinity was 51 %. In figure 4.12 a clear correlation can be seen between the crystallinity and the charge retention. As the samples degree of crystallinity is increased so is the samples charge retention. From figure 4.12 it seems that the importance of the crystallinity is increased with the isothermal temperature of the experiments. This is seen as the beginning of the curves slope in figure 4.12 are shifted upwards in crystallinity with increased experimental temperature. Figure 4.12 with absolute values, if that should be of interested, can be found in appendix G on page 107.

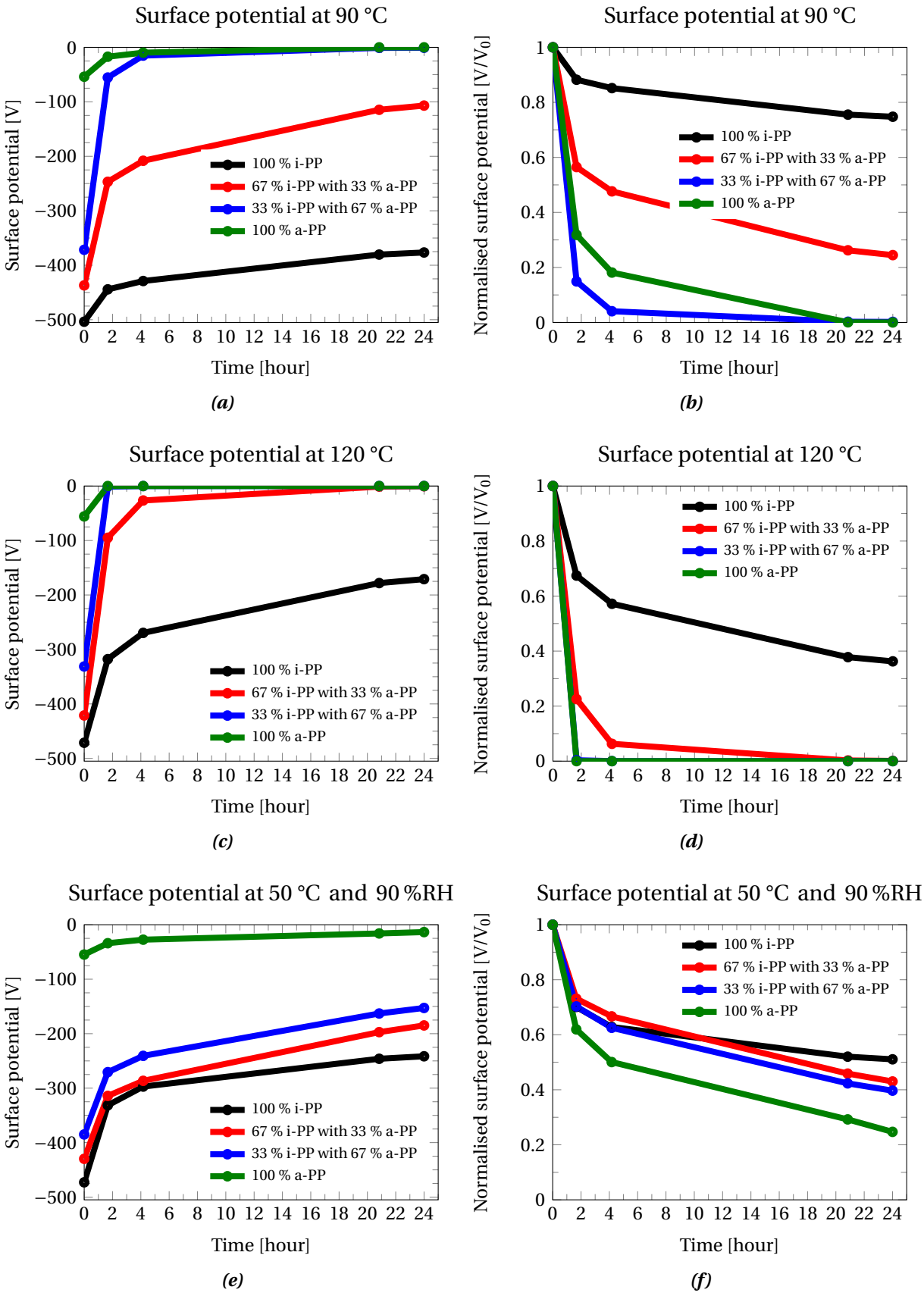

Figure 4.11: *The surface potential decay for samples where the crystallinity has been controlled by mixing a-PP with i-PP, while all other process parameters have been the same. The graphs to the left show the corrected potential decay in absolute values and the graphs to the right show the potential decay in normalised values, with respect to the start of the experiment.*

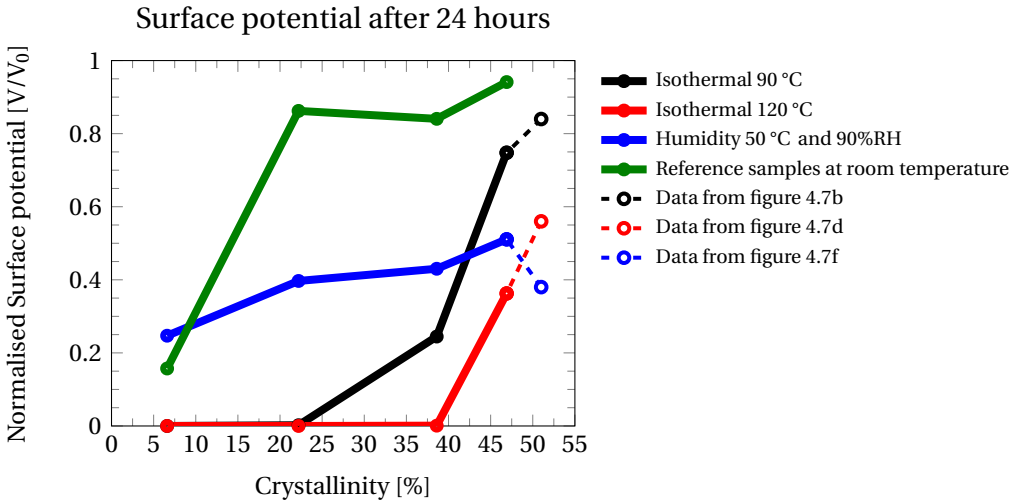

Figure 4.12: *Shows the normalised surface potential after 24 hours versus the sample crystallinity, for the isothermal and humidity experiments presented in this section. A clear tendency is seen, between increased crystallinity and increased charge retention.*

Figure 4.13a, figure 4.13c and figure 4.13e show the measured thermally stimulated potential decay and figure 4.13b, figure 4.13d and figure 4.13f show the corresponding calculated thermally stimulated current, for the four sample types at three different linear heating rates. The used heating rates were 1 K/min, 3 K/min and 7.5K/min. The first to be notice between the thermally stimulated current figures is that as the heating rates are increased so are the magnitude of the peaks and the area under the peaks; be aware of the y-axis scaling in figure 4.13b, figure 4.13d and figure 4.13f. Another thing that is also seen, as the heating rate is increased is, that the position of the current peaks are shifted upwards in temperature and more peaks are revealed. These two effects are very distinct between figure 4.13b and figure 4.13f. In figure 4.13f multiple peaks have been introduced, compared with figure 4.13b, for the samples consisting of 100 % i-PP (black curves) and $^2/_3$*i-PP and* $^1/_3$*a-PP* (red curves). Also the current peak in figure 4.13f, for the sample consisting of $^1/_3$*i-PP and* $^2/_3$*a-PP* (blue curve) has been broad, compared to the released current for the same sample type in figure 4.13b, indicating two, or more, current peaks that have fused into one broad in figure 4.13f. All these effects fit well with the theory described in section 2.4. When comparing the different sample types within the same heating rate, it is seen the same tendency as from the isothermal experiments. Namely that the samples with the highest degree of crystallinity shows the best charge retention. From figure 4.13b, which is the experiments close to isothermal conditions, an understanding is achieved of the bad performance of the samples consisting of $^1/_3$*i-PP and* $^2/_3$*a-PP* and 100 % a-PP, at the 90 °C isothermal experiments. In figure 4.13b it is seen that these two samples have their main current peak under or very close to 90 °C which of course will result in a fast discharging at 90 °C. The same applies for the sample which contain $^2/_3$*i-PP and* $^1/_3$*a-PP* at the 120 °C isothermal experiment, as it has its current peak close to 120 °C; see figure 4.13b. The temperature at which the largest current peak is occurring in figure 4.13b is at 149 °C, 139 °C, 111 °C and 60 °C for the samples containing 100 % i-PP, 67 % i-PP, 33 % i-PP and 100 % a-PP respectively. These temperatures can be seen as 'critical temperatures' which the samples should be kept well below to avoid significant discharging. The term "well below" can not be well defined as it depend on the shape of the released current seen in figure 4.13b. In addition to examining the critical temperatures of the different samples types, the thermally stimulated current was also thought to reveal the activation energies of the energetic traps.

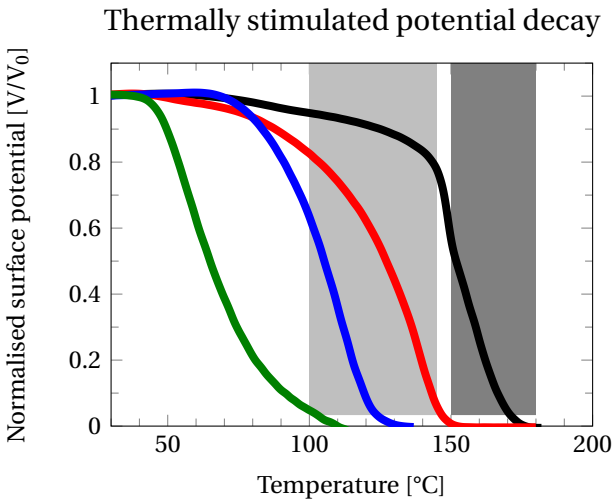

***(a)** See legend in figure **(b)**.*

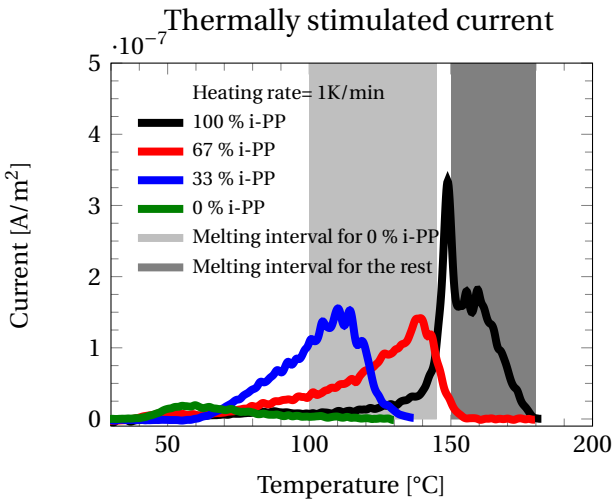

(b)

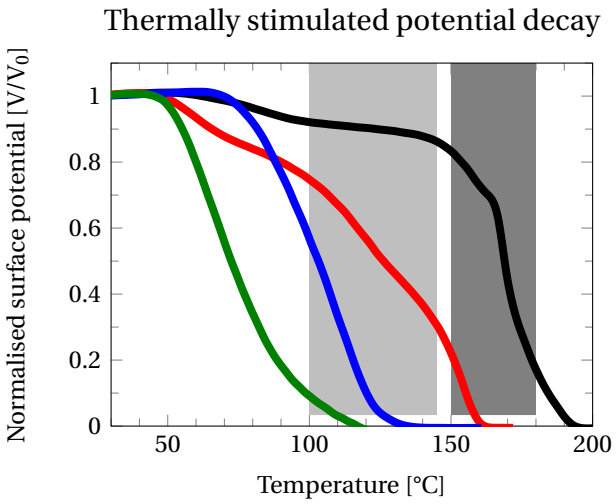

***(c)** See legend in figure **(d)**.*

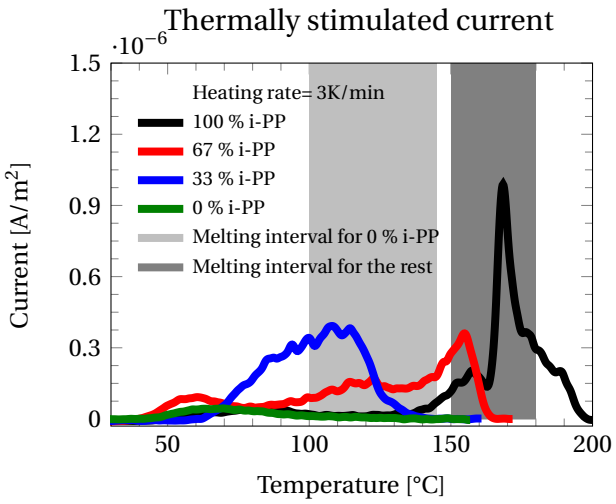

(d)

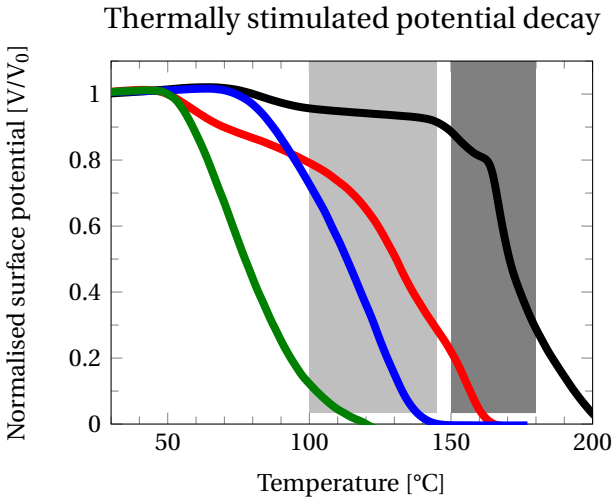

***(e)** See legend in figure **(f)**.*

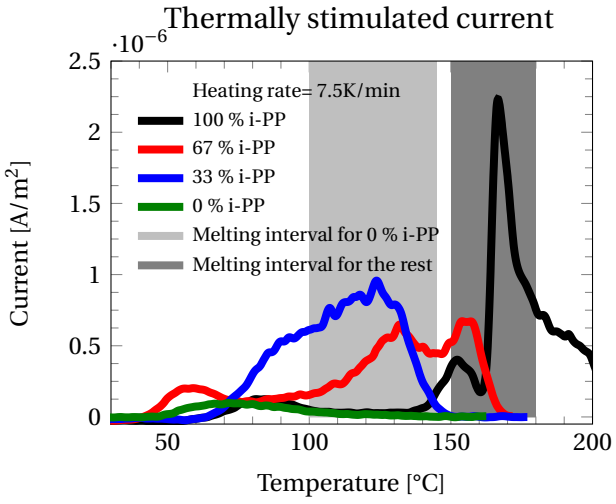

(f)

***Figure 4.13:** The graphs to the left show the thermally stimulated potential decay and the graphs to the right show the related calculated thermally stimulated currents. Three different heating rates have been used, which are stated in the right graphs legend. What is seen is that as the crystallinity is increased the current peaks are shifted towards a higher temperature, which means an electret with a better charge retention. As the heating rate is increased more peaks/traps are relieved. Both effects have also been foreseen by the theory.*

With these activation energies it should be possible to predict the potential decay either over longer periods of time at a relative low temperature compared to the electrets critical temperature or for a temperature close to the critical temperature for a short periods of time; for example at isothermal conditions at 90 °C or 120 °C.

Unfortunately most of the released current, in figure 4.13b, figure 4.13d and figure 4.13f, from the samples consisting of 100 % i-PP are within the melting interval of i-PP, making it impossible to determined any activation energies from that part of the released current, as the theory does not apply here. The same goes for some of the released current from the sample consisting of $^{2}/_{3}$*i-PP and* $^{1}/_{3}$*a-PP*. The thermally stimulated current from the two sample types with the least amount of i-PP are released before the samples enter the melting interval. Which should make it relatively easy to determined their activation energy. However, as these two samples more or less ware completely discharged within the first 2 hours at the isothermal experiments (see figure 4.11a and figure 4.11c), there is little meaning in determining their activations energies. As the accuracy of the activation energies can not be confirmed by experimental data, where both a significant potential decay and a significant charge retention are seen. Instead the focus will be on determining the activation energies for the sample consisting of 100 % i-PP and the sample consisting of $^{2}/_{3}$*i-PP and* $^{1}/_{3}$*a-PP*. The data that will be used is the released current where the heating rate was 7.5 K/min, as these data contains the most current peaks to work with.

Figure 4.14a shows the thermally stimulated current for the sample consisting of $^{2}/_{3}$*i-PP and* $^{1}/_{3}$*a-PP* at the heating rate of 7.5 K/min, along with three fits, that can describe the released current up to 150 °C. The three fits are based on the differential equation that describes the general second order reaction kinetic, which were discussed in section 2.4.2 on page 27:

$$I = -\frac{dn}{dt} = \frac{n^2}{\frac{A_n}{A_h}(N-n)+n}\nu \exp\left(\frac{-E_a}{k_b T}\right) \tag{4.1}$$

As ν, which is the attempt-to-escape frequency, and E_a, which is the activation energy, are correlated, one of them will have to be fixed to get a meaningful fit. In this thesis ν has been fixed to $\nu = 10^{13}\,\mathrm{s}^{-1}$ as ν normally is in the interval of $10^{12}\,\mathrm{s}^{-1}$ to $10^{14}\,\mathrm{s}^{-1}$ [**?**]. n is the number of electrons in the samples at any given time. N, which is the number of available traps has been set to n_0 (which is the number of charges on the electret at t=0) as it is assumed that the deepest traps are filled first, and that the effect of traps with lower energies, than occupied at $t = 0$, can be neglected. The ratio A_n/A_h describes the probability of re-trapping, where $A_n/A_h = 0$ means that re-trapping does not occur and $A_n/A_h = 1$ means that re-trapping of electrons occurs just as often as non-retrapping. There is no theoretical upper limit for the A_n/A_h ratio. For the three fits seen in figure 4.14a the A_n/A_h ratio has been fixed to $A_n/A_h = 0.5$ as this value gives the best fit to the flange (the right side of a current peak) of the three different current peaks. The activation energies for the three fits have been determined from the temperature position of the current peaks by numerical approach. After determining the activation energies for fit A and fit C, which were 0.98 eV and 1.21 eV respectively, the activation energy for fit B could be determined from the peak that occurred when subtracting fit A and fit C from the experimental data. The activation energy for fit B was determined to 1.09 eV. The sum of fit A, B and C account for 70 % of the released current in figure 4.14a and it is therefore fair to assume, the existence of minimum one more trap

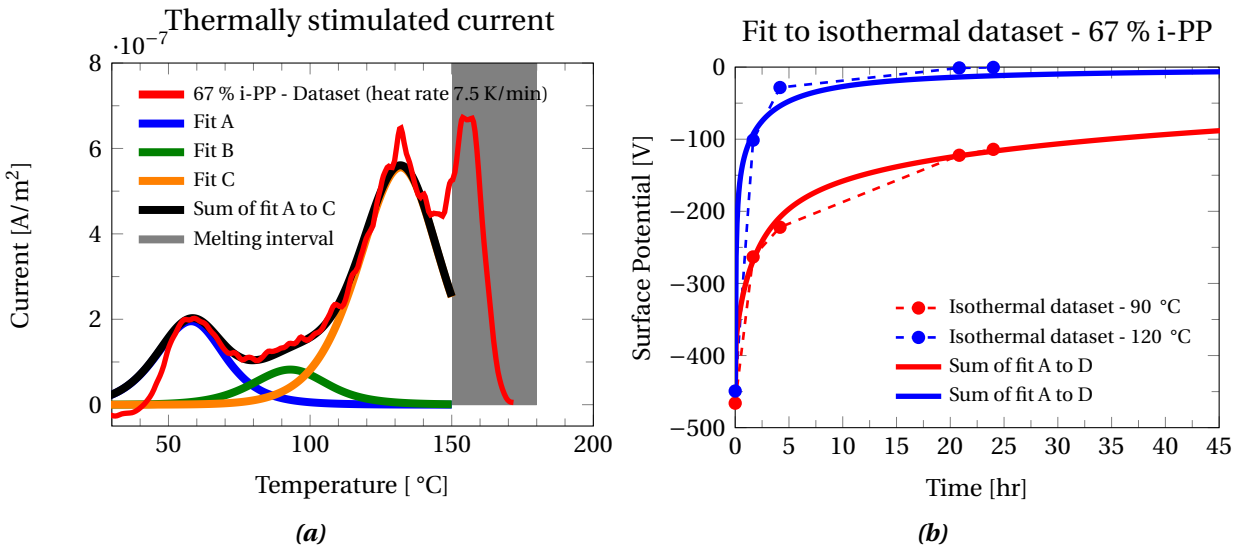

(a) ***(b)***

Figure 4.14: ***(a)*** *Shows the calculated released current for the sample type consisting of* 2/3 i-PP and 1/3 a-PP *at a heating rate of 7.5 K/min, along with three fits that accounts for the released current up to the melting of the sample. The three activations energies along with other relevant parameters for the fits can be seen in table 4.4.* ***(b)*** *Shows, for the sample type consisting of* 2/3 i-PP and 1/3 a-PP*, the theoretical isothermal potential decay (solid curves), together with the experimental data (dots) presented in figure 4.11a and figure 4.11c. The theoretical potential decay is based on the three activations energies determined from figure 4.14a and a fourth activations energies determined from a best fit approach to the* 90 °C *isothermal experimental data (red dots). As seen the theoretical predicted potential decay fits very well with the experimental data. The fourth activation energy and the two fits* R^2 *values are seen in table 4.4.*

(67 % i-PP)	**Based on**	**Weighting**	**$E_{\#}$ [eV]**	**Peak Temperature**
Fit A	TSC†	14.2 %	0.98	58 °C
Fit B	TSC	6.6 %	1.09	93 °C
Fit C	TSC	49.1 %	1.21	132 °C
Fit D	TSPD‡	30.1 %	1.30	161 °C
$\nu = 10^{13}\,\mathrm{s}^{-1}$	N=n_0	$A_n/A_h = 0.5$	$R^2_{90\,^\circ\mathrm{C}} = 0.997$	$R^2_{120\,^\circ\mathrm{C}} = 0.993$

Table 4.4: *Show the activation energies, and other relevant parameters for the four fits in figure 4.14a and figure 4.14b.* † *Thermally stimulated Current.* ‡ *Thermally stimulated Potential Decay.*

with an activation energy above 1.26 eV; which correspond to a current peak above 150 °C. The activation energy of this fourth trap will be determined in a little while. The weighting of the different fits in figure 4.14a has been determined by comparing the area under the curves with the area under the calculated released current (the red curve). All the above mentioned values are summarise in table 4.4.

The last trap, which is assumed to exist with an activation energy above 1.26 eV, can be determined from the isothermal experiments by a best fit approach. The term "best-fit approach" corves how equation (4.1) has been mathematical fitted to experimental data points.

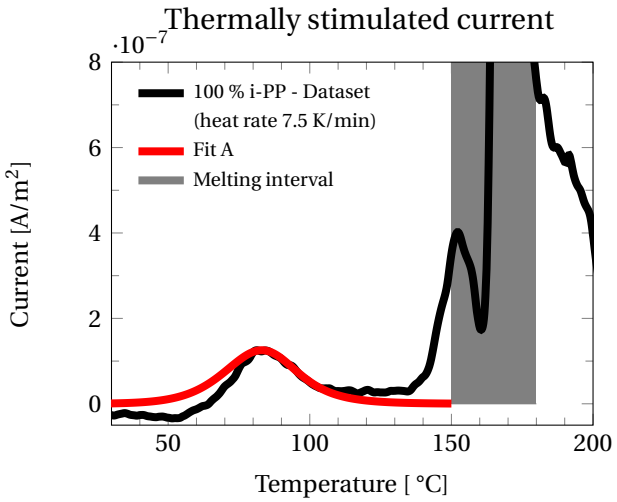

Figure 4.15: *Shows the calculated released current for the sample type consisting of 100 % i-PP at a heating rate of 7.5 K/min. Only one current peak is seen before the sample begins to melt, meaning that only one activation energy can be determined from the thermally stimulated current. The activation energy along with other relevant parameters for the fit can be seen in table 4.5.*

MATLAB [**?**] has been used for this purpose with the build in function *lsqcurvefit* which is a solver for non-linear curve-fitting problems in least squares sense. The last and fourth activation energy was determined by using the three activation energies and their weighting determined from figure 4.14a, and then assuming the existence of one more trap that should account for the last 30 % of the charges. This has been done using the 90 °C isothermal data, giving an activation energy for the last trap on 1.30 eV. The uncertainty from the fit on this activation energy is ±0.004 eV, which is much smaller than the uncertainty given by the fixed value of ν; this was discussed in section 2.4.2 on page 30. The solid red and blue curve in figure 4.14b is the theoretical potential decay at 90 °C and 120 °C respectively for the sample type consisting of $^2/_3$*i-PP and* $^1/_3$*a-PP* using the four above determined activation energies and their weighting. As seen the theoretical predicted decay fits very well with what has been observed experimentally the first 24 hours, and when extrapolating the fits beyond the first 24 hours the predicted decay seems reasonable. The coefficient of determination (R^2-values) for the two predicted decays in figure 4.14b are 0.997 and 0.993 for the 90 °C fit and the 120 °C fit respectively. These values are also summarise in table 4.4.

The determination of the activation energies for the sample consisting of 100 % i-PP is done with the same approach as for the sample consisting of $^2/_3$ *i-PP and* $^1/_3$ *a-PP* . However, as seen in figure 4.15, only a single current peak is visible, for the released current with a heating rate of 7.5 K/min. before the sample begins to melt. As the current peak is located at 83 °C the activation energy is 1.06 eV with $\nu = 10^{13}\,\mathrm{s}^{-1}$, $A_n/A_h = 0.5$ and $N = n_0$. The weighting of fit A in figure 4.15 has been determined to 10.7 % of the total released current. The above mentioned values are also summarised in table 4.5. From the released current in figure 4.15 it is fair to assume the existence of minimum one more trap with an activation energy above 1.26 eV; which, as previously mentioned, corresponds to a current peak above 150 °C.

In figure 4.16a a best fit approach, only using the data from the 90 °C isothermal experiment, is seen for the sample consisting of 100 % i-PP. This has been done using the activation energy and its weighting determined from the released current in figure 4.15 and the assumption of

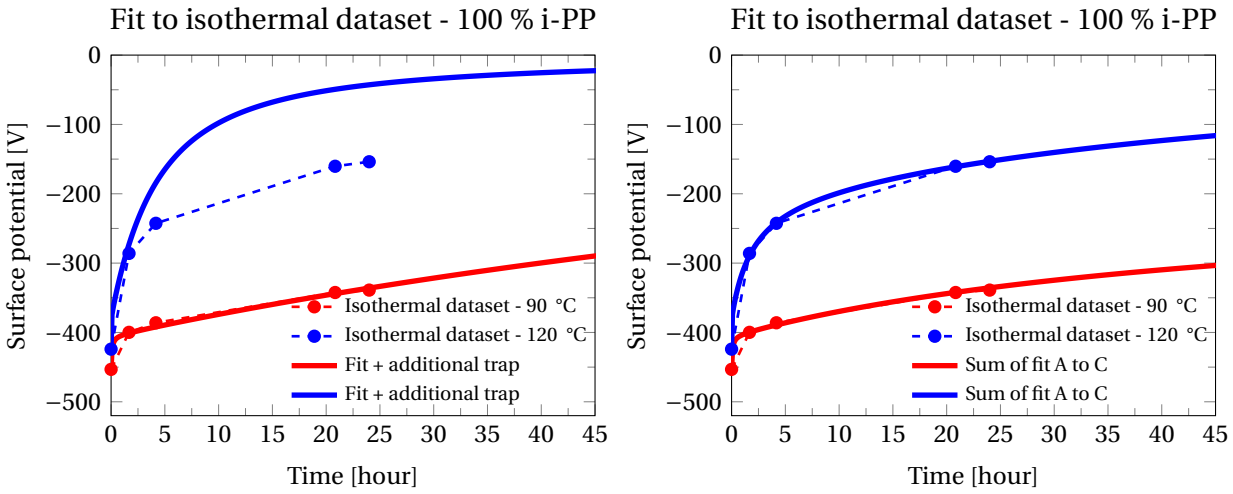

***(a)** - with one additional trap* *(b) - with two additional traps*

***Figure 4.16:** Shows, for the sample type consisting of 100 % i-PP, the theoretical isothermal potential decay (solid curves), together with the experimental data (dots) presented in figure 4.11a and figure 4.11c. **(a)** The theoretical potential decay based on the activation energy determined from figure 4.15 and **one** additional activation energy determined from a best fit approach to the 90 °C isothermal experimental data (red dots). **(b)** The theoretical potential decay based on the activation energy determined from figure 4.15 and **two** additional activation energies determined from a best fit approach to both the 90 °C and 120 °C isothermal experimental data (red and blue dots). As seen the theoretical predicted potential decay fits very well with the experimental data. All three activation energies and the two fits R^2-values are seen in table 4.5.*

(100 % i-PP)	**Based on**	**Weighting**	**$E_{\#}$ [eV]**	**Peak Temperature**
Fit A	TSC†	10.7 %	1.06	83 °C
Fit B	TSPD‡	40.3 %±2.7%	1.29	161 °C
Fit C	TSPD	49.0 %±2.7%	1.41	199 °C
$\nu = 10^{13}\,\mathrm{s}^{-1}$	N=n_0	$A_n/A_h = 0.5$	$R^2_{90\,^{\circ}\mathrm{C}} = 0.998$	$R^2_{120\,^{\circ}\mathrm{C}} = 1.000$

***Table 4.5:** Show the activation energies, and other relevant parameters for the fits in figure 4.15 and figure 4.16b.† Thermally stimulated Current. ‡ Thermally stimulated Potential Decay.*

one more trap that should account for the rest of the charges. The result is a good fit to the data from the 90 °C isothermal experiment, with the additional trap with an activation energy of 1.34 eV. However, when trying to describe the decay for the 120 °C isothermal experiment, with the two above mentioned activation energies it resulted, as seen by the blue curve in figure 4.16a, in a significant underestimation of the charge retention. This indicates that there exist yet another trap with an activation energy above 1.34 eV, which will result in a larger charge retention for the fit at 120 °C.

Figure 4.16b shows the results of a best fit approach to the data from both the 90 °C and the 120 °C isothermal experiments. The activation energy and its weighting determined from the realised current in figure 4.15 has been used together with the assumption of two additional

traps that should account for the rest of the charges. This resulted in the two activation energies of 1.29 eV and 1.41 eV with the weightings 40.3 % and 49.0 % respectively. Both activation energies, theoretical current peaks lies well in or above the melting interval of i-PP; at 161 °C and 199 °C respectively. As see in figure 4.16b, the theoretical predicted decay fits very well with the experimental data from the 90 °C and the 120 °C isothermal experiments. Moreover, when extrapolating the fits beyond the first 24 hours the predicted decay seems reasonable. The R^2-values for the two predicted decays in figure 4.16b are 0.998 and 1.000 for the 90 °C fit and the 120 °C fit respectively. The above mentioned values are also summarise in table 4.5.

The determination of the activation energies for the samples consisting of 100 % i-PP and $^2/_3$ *i-PP and* $^1/_3$ *a-PP* have shown that the theory discussed in section 2.4 can describe the potential decay for electrets, giving a powerful tool of estimating the lifetime of an electret at different thermal conditions.

4.5 Summary

No improvement in the charge retentions was seen with the imprinted surfaces. In spite of the fact that, it is here the charges are located. Instead it was seen that the sample preparation had a much larger influence on the charge retention, than a structured surface. The largest difference was seen between the samples types *levelled surface* and *levelled surface which had been slowly cooled*. The difference between these two types of sample, for the normalised surface potential after 24 hours, was for the isothermal experiments at 90 °C, isothermal experiments at 120 °C, and the humidity induced potential decay, 16 %-point, 8 %-point and 10 %-point respectively.

In the experiments where particles were introduced to the polymer matrix it was seen that, aluminium oxide and calcium carbonate could enhance the charge stability. At the 90 °C isothermal experiments it was seen that the sample with no particles, after 24 hours had 81 % left of its initial potential. For the samples with calcium carbonate particles, aluminium oxide micron-size particles and aluminium oxide nano-size particles the corresponding numbers were 95 %, 92 % and 96 % respectively. What was also seen from the particle experiments, was that the sample preparation, has an equally large influence, on the electret charge retention, as the particles themselves.

From the experiments where the cooling rate was controlled it was seen that the size of the spherulites and the number of the spherulites had a great influence on the charge retention in polypropylene. As the size of the spherulites became smaller and as the spherulites grew in numbers the charge retention was increased. This indicates that the crystalline areas in an electret material plays a significant role for the charge retention. A huge difference was also seen in the thermally stimulated current, where the location of the maximum current was at 171 °C and 151 °C for the sample type with *small spherulites* and *large spherulites* respectively. However, as these temperatures lied within the melting interval (150 °C to 180 °C) of polypropylene the activations energies for theses samples could not be determined, as the theory described in chapter 2, regarding activation energies, only apply for materials where the phase state is preserved. The series of experiments where different cooling rates were

used, could not be conducted while the degree of the crystallinity was held constant, for this reason a-PP was mixed with i-PP.

By mixing a-PP with i-PP the degree of crystallinity could be controlled while all other sample preparation parameters could be kept identical. In this way four sample types with different degree og crystallinity was obtained. Here it was seen that the sample with the highest degree of crystallinity showed the best charge retention. And that the importance of the crystallinity is increased with increased temperature. For the two samples with the highest degree of crystallinity, it were possible to determined the activation energies for their traps. This was done using the data form the thermally stimulated current and the isothermal experiments. Here it was shown that the theory discussed in section 2.4 can be used to describe the potential decay for an electret material. Another thing revealed by the thermally stimulated current was the 'critical temperatures' which the samples should be kept well below to avoid significant discharging. The term "well below" can not be well defined as it depends on the shape, of the released current as a function of temperature.

Chapter 5

CONCLUSION

The goals of this Ph.D. project have been to get a broader understanding of the key parameters that influence the charge stability of polymer electrets and how the charges are distributed. This has been archived using polypropylene as an electret polymer model system. Polypropylene was chosen as the polymer for the model system due to the limited charge lifetime compared to other much more stable electrets, e.g. fluoropolymers. This made it possible to study the performance of polypropylene as an electret material much faster than other more stable electret polymers.

Theoretical considerations about the crystalline regions, known as spherulites, in polypropylene were made under the assumption that these regions support the best trap sites for electrical charges. From these considerations two conclusions could be drawn:

- If it is the number of spherulites that is the critical parameter for the charge retention, an electret with many small spherulites would significantly outperform an electret with fewer larger spherulites; both having the same crystallinity.
- If it is the accessible area/volume of the spherulites that is the critical parameter for the charge retention, an electret with high crystallinity will outperform an electret with low or zero crystallinity, regardless the size of the spherulites.

It turns out that both the number of spherulites and the degree of crystallinity plays a significant role, one that should not be overlooked, regarding polypropylenes charge retention. This will be elaborated in a little while.

Samples with an imprinted surface, levelled and not levelled (undulated) surfaces and levelled surface which had been slowly cooled, were prepared. From a series of experiments, it was seen that the sample preparation had a much larger influence on the charge retention, than an imprinted surface. In fact no improvement or deterioration in the charge retentions, was seen for samples with an imprinted surface. This observation was made in spite of the fact that it is at the surface the charges are located. The largest difference between the above mentioned samples were between the samples types *levelled surface* and *levelled surface which had been slowly cooled*. In general terms is could be concluded, regarding charge retention, that a non-levelled surface is better than a levelled surface which had been slowly cooled, and that a levelled surface is better than a surface that has not been levelled:

$$\underbrace{\text{Levelled surface} > \text{not levelled surface} > \text{levelled surface which had been slowly cooled}}_{\text{charges stability}}$$

The influence of the particles, silicon dioxide, calcium carbonate and aluminium oxide, on polypropylenes charge retention was investigated in a master project made by Theofanis Spanos [**?**]. In these experiments particles were introduced to the polymer matrix and it was seen that, aluminium oxide and calcium carbonate could enhance the charge stability. What was also seen from the particle experiments, was that the sample preparation, seemed to have an equally large influence, on the electret charge retention, as the particles themselves.

The size of the spherulites in polypropylene was controlled through different cooling methods, from polypropylenes melted state. The spherulites were visualised with a scanning electron microscope, after a selective etch to enhance the contrast between the amorphous and crystalline regions. The effect on polypropylene charge retention was very clear. The smaller the spherulites were and the more there were of them, the better. This shows that the crystalline regions, and in particular the size of the spherulites, in polypropylene as an electret material, plays a significant role, for the charge retention. Three different cooling methods were used, designated: *slowly cooled*, *medium cooled* and *fast cooled*, resulting in spherulites in three different size intervals, 50 µm to 100 µm, 3 µm to 7 µm, and 0.7 µm to 1.5 µm respectively. Isothermal experiments at 90 °C and 120 °C were conducted, where it was seen that the largest difference in charges retention was between the samples that had been *slowly cooled* and *fast cooled*. A huge difference was also seen in the thermally stimulated current, where the location of the maximum current was at 171 °C and 151 °C for the sample type *fast cooled* and *slowly cooled* respectively. However, as these temperatures lies within the melting interval (150 °C to 180 °C) of polypropylene the activation energies for the samples could not be determined, as the theory described in chapter 2, regarding activation energies, only applies for materials where the phase state is preserved.

The experiments where the cooling rate had been controlled could not be conducted while the degree of the crystallinity was kept constant, for this reason a-PP was mixed with i-PP. In this way the degree of crystallinity could be controlled in the samples, while all other preparation parameters could be kept identical. In these experiments four samples with crystallinity ranging from 7 % to 47 % was produced. The conclusion from these experiments were also very clear, namely that the charges retention is favoured by high crystallinity. This becomes more pronounced at higher temperatures, meaning that the effect of high crystallinity plays a larger role for the charge retention when the electret samples are exposed to higher temperatures. The activation energies for the traps in the two samples with the highest crystallinity (47 % and 39 %) could be determined from the thermally stimulated current and the isothermal experiments. Here it was shown that the theory discussed in section 2.4 can be used to describe the potential decay for an electret material. Three traps were determined for the sample with a crystallinity of 47 % and four traps were determined for the sample with a crystallinity of 39 %. Another thing reviled by the thermally stimulated current was the 'critical temperatures' which the samples should be kept well below to avoid significant discharging. The 'critical temperature' is here defined as the temperature where the largest current peak occurs, for a heating rate as close to isothermal conditions as possible, in this case a heating rate of 1 K/min. The term "well below" can not be well defined as it depend

on the shape of the released current as a function of temperature. The 'critical temperature' for the four sample types were, 149 °C, 139 °C, 111 °C and 60 °C for the sample with the crystallinities of 47 %, 39 %, 22 % and 7 % respectively.

Chapter 6
OUTLOOK

The work done in this thesis has given a broader understanding of which key parameters that influence the charge stability of polypropylene electrets, and how the charges are distributed. However, a lot is still unknown. First of all it would be extremely relevant to investigate if the effects seen in polypropylene, regarding the degree of crystallinity and the size of the crystalline region, also happens in other semi-crystalline polymers, such as Fluorinated Ethylene Propylene (FEP). Time unfortunately prevented this from being investigated.

Sample preparation, which ensured the formation of spherulites at the surface was used. This was done so the effect of the crystalline regions could be studied. As the importance of these regions now are known, it could be of interest to study how the charge retention of an electret is affected by a transcrystalline surface. A transcrystalline surface, which were mentioned in section 2.3, has that intriguing property that the surface has a crystallinity close to 100 % due to all of the crystals that have grown perpendicular to the surface.

The study of the effect by a transcrystalline surface could be combined with a study of the metal choice as the back electrode. As this metal layer could have an influence on the surface crystallinity if the polymer layer are thin enough (below 100 μm), and in the case where the surface is not in contact with another solid material upon cooling, from its melted state.

In this thesis a good understanding was achieved on how the charges behaves when thermally stimulated. Again this theory was only tested on polypropylene, and it would of course be relevant to investigate, if the same understanding also applies for other electret materials. What is still needed regarding discharge mechanisms, is the understanding at high humidity. It could be of great use to develop a theory that explained this. A place to start would by to investigate if it is the relative humidity or the absolute humidity that dominates the discharging of electrets, and if this process is related to how far from the dew point the discharging is occurring. Another thing to consider is whether the humidity effectively is lowering the activation energies of the traps used to explained the thermal discharging. In this case the activation energy can be seen as an function of humidity and the theory describing the thermal discharging can, after a modification of the activation energy, also be used to explain the discharging at high humidity.

Literature has already, to some extent, explained what happens when corona charging an electret at elevating temperature [**?**, **?**, **?**, **?**], it could be interesting to see if some of the same phenomenon also appearers when corona charging at high humidity. In particular if the charge retention of an electret could be enhanced in this way.

BIBLIOGRAPHY

Appendix A

"ELECTRET" SEARCH AT DTU DATABASE

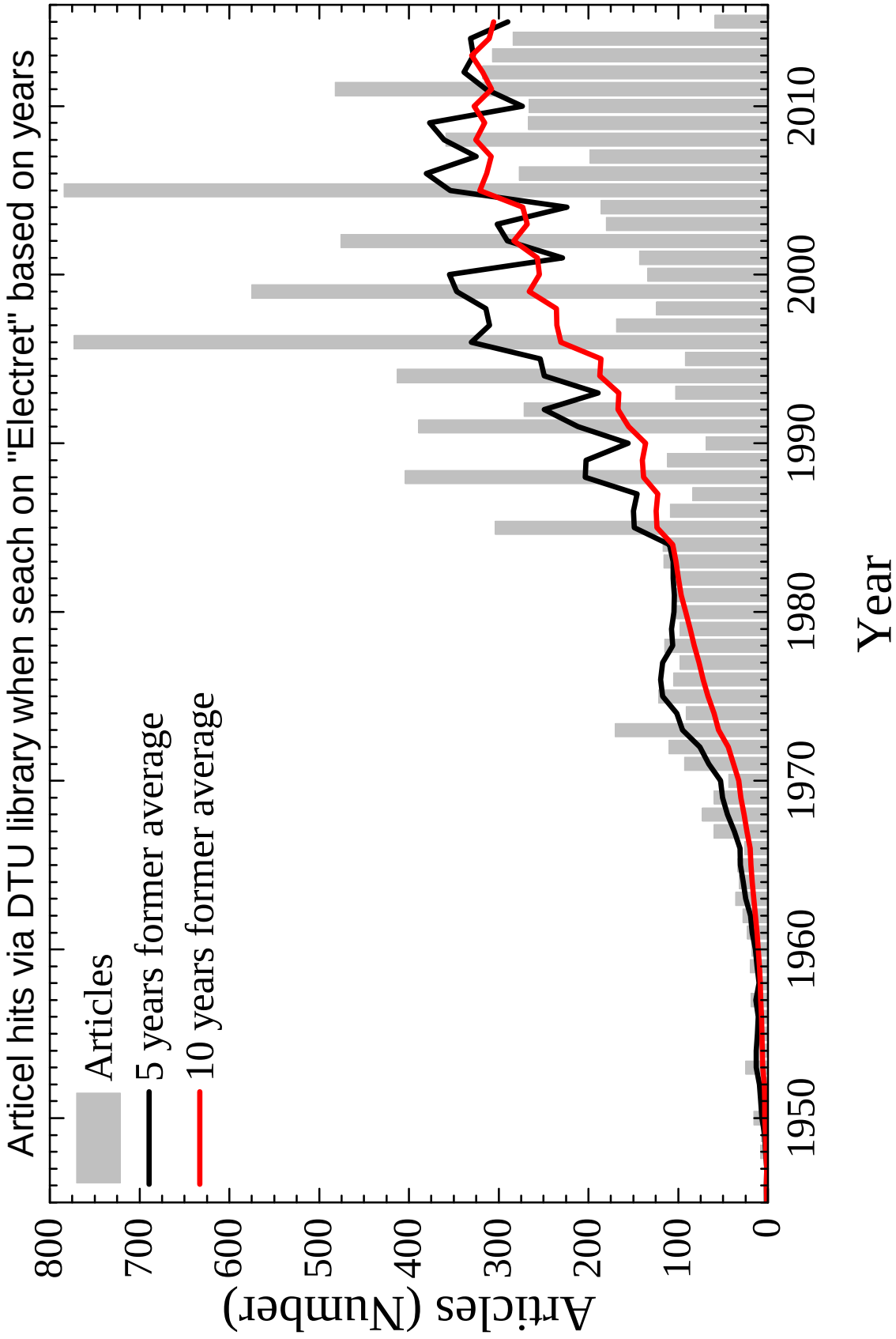

Figure A.1: *The figure shows the number of articles that appears when only using the word "electret" at the DTU article database. The data is from 27-05-2015. http://www.bibliotek.dtu.dk/*

Appendix B

ACTIVATION ENERGY

This appendix is a supplement to section 2.4 on page 24 in the theory chapter. The purpose of this appendix is to give a more detailed derivation of the mathematics, behind the activations energies; should this be of interested or need.

B.1 Absent Re-trapping

The decay of electrons, when **re-trapping is negligible**, is given by [**?**, **?**]:

$$I = -\frac{dn}{dt} = n\nu \exp\left(\frac{-E_a}{k_b T}\right) \tag{B.1}$$

n is the number of electrons on/in the sample at any given time, ν can be interpret as an attempt-to-escape frequency and multiply with $\exp\left(\frac{-E_a}{k_b T}\right)$, this term is the probability per unit time that an electron will escape its trap.

B.1.1 Constant Temperature

The solution to equation (B.1) for constant temperature is:

$$\begin{aligned} \int_{n_0}^{n} \frac{1}{n} dn &= -\nu \int_0^t \exp\left(\frac{-E_a}{k_b T}\right) dt \\ \ln\left(\frac{n}{n_0}\right) &= -\nu \exp\left(\frac{-E_a}{k_b T}\right) t \\ n &= n_0 \exp\left(t\nu \exp\left(\frac{-E_a}{k_b T}\right)\right) \end{aligned} \tag{B.2}$$

Inserting equation (B.2) into equation (B.1) give: (constant temperature - no ret-rapping)

$$\underline{\underline{I = n_0 \exp\left(-t\nu \exp\left(\frac{-E_a}{k_b T}\right)\right) \cdot \nu \exp\left(\frac{-E_a}{k_b T}\right)}} \tag{B.3}$$

B.1.2 Linear Increased Temperature

Equation (B.1) can be rewritten to be a function of an linear increased temperature instead of time. This is done by changing the time variable to temperature: $T' = T_0 + \beta t \Rightarrow dt = d\left(\frac{T'}{\beta} - \frac{T_0}{\beta}\right)$. Where $T_0 = 0\,\mathrm{K}$. Giving:

$$I = -\frac{dn}{dT} = n\frac{\nu}{\beta}\exp\left(\frac{-E_a}{k_b T}\right) \tag{B.4}$$

The solution to equation B.4, for linear increased temperature is:

$$\begin{aligned}
\int_{n_0}^{n}\frac{1}{n}dn &= -\frac{\nu}{\beta}\int_0^T \exp\left(\frac{-E_a}{k_b T'}\right)dT' \\
\ln\left(\frac{n}{n_0}\right) &= -\frac{\nu}{\beta}\int_0^T \exp\left(\frac{-E_a}{k_b T'}\right)dT' \\
n &= n_0\exp\left(-\frac{\nu}{\beta}\int_0^T \exp\left(\frac{-E_a}{k_b T'}\right)dT'\right)
\end{aligned} \tag{B.5}$$

Inserting equation (B.5) into equation (B.4) give: (linear increase temperature - no re-trapping)

$$\underline{\underline{I = n_0\exp\left(-\frac{\nu}{\beta}\int_0^T \exp\left(\frac{-E_a}{k_b T'}\right)dT'\right)\cdot\nu\exp\left(\frac{-E_a}{k_b T}\right)}} \tag{B.6}$$

B.1.3 Extract the Activation Energies

If equation (B.6) is differentiated with respect to the temperature and solve for equal to zero, one have a relationship between the peak temperature, T_p and the activation energy, E_a. In the following the product rule are used $\left((f\cdot g)' = f'\cdot g + f\cdot g'\right)$:

$$\begin{aligned}
\frac{d}{dT}\left[n_0\exp\left(-\frac{\nu}{\beta}\int_0^T \exp\left(\frac{-E_a}{k_b T'}\right)dT'\right)\cdot\nu\exp\left(\frac{-E_a}{k_b T}\right)\right] &= 0 \\
n_0\exp\left(-\frac{\nu}{\beta}\int_0^{T_p} \exp\left(\frac{-E_a}{k_b T'}\right)dT'\right)\cdot\frac{E_a}{k_b T_p^2}\nu\exp\left(\frac{-E_a}{k_b T_p}\right) - & \\
\frac{n_0\nu^2}{\beta}\exp\left(\frac{-E_a}{k_b T_p}\right)^2\exp\left(-\frac{\nu}{\beta}\int_0^{T_p} \exp\left(\frac{-E_a}{k_b T'}\right)dT'\right) &= 0
\end{aligned}$$

$$\begin{aligned}
\frac{E_a}{k_b T_p^2} &= \frac{\nu}{\beta}\exp\left(\frac{-E_a}{k_b T_p}\right) \\
\frac{E_a}{k_b T_p}\cdot\frac{\beta}{\nu T_p} &= \exp\left(\frac{-E_a}{k_b T_p}\right) \qquad \text{(B.7)} \\
\underline{\underline{\frac{E_a}{k_b T_p}}} &= \underline{\underline{\ln\left(\frac{T_p\nu}{\beta}\right) + \ln\left(\frac{T_p k_b}{E_a}\right)}} \qquad \text{(B.8)}
\end{aligned}$$

Equation (B.8) can also be obtained by directly differentiating equation (B.4). By a graphical determination it is found that if the therm $\ln\left(T_p k_b / E_a\right)$ is set to -3.52 the relation between E_a and T_p is given to ±0.5 %, within the intervals $10^{12} < \nu/\beta < 10^{16}$ and $273 < T_p < 773$ (°K), by the relationship:

$$\underline{\underline{\frac{E_a}{k_b T_p} \approx \ln\left(\frac{T_p \nu}{\beta}\right) - 3.52}} \tag{B.9}$$

Figure B.1 shows the error the approximation made in equation (B.9) give for different ratios of ν/β.

From equation (B.7), ν can be expressed by the peak temperature as:

$$\begin{aligned} \frac{E_a}{k_b T_p} \cdot \frac{\beta}{\nu T_p} &= \exp\left(\frac{-E_a}{k_b T_p}\right) \\ \nu &= \exp\left(\frac{E_a}{k_b T_p}\right) \frac{\beta E_a}{k_b T_p^2} \end{aligned} \tag{B.10}$$

Inserting equation (B.10) into equation (B.6) yields:

$$I(T) = n_0 \exp\left(-\exp\left(\frac{E_a}{k_b T_p}\right) \cdot \frac{E_a}{k_b T_p^2} \int_0^T \exp\left(\frac{-E_a}{k_b T'}\right) dT'\right) \cdot \frac{\beta E_a}{k_b T_p^2} \exp\left(\frac{E_a}{k_b T_p}\right) \exp\left(\frac{-E_a}{k_b T}\right) \tag{B.11}$$

which then can be used in a fitting routine for the release current experimental obtained. A full fit with equation (B.11) is easiest done by a fitting routine, which can run many iteration in a short amount of time. This is a bit more comprehensive method than just using the peak temperature and equation (B.9), but in addition to find E_a, values for ν, can also be determined, which definitely is this method strength.

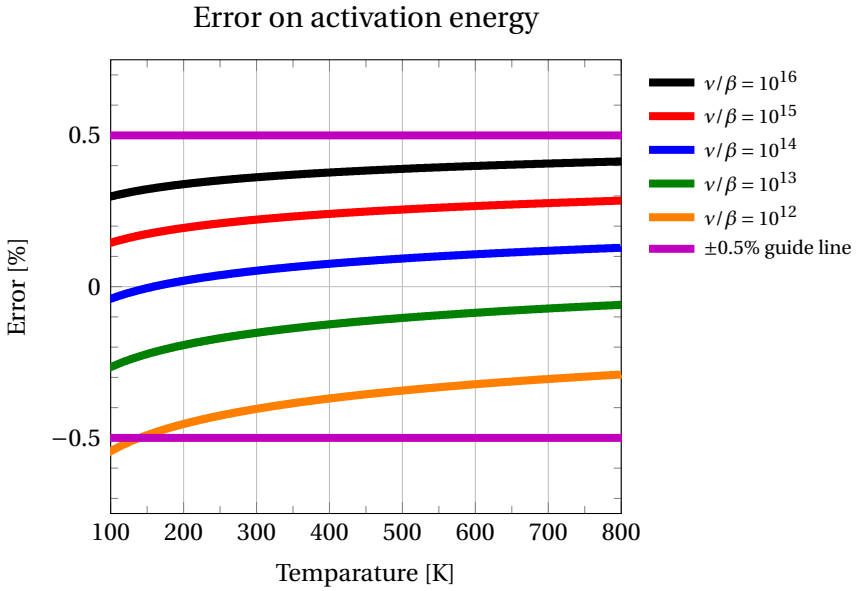

Figure B.1: *Shows the error the approximation made in equation (B.9) give for different values of ν/β.*

B.2 When Re-trapping Occurring

The decay of electrons, when **re-trapping is occurring**, are given by [**?**, **?**, **?**]:

$$I = -\frac{dn}{dt} = \frac{n^2}{\frac{A_n}{A_h}(N-n)+n}\nu \exp\left(\frac{-E_a}{k_b T}\right) \tag{B.12}$$

N being number of traps with energy E_a, A_h is the probability coefficient of an electron recombining with a hole in a recombination centre and A_n is the probability coefficient of an electron being re-trapped. The solution to equation (B.12) when $A_n/A_h = 1$ it given in the following. For $A_n/A_h \neq \{0,1\}$ an numerical approach is needed.

B.2.1 Constant Temperature

The solution to equation (B.12) for constant temperature is:

$$\begin{aligned}
\int_{n_0}^{n} \frac{1}{n^2} dn &= -\frac{\nu}{N}\int_0^t \exp\left(\frac{-E_a}{k_b T}\right) dt \\
\frac{1}{n_0} - \frac{1}{n} &= -\frac{\nu}{N}\exp\left(\frac{-E_a}{k_b T}\right) t \\
\frac{1}{n} &= \frac{\nu}{N}\exp\left(\frac{-E_a}{k_b T}\right) t + \frac{1}{n_0}
\end{aligned} \tag{B.13}$$

Inserting equation (B.13) into equation (B.12) yields:

$$I = \left(\frac{\nu}{N}\exp\left(\frac{-E_a}{k_b T}\right) t + \frac{1}{n_0}\right)^{-2} \cdot \frac{\nu}{N}\exp\left(\frac{-E_a}{k_b T}\right) \tag{B.14}$$

equation (B.14) simplified:

$$\underline{\underline{I = \frac{n_0^2 \nu}{N}\exp\left(\frac{-E_a}{k_b T}\right)\left(1 + \frac{n_0 \nu}{N}\exp\left(\frac{-E_a}{k_b T}\right) t\right)^{-2}}}$$

B.2.2 Linear Increased Temperature

Equation (B.12) can be rewritten to be a function of an linear increased temperature instead of time. This is done by changing the time variable to temperature: $T' = T_0 + \beta t \Rightarrow dt = d\left(\frac{T'}{\beta} - \frac{T_0}{\beta}\right)$. Where $T_0 = 0\,\mathrm{K}$. Giving:

$$I = -\frac{dn}{dT} = \frac{n^2}{\frac{A_n}{A_h}(N-n)+n}\frac{\nu}{\beta}\exp\left(\frac{-E_a}{k_b T}\right) \tag{B.15}$$

The solution to equation B.15, for linear increased temperature is:

$$\begin{aligned}\int_{n_0}^{n}\frac{1}{n^2}dn &= -\frac{\nu}{N\beta}\int_0^T \exp\left(\frac{-E_a}{k_bT'}\right)dT' \\ \frac{1}{n_0}-\frac{1}{n} &= -\frac{\nu}{N\beta}\int_0^T \exp\left(\frac{-E_a}{k_bT'}\right)dT' \\ \frac{1}{n} &= \frac{\nu}{N\beta}\int_0^T \exp\left(\frac{-E_a}{k_bT'}\right)dT'+\frac{1}{n_0}\end{aligned} \tag{B.16}$$

Inserting equation (B.16) into equation (B.15) yields:

$$I=\left(\frac{\nu}{N\beta}\int_0^T \exp\left(\frac{-E_a}{k_bT'}\right)dT'+\frac{1}{n_0}\right)^{-2}\cdot\frac{\nu}{N}\exp\left(\frac{-E_a}{k_bT}\right) \tag{B.17}$$

equation (B.17) simplified:

$$\underline{\underline{I=\frac{n_0^2\nu}{N}\exp\left(\frac{-E_a}{k_bT}\right)\left(1+\frac{n_0\nu}{N\beta}\int_0^T \exp\left(\frac{-E_a}{k_bT'}\right)dT'\right)^{-2}}} \tag{B.18}$$

B.2.3 Extract the Activation Energies

If equation (B.18) is differentiated with respect to the temperature and solve for equal to zero, one have a relationship between the peak temperature, T_p and the activation energy, E_a. In the following the product rule are used $\left((f\cdot g)'=f'\cdot g+f\cdot g'\right)$:

$$\begin{aligned}\frac{d}{dT}\left[\frac{n_0^2\nu}{N}\exp\left(\frac{-E_a}{k_bT}\right)\left(1+\frac{n_0\nu}{N\beta}\int_0^T \exp\left(\frac{-E_a}{k_bT'}\right)dT'\right)^{-2}\right] &= 0 \\ \frac{n_0^2\nu E_a}{Nk_bT_p^2}\exp\left(\frac{-E_a}{k_bT_p}\right)\cdot\left(1+\frac{n_0\nu}{N\beta}\int_0^{T_p} \exp\left(\frac{-E_a}{k_bT'}\right)dT'\right)^{-2} - & \\ \frac{n_0^2\nu}{N}\exp\left(\frac{-E_a}{k_bT_p}\right)\cdot\frac{2n_0\nu}{N\beta}\exp\left(\frac{-E_a}{k_bT_p}\right)\left(1+\frac{n_0\nu}{N\beta}\int_0^{T_p} \exp\left(\frac{-E_a}{k_bT'}\right)dT'\right)^{-3} &= 0\end{aligned}$$

$$
\begin{aligned}
\frac{n_0^2 \nu E_a}{N k_b T_p^2} &= \frac{2 n_0^3 \nu^2}{N^2 \beta} \exp\left(\frac{-E_a}{k_b T_p}\right)\left(1 + \frac{n_0 \nu}{N\beta}\int_0^{T_p} \exp\left(\frac{-E_a}{k_b T'}\right) dT'\right)^{-1} \\
\frac{E_a}{k_b T_p^2} &= \frac{2 n_0 \nu}{N\beta} \exp\left(\frac{-E_a}{k_b T_p}\right)\left(1 + \frac{n_0 \nu}{N\beta}\int_0^{T_p} \exp\left(\frac{-E_a}{k_b T'}\right) dT'\right)^{-1} \\
\frac{E_a}{k_b T_p^2} &= 2\exp\left(\frac{-E_a}{k_b T_p}\right)\cdot\left(\frac{n_0 \nu}{N\beta} + \int_0^{T_p} \exp\left(\frac{-E_a}{k_b T'}\right) dT'\right)^{-1} \\
\exp\left(\frac{-E_a}{k_b T_p}\right) &= \frac{E_a}{2 k_b T_p}\left(\frac{N\beta}{n_0 \nu T_p} + \frac{1}{T_p}\int_0^{T_p} \exp\left(\frac{-E_a}{k_b T'}\right) dT'\right) \\
\frac{-E_a}{k_b T_p} &= \ln\left(\frac{E_a}{2 k_b T_p}\right) + \ln\left(\frac{N\beta}{n_0 \nu T_p} + \frac{1}{T_p}\int_0^{T_p} \exp\left(\frac{-E_a}{k_b T'}\right) dT'\right) \\
\underline{\underline{\frac{E_a}{k_b T_p}}} &= \underline{\underline{\ln\left(\frac{2 k_b T_p}{E_a}\right) - \ln\left(\frac{N\beta}{n_0 \nu T_p} + \frac{1}{T_p}\int_0^{T_p} \exp\left(\frac{-E_a}{k_b T'}\right) dT'\right)}}
\end{aligned}
\tag{B.19}
$$

As $\frac{1}{T_p}\int_0^{T_p} \exp\left(\frac{-E_a}{k_b T'}\right) dT' \ll \frac{N\beta}{n_0 \nu T_p}$ it can be neglected, and by a graphical determination it is found that if the therm $-\ln\left(2T_p k_b / E_a\right)$ is set to -3.47 the relation between E_a and T_p is given to $\pm 0.5\,\%$, within the intervals $10^{12} < \nu n_0/\beta N < 10^{16}$ and $273 < T_p < 773$ (°K). Given by the relationship:

$$
\underline{\underline{\frac{E_a}{k_b T_p} \approx \ln\left(\frac{n_0 \nu T_p}{N\beta}\right) - 3.47}} \tag{B.20}
$$

Figure B.2 shows the error the approximation made in equation (B.20) give for different ratios of $\nu n_0/\beta N$.

From equation (B.19), ν can be expressed by the peak temperature as:

$$
\begin{aligned}
\frac{E_a}{k_b T_p} &= \ln\left(\frac{2 k_b T_p}{E_a}\right) - \ln\left(\frac{N\beta}{n_0 \nu T_p} + \frac{1}{T_p}\int_0^{T_p} \exp\left(\frac{-E_a}{k_b T'}\right) dT'\right) \\
\exp\left(\frac{-E_a}{k_b T_p}\right) &= \frac{E_a}{2 k_b T_p}\left(\frac{N\beta}{n_0 \nu T_p} + \frac{1}{T_p}\int_0^{T_p} \exp\left(\frac{-E_a}{k_b T'}\right) dT'\right) \\
\exp\left(\frac{-E_a}{k_b T_p}\right) &= \frac{E_a}{2 k_b T_p}\frac{N\beta}{n_0 \nu T_p} + \frac{E_a}{2 k_b T_p^2}\int_0^{T_p} \exp\left(\frac{-E_a}{k_b T'}\right) dT' \\
\frac{E_a}{2 k_b T_p}\frac{N\beta}{n_0 \nu T_p} &= \exp\left(\frac{-E_a}{k_b T_p}\right) - \frac{E_a}{2 k_b T_p^2}\int_0^{T_p} \exp\left(\frac{-E_a}{k_b T'}\right) dT' \\
\nu &= \left(\frac{2 n_0 k_b T_p^2}{E_a N\beta}\exp\left(\frac{-E_a}{k_b T_p}\right) - \frac{n_0}{N\beta}\int_0^{T_p} \exp\left(\frac{-E_a}{k_b T'}\right) dT'\right)^{-1}
\end{aligned}
\tag{B.21}
$$

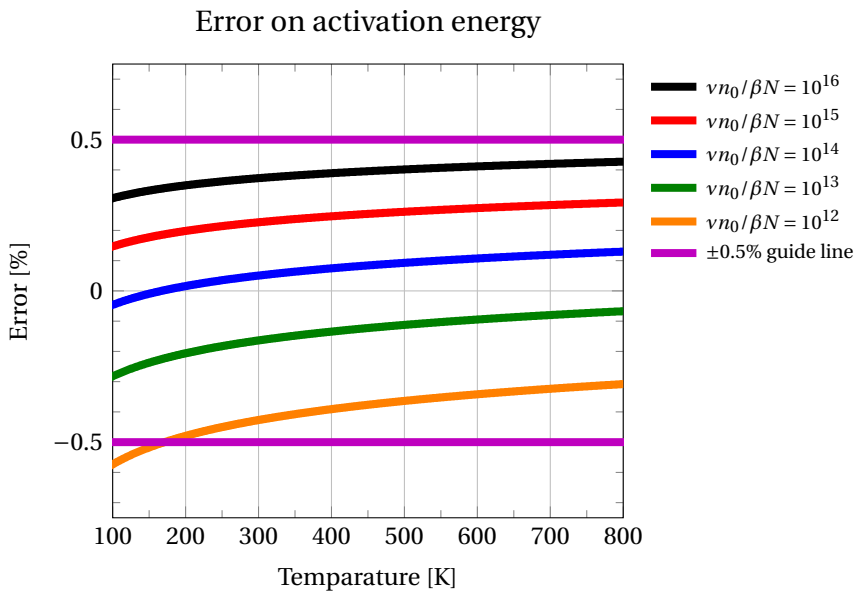

Figure B.2: *Shows the error the approximation made in equation (B.20) give for different values of* $\nu n_0/\beta N$.

Equation (B.21) can in combination with equation (B.18) be used in a fitting routine to remove ν as a variable. This can significantly make the fitting routine easier as an increasing in both ν and E_a will shift the current peak in the same direction. Unfortunately this simplification in a fitting routing is only possible when $A_n/A_h = 1$. As stated in the start of subsection 2.4.2 if $A_n/A_h \neq \{0,1\}$ an purely numerical approach is needed to describe the behaviour of the charges when thermal stimulated.

Appendix C

PRODUCT SPECIFICATION ISOTACTIC-POLYPROPYLENE

SIGMA-ALDRICH®

sigma-aldrich.com

3050 Spruce Street, Saint Louis, MO 63103, USA
Website: www.sigmaaldrich.com
Email USA: techserv@sial.com
Outside USA: eurtechserv@sial.com

Product Specification

Product Name:
Polypropylene - Isotactic, average M_w ~250,000, average M_n ~67,000

Product Number: **427888**
CAS Number: 9003-07-0
MDL: MFCD00084447
Formula: C3H6

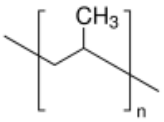

TEST	Specification
Appearance (Color)	Colorless
Appearance (Form)	Beads
Infrared spectrum	Conforms to Structure
Melt Index g/10 min; 230℃, 2.16 kg	10 - 14

Specification: PRD.0.ZQ5.10000052063

Properties

(from web site: http://www.sigmaaldrich.com/catalog/product/aldrich/427888?lang=en&region=DK)

Related Categories	Hydrophobic Polymers, Materials Science, Olefins, Polymer Science, Polymers, More...
melt index	12 g/10 min (230°C/2.16kg)
mol wt	average M_n ~67,000
	average M_w ~250,000
hardness	100 (Rockwell R, ASTM D 785-A)
transition temp	T_m 160-165 °C
density	0.9 g/mL at 25 °C(lit.)

Appendix D

PRODUCT SPECIFICATION ATACTIC-POLYPROPYLENE

Goodfellow

ACKNOWLEDGEMENT OF ORDER

Ermine Business Park
Huntingdon PE29 6WR England
Telephone +44 1480 424 800
Fax +44 1480 424 900

Your order has been entered as shown on this sheet. If your
If your requirements have been interpreted incorrectly in any respect,

Unless previously agreed by us in writing
This order is subject to our standard conditions
of sale, copies of which are available on request.

Department of Micro and Nanotechnology
Technical University of Denmark
Orsteds Plads
DK-2800 LYNGBY
DENMARK

For the attention of:
Anders Thyssen

Your order number	Anders Thyssen
	Credit Card
Date of your order	21-October-2014
Our order reference	**LS433924/A F S**
Customer reference no.	11290-76
Date of receipt of order	21-October-2014
Date of acknowledgement	7-November-2014
Despatch forecast	4-November-2014
Terms of payment	Net 30 days
Terms of despatch	Free delivered excluding Import duty and tax
Your order was placed by	E-mail

Item	Catalogue number	Description
1		Polypropylene ~~Granule~~ Waxy gel PP Condition : Atactic Molecular weight : 12,000 g/mol Quantity ordered : 500 g Price : GBP 0.29/g Physical Form : Waxy solid Molecular weight (Mw) approx : 12,000 Density : 0.85 Refractive Index : 1.4735 Brookfield viscosity : 240cp (149°C) Flash point : >149°C Softening Point - R&B : 121°C Soluble in Chlorinated hydrocarbons, diethyl ether, hydrocarbons, isoamyl acetate & toluene Insoluble in more polar organic solvents with small hydrocarbon groups even at elevated temperatures --- J N Murray 22-October-2014 : Thank you for your payment received today via credit card. ---

Despatch to:
as shown above

Original invoice to:
as shown above

Additional notes
Order being paid for by Credit Card

Charges

Goods total	145.00
UK VAT at zero %	
Invoice total GBP	145.00

Goodfellow Cambridge Limited

VAT registration GB 212 8527 79

Registered office: Units C1+C2, Spitfire Close, Ermine Business Park, HUNTINGDON PE29 6WR Registered in England and Wales no. 1188162

Appendix E

HUMIDITY POTENTIAL DECAY - IMPRINT

Additional data for section 4.1 on page 54. Se figure text.

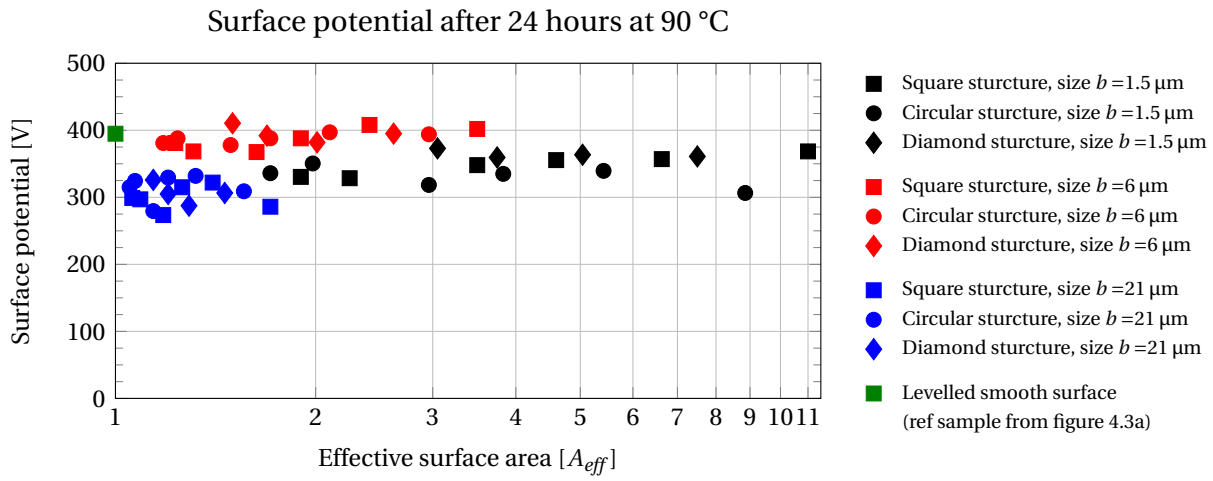

(a)

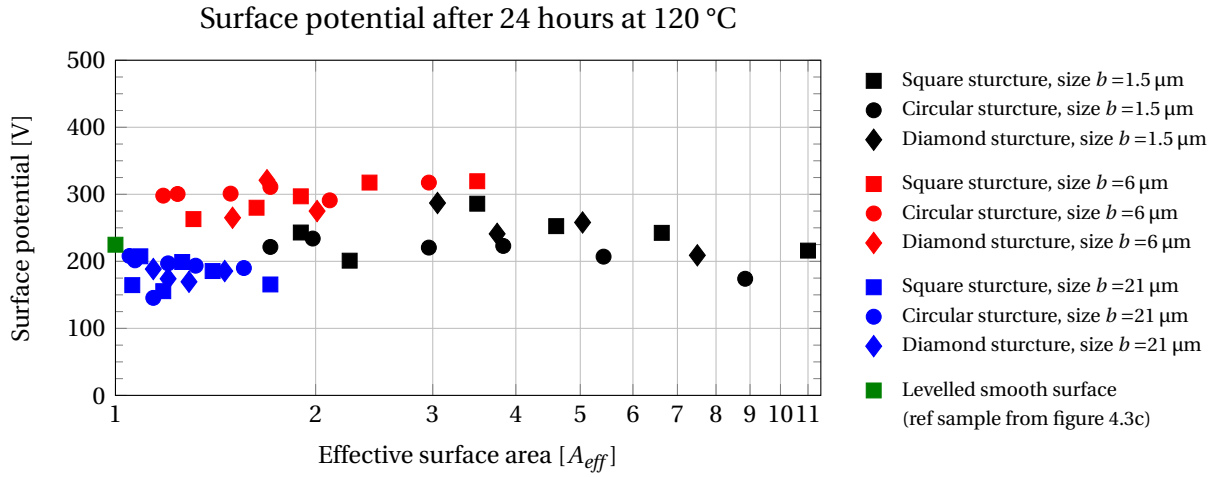

(b)

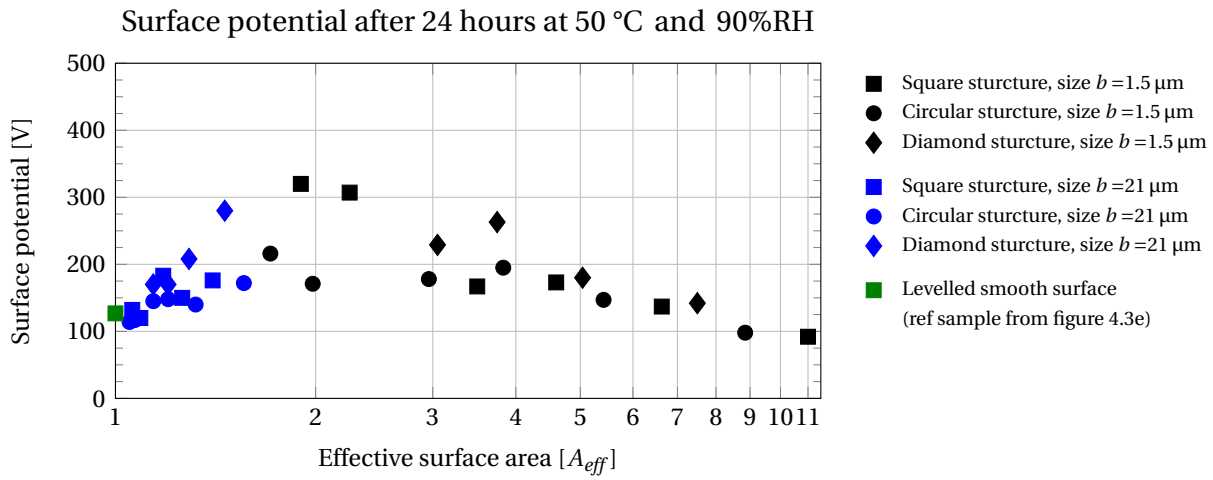

(c)

Figure E.1: *The surface potential after 24 hours, plotted against the effective surface area, for the humidity potential decay experiment. The data is for the samples with had been imprinted with a patterned to increase the effective surface area, see section 4.1.*

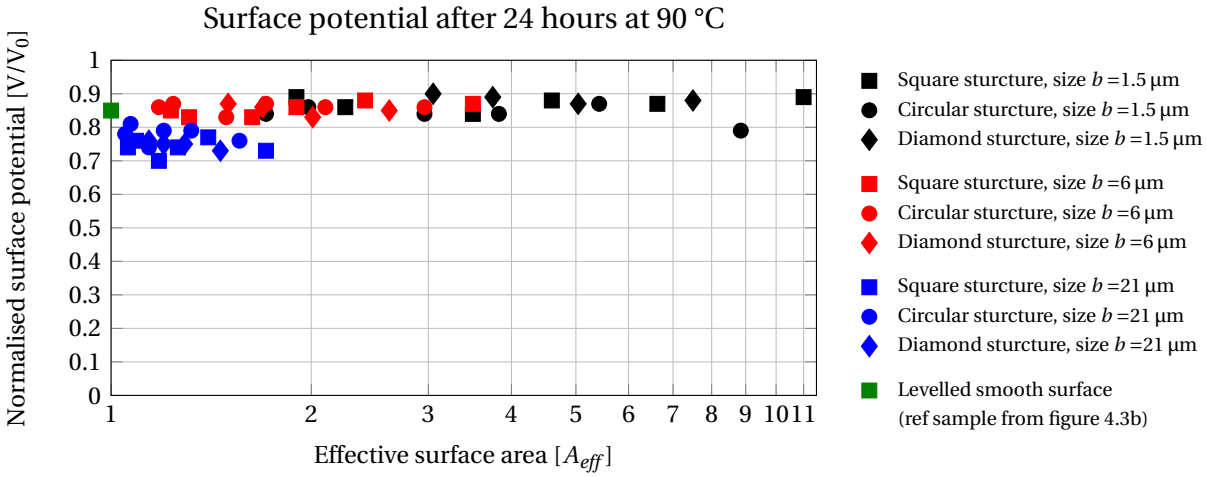

(a)

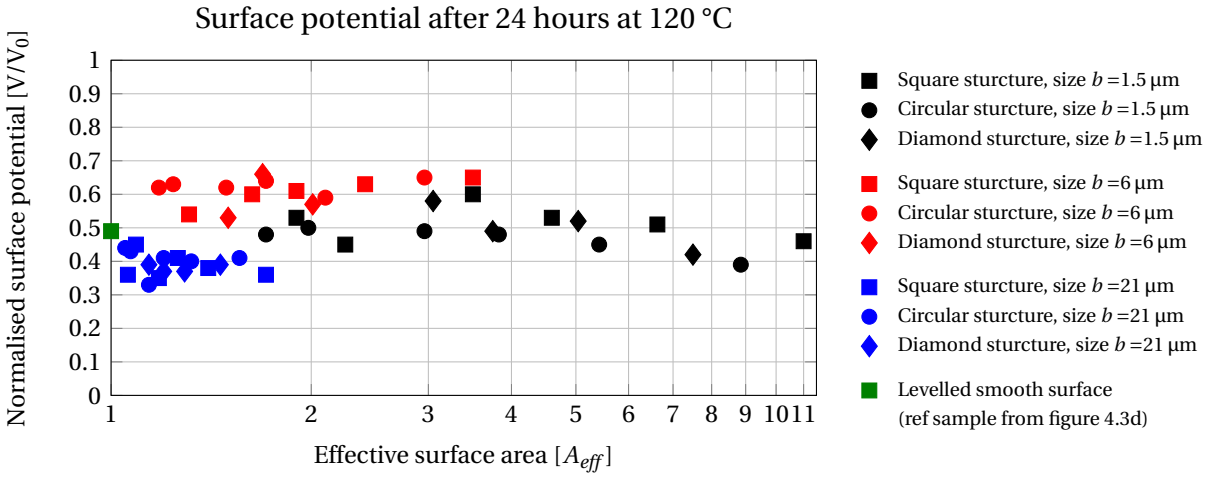

(b)

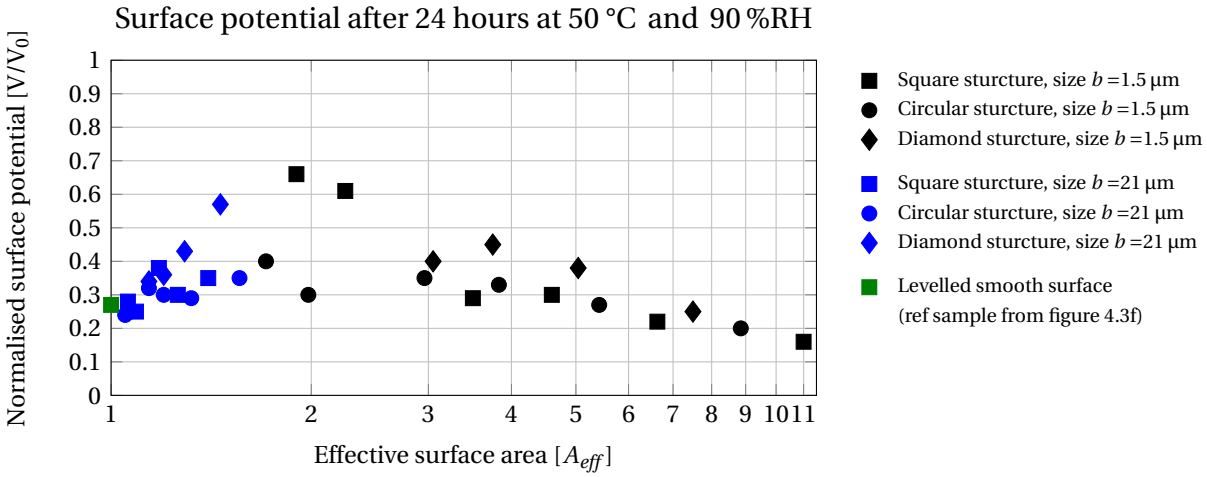

(c)

Figure E.2: *The normalised surface potential after 24 hours, plotted against the effective surface area, for the humidity potential decay experiment. The data is for the samples with had been imprinted with a patterned to increase the effective surface area, see section 4.1.*

Appendix F

PRODUCT SPECIFICATION - PARTICLES

SIGMA-ALDRICH® sigma-aldrich.com

3050 Spruce Street, Saint Louis, MO 63103, USA
Website: www.sigmaaldrich.com
Email USA: techserv@sial.com
Outside USA: eurtechserv@sial.com

Product Specification

Product Name:
Aluminum oxide – powder, ≤10 µm avg. part. size, 99.5% trace metals basis

Product Number:	**265497**
CAS Number:	1344-28-1
MDL:	MFCD00003424
Formula:	Al2O3
Formula Weight:	101.96 g/mol

Al_2O_3

TEST	Specification
Appearance (Color)	White
Appearance (Form)	Powder
X-Ray Diffraction	Conforms to Structure
Average Particle Size	≤ 10 micron
Trace Metal Analysis	≤ 6000.0 ppm
Purity	Meets Requirements
99.5% Based on Trace Metals Analysis	

Specification: PRD.0.ZQ5.10000021451

Denmark Home 544833 - Aluminum oxide

SIGMA-ALDRICH

544833 ALDRICH

Aluminum oxide

nanopowder, <50 nm particle size (TEM)

Synonym: **Alumina**

SDS SIMILAR PRODUCTS

CAS Number 1344-28-1 | **Linear Formula** Al_2O_3 | **Molecular Weight** 101.96 | **EC Number** 215-691-6

MDL number MFCD00003424 | **PubChem Substance ID** 24878787 | **eCl@ss** 38120402

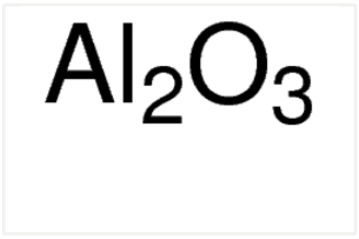

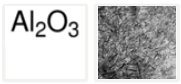

Properties

Related Categories	13: Al, Aluminum, Biocompatible Ceramics, Biomaterials, Materials Science, More...
description	**gamma phase**
form	**nanopowder**
particle size	**<50 nm (TEM)**
surface area	**>40 m^2/g (BET)**
mp	**2040 °C(lit.)**

Description

Packaging
10, 50 g in glass bottle

Price and Availability

SKU-Pack Size	Availability	Price (EUR/DKK)	Quantity
544833-10G	Only 3 left in stock (more on the way) - FROM	~~24.39~~ **174.24**	0
544833-50G	Available to ship on 16.10.15 - FROM	~~70.70~~ **573.84**	0

Bulk orders?

ADD TO CART

Suggested Laboratory Gloves

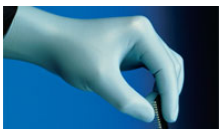

This substance has been tested against several types of hand protection for CE compliance. Click below to find the recommended gloves for handling this product.

FOR SPLASH & IMMERSION PROTECTION

Did you use this product in your Paper? If so click here.
Set your institution to view full text papers.

Personalized Product Recommendations

SIGMA-ALDRICH® sigma-aldrich.com

3050 Spruce Street, Saint Louis, MO 63103, USA
Website: www.sigmaaldrich.com
Email USA: techserv@sial.com
Outside USA: eurtechserv@sial.com

Product Specification

Product Name:
Silicon dioxide – nanopowder, 10–20 nm particle size (BET), 99.5% trace metals basis

Product Number:	**637238**
CAS Number:	7631-86-9
MDL:	MFCD00011232
Formula:	O2Si
Formula Weight:	60.08 g/mol

SiO_2

TEST	Specification
Appearance (Color)	White
Appearance (Form)	Powder
Particle Size	Conforms
10-20 nm (BET)	
ICP Major Analysis	Confirmed
Confirms Silicon Component	
Trace Metal Analysis	$\leq$ 6000.0 ppm
Purity	Meets Requirements
99.5% Based On Trace Metals Analysis	

Specification: PRD.0.ZQ5.10000026590

SIGMA-ALDRICH® sigma-aldrich.com

3050 Spruce Street, Saint Louis, MO 63103, USA
Website: www.sigmaaldrich.com
Email USA: techserv@sial.com
Outside USA: eurtechserv@sial.com

Product Specification

Product Name:
Calcium carbonate – powder, ≤30 µm particle size, 98%

Product Number:	**310034**
CAS Number:	471-34-1
MDL:	MFCD00010906
Formula:	CCaO3
Formula Weight:	100.09 g/mol

$CaCO_3$

TEST	Specification
Appearance (Color)	White
Appearance (Form)	Powder
Complexiometric EDTA % Ca	39.0 - 41.0 %
Average Particle Size	≤ 30 micron
ICP Major Analysis Confirms Calcium Component	Confirmed

Specification: PRD.0.ZQ5.10000028072

Appendix G

Surface Potential vs. Crystallinity

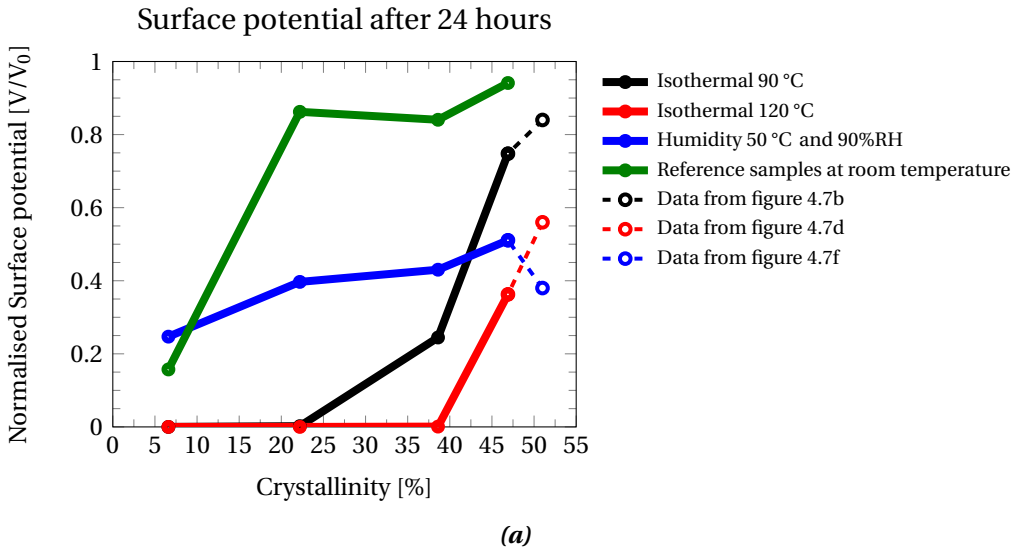

(a)

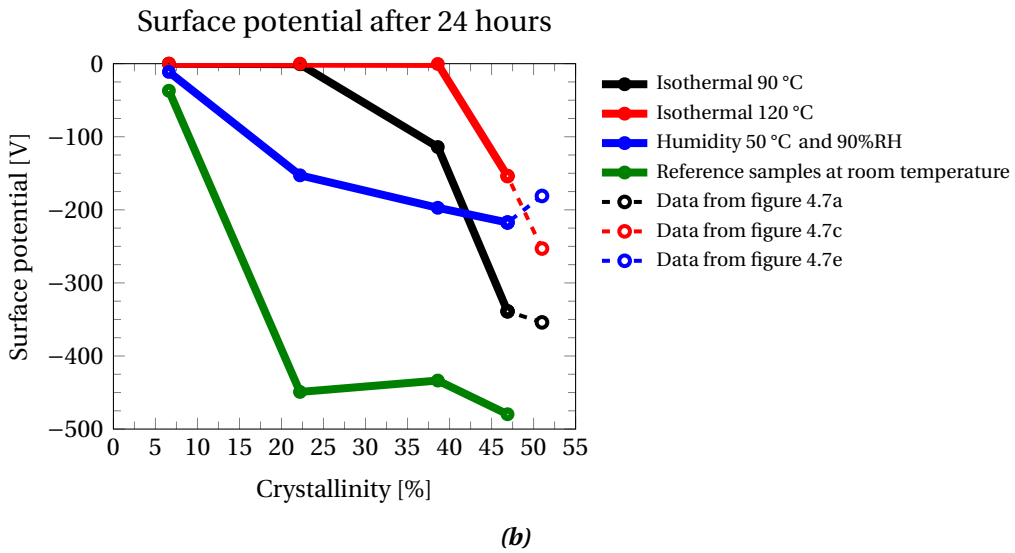

(b)

Figure G.1: ***(a)*** *Shows the normalised surface potential after 24 hours versus the sample crystallinity, for the isothermal and humidity experiments presented in section 4.4. A clear tendency are seen, between increased crystallinity and increased charge retention.* ***(b)*** *Same plot as (a) but with absolute values instead of normalised.*

Appendix H

LIST OF PUBLICATIONS

Parts of the performed research in the Ph.D. thesis have been presented at conferences and published in scientific Journals.

- A. Thyssen, K. Almdal and E. V. Thomsen, *"Imprint enhanced polypropylene"*, Proceeding, IEEE 15th International Symposium on Electrets (ISE15), 2014, pp. 48.
- A. Thyssen, K. Almdal and E. V. Thomsen, *"Electret Stability Related to Spherulites in Polypropylene"*, Poster, IEEE 15th International Symposium on Electrets (ISE15), 2014.
- A. Thyssen, K. Almdal and E. V. Thomsen, *"Electret Stability Related to Spherulites in Polypropylene"*, IEEE Transactions on Dielectrics and Electrical Insulation, Vol. 22, No. 5, pp. 2858-2863, Oct. 2015. doi: 10.1109/TDEI.2015.004891
- A. Thyssen, K. Almdal and E. V. Thomsen, *"Electret Stability Related to the Crystallinity in Polypropylene"*, Proceeding, IEEE Sensors 2015, 2015, pp. 1879-1882.
- A. Thyssen, K. Almdal and E. V. Thomsen, *"Electret Stability Related to the Crystallinity in Polypropylene"*, IEEE Transactions on Dielectrics and Electrical Insulation, Submitted Jannuar-2016, *Status: under submission.*

H.1 IEEE ISE15 2014

A. Thyssen, K. Almdal and E. V. Thomsen *"Imprint enhanced polypropylene"* Proceeding, IEEE 15th International Symposium on Electrets (ISE15), 2014, pp. 48.

Imprint enhanced polypropylene

Anders Thyssen[1], Kristoffer Almdal[1], Erik V. Thomsen[1]
[1]Technical University of Denmark, Department of Micro- and Nanotechnology, 2800 Kgs. Lyngby Denmark
Anders.Thyssen@nanotech.dtu.dk

I. Introduction

Polypropylene is used as a model system for investigating the discharge mechanisms in polymer electret materials. The goal is to get an understanding of how to enhance the temperature and humidity stability for polypropylene and to be able to transfer this knowledge to other electret polymers. Polypropylene is chosen as a model system due to the limited charge lifetime compared to other much more stable electrets. This makes it possible to see improvements in the performance of polypropylene much faster than other more stable electret polymers.

II. Sample Preparation and Measurements

All samples consist of a support structure and a spin coated layer of polypropylene, with an M_w of 250,000 g/mol and a M_n on 67,000 g/mol.

The support structures consist of a single side polished 4" highly doped silicon wafer with 20 nm/100 nm Ti/Au on the back side and 100 nm Ti of the front side. This is done to ensure good electrical conductivity throughout the support structure and to ensure polypropylene adherence to the front side. The silicon wafer has been chosen due to its flatness.

The polypropylene is spin coated on to the support structure, from a 10 wt.% polypropylene/cyclohexane solution. The spin coating is performed in two steps both at 500 rpm, to reach a final thickness of around 30-40 µm.

Even though a spin coating technique is used to apply the polypropylene to the surface of the samples, the polypropylene is not as flat as expected. The samples are therefore flattened in a press at 180 °C. Some of the samples are later on imprinted with a custom made stamp at 120 °C. The cooling after flattering and imprint is done rapidly by placing the samples on an aluminium block at ambient conditions, unless otherwise stated.

The two stamps used in this abstract both consist of different areas with periodic structures of squares, circles and diamonds. The side lengths and diameter for the elements in the periodic structures are 1.5 µm and 21 µm respectively for the two stamps.

All samples are negative corona charged to approximately -500 V, and are left for minimum 12 hr. to settle. After this period the experiments begins.

The objective of the experiments is to investigate the stability with respect to the temperature and humidity of imprinted vs. non-imprinted surfaces. The potential of the samples are measured five times over a period of 24 hr. In between the measurements the samples are placed in an oven at 90 °C or a climate chamber at 50 °C and 90 %RH, depending on the specific experiment.

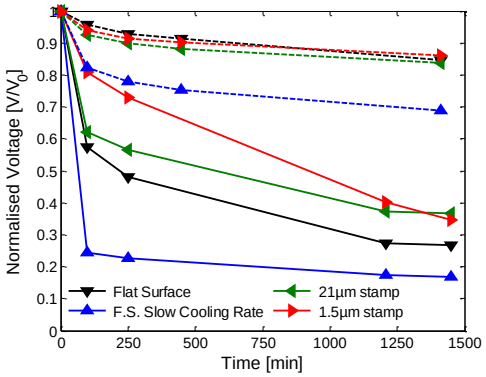

Fig. 1: The normalised average voltage decay, for polypropylene samples with and without surface imprint, at 50 °C and 90 %RH (solid lines) and at 90 °C and <2 %RH (dash lines) over a period of 24 hr.

III. Results and Discussion

The values plotted in fig. 1 are average values from different samples of the same type, and different location on each sample. Some of the samples have been slowly cooled down from 180 °C before charging.

The dashed lines in fig. 1 show the normalised voltage decays for the samples that have been in an oven. It is seen that there is a pronounced stability difference between the samples that has been cooled rapidly and slowly, respectively. No difference in temperature stability is seen between the imprinted surfaces and the non-imprinted surfaces.

The solid lines in fig. 1 show the normalised voltage decays for the samples that have been in a climate chamber. It is seen that after 1450 min. the slowly cooled samples only have about 17% left of its initial voltage, while the non-imprinted samples have about 27% left, the samples with imprint however, have about 36% of its initial voltage left. No pronounced difference is seen between the two different samples made with different stamps.

Using polypropylene as a model system is looking promising. The decay in the potential is happening relatively fast, making it possible to see any enhancement, as a result of mechanical manipulation one might introduce to the material, in a reasonable amount of time. The data in fig. 1 indicate that it is possible that an imprinted surface is more stable in high humidity than and non-imprinted surface, and that the cooling rate under the sample preparation is an important factor.

Future plans are to further investigate what the cooling rate and imprinted surface does to enhance both the humidity and temperature stability. The plan later on is also to introduce particles in the polypropylene model system. The goal is also to make a model that can explain the discharge mechanism for surface and bulk charges.

H.2 IEEE ISE15 2014 - Poster

A. Thyssen, K. Almdal and E. V. Thomsen *"Electret Stability Related to Spherulites in Polypropylene"* Poster, IEEE 15th International Symposium on Electrets (ISE15), 2014.

Electret Stability Related to Spherulites in Polypropylene

Anders Thyssen, Kristoffer Almdal and Erik V. Thomsen
Department of Micro and Nanotechnology, Technical University of Denmark, 2800 Kgs. Lyngby, Denmark
Anders.Thyssen@nanotech.dtu.dk

Motivation

Polypropylene is used as a model system for investigating the discharge mechanisms in polymer electret materials. The goal is to get an understanding of how to enhance the temperature and humidity stability for polypropylene and to be able to transfer this knowledge to other electret polymers. Polypropylene is chosen as a model system due to the limited charge lifetime compared to other much more stable electrets. This makes it possible to see improvements in the performance of polypropylene much faster than other more stable electret polymers.

Sample preparation

- Spin coated polypropylene layer
- Levelled in a press at 10 bar and 180°C, polypropylene thickness ≈ 30 µm
- Three cooling treatments:
  - Slow cooling – Cooled from 180°C to room temperature in 5 min.
  - Medium cooling – Placed on marble table, from 180°C to room temperature in ≈ 10 sec
  - Fast cooling – Ice bath, from 180°C to 0°C ≈ 1 sec.
- Corona charged to -500 V
- Isothermal and humidity stability experiments

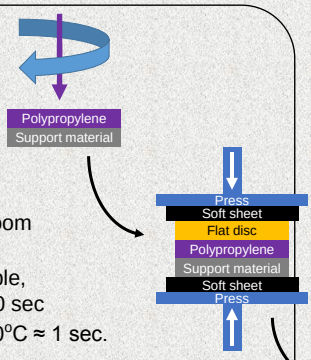

Spherulites size

Depending on the cooling method, spherulites of different size, concentration and ratio between spherulites and non-spherulites area are formed. This has been confirmed for the samples that has been slowly and medium cooled. It is believed that the spherulites in the samples that has been cooled fast are too small, if any, to be seen in optical microscopy AFM or SEM techniques.

	Slowly cooled	Medium Cooled	Fast Cooled
Concentration	40,000 cm^{-1}	44,500 cm^{-1}	NA
Mean spherulite area	1,800 μm^2	600 μm^2	<1 μm^2
Mean spherulite/non-spherulites ratio	62 %	26 %	NA

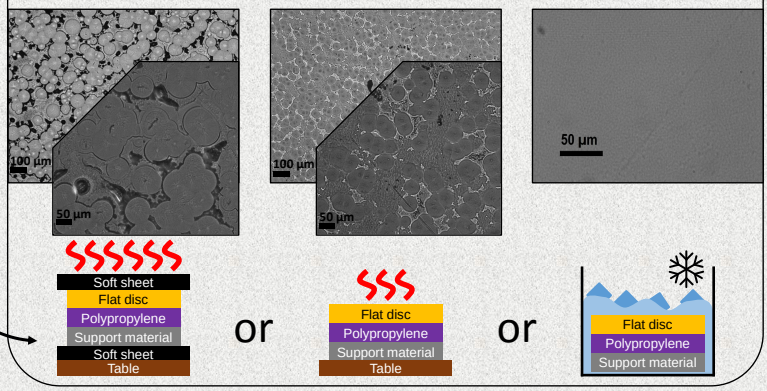

Results

Isothermal experiments at 90°C and 120°C along with a humidity experiment at 50°C with 90% relative humidity has been conducted. Each data point is an average from five different measuring points from five different samples, a total of 25 measurements per data point. In general there is a tendency that the faster the samples have been cooled, from its melting state to its solid, the more stable the charges become, both in respect to temperature and humidity. (*Fig. 1-3)*

Fig. 4 shows the normalised voltage after 25 hr. from the three experiments, seen in Fig. 1 to 3, vs. the spherulites area. The graph in Fig. 4 indicate that there are some charge stability to gain by controlling of the size of the spherulites. This could be, as here presented, by thermal methods or it could be by nucleation agents.

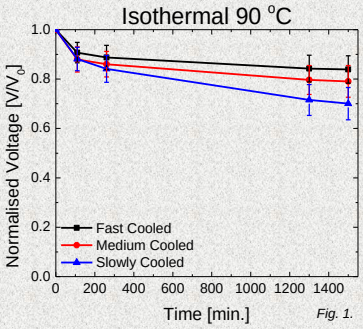

Fig. 1.

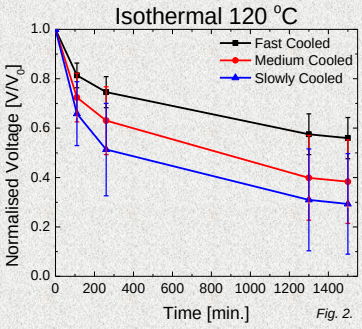

Fig. 2.

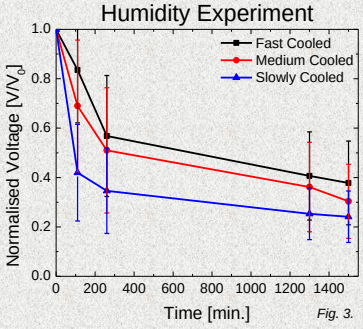

Fig. 3.

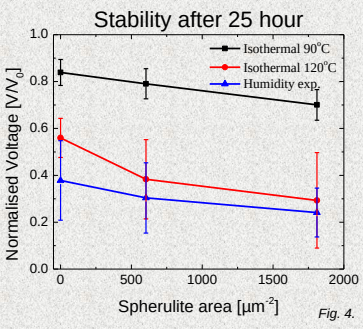

Fig. 4.

Fig. 5 shows thermal stimulated (TS) voltage decay. As seen the charge release happens at higher temperature for the fast cooled samples then the slowly cooled samples. The effect it thought to be related to the different sizes of the spherulites.

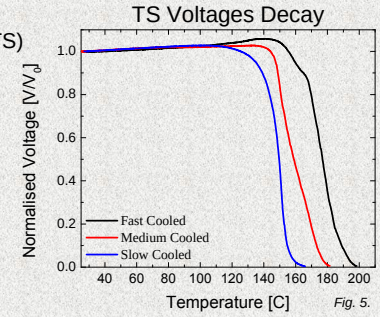

Fig. 5.

Conclusion

Smaller spherulites give more stable electrets

- Fast cooling enhances charge stability
- Fast cooling push charge release towards higher temperature
- Polypropylene is a promising model system for electret polymers
- Further investigating of how the spherulites, if any, looks in the fast cooled samples are needed.
- Further investigating of how to controls the spherulites size are planed

Technical University of Denmark
DTU Nanotech
Department of Micro- and Nanotechnology

Anders Thyssen, Ph.D. Student,
Ørsteds Plads 345Ø, 2800 Kgs. Lyngby, Denmark
Anders.Thyssen@nanotech.dtu.dk

Contact info

H.3 Transactions on Dielectrics and Electrical Insulation 2015

A. Thyssen, K. Almdal and E. V. Thomsen *"Electret Stability Related to Spherulites in Polypropylene"* IEEE Transactions on Dielectrics and Electrical Insulation, Vol. 22, No. 5, pp. 2858-2863, Oct. 2015. DOI: 10.1109/TDEI.2015.004891

Electret Stability Related to Spherulites in Polypropylene

Anders Thyssen, Kristoffer Almdal and **Erik V. Thomsen**
Technical University of Denmark
Department of Micro and Nanotechnology
Ørsteds Plads 345Ø, 2800 Kgs. Lyngby, Denmark

ABSTRACT

Electret charge stability has been related to the size of the spherulites in polypropylene. As the size of the spherulites is decreased the stability is increased. This is seen for isothermal conditions at 90 and 120 °C as well as for 90 % relative humidity at 50 °C. The charge release temperature is also increased in thermally stimulated voltage discharge experiments as the size of the spherulites is decreased. The size of the spherulites is controlled though the cooling rate from polypropylenes liquid state.

Index Terms - **Crystals, electrets, humidity measurement, polypropylene films, spherulite.**

1 INTRODUCTION

POLYPROPYLENE is used for investigating the discharge mechanisms in polymer electret materials. The goal is to get an understanding of how to enhance the temperature and humidity charge stability for polypropylene and to be able to transfer this knowledge to other electret polymers. The choice of polypropylene as a model system is taking advantage of the limited charge lifetime in this system compared to other much more stable electrets, thus enabling a faster observation of performance improvements in polypropylene electrets as compared to more stable polymer electrets.

It has previously been reported that the charges in semicrystalline electret polymers are located at the center of the spherulites and at spherulictic boundaries [1]. In this article, the relation between charge stability in polypropylene electrets, and the size of the spherulites is investigated.

Through different means, one can control the size of the spherulites; the most common method is adding nucleation agents [2–4], which the plastics industry is using in large scale. However, process temperature and cooling rate also play an important role when spherulites are formed [5–7]. In this work the final size of the spherulites are controlled by the heating and cooling rates. The reason for this is that the possible influence from the nucleation agents are unwanted, at this present state of our investigation.

2 EXPERIMENTAL PROCEDURES

This section covers the details regarding sample preparation and experimental procedures.

Manuscript received on 5 September 2014, in final form 3 April 2015, accepted 13 April 2015.

2.1 SUPPORT STRUCTURE AND SPIN COATING

All samples consist of a support structure and a spin coated layer of isotactic polypropylene, with a weight average molecular weight of 250,000 g/mol and a number average molecular weight of 67,000 g/mol.

The support structures consist of a single side polished, 10 cm diameter, highly doped silicon wafer with a 100 nm thick layer of titanium on the front side. The titanium is to provide good electrical conductivity throughout the support structure and to ensure the adhesion of polypropylene to the front side. A highly doped silicon wafer as support structure has been chosen due to its very low electrical resistivity, which is below 0.025 Ωcm, and flatness.

The polypropylene is spin coated on to the support structure, from a 10/90 wt% polypropylene/cyclohexane solution. Prior to spin coating the solution has been heated to 120 °C under pressure for at least 18 hours to ensure complete dissolution of the polypropylene beads. Upon use, the solution is cooled to 77 °C, which is a metastable state for the solution. The time window of use, at 77 °C, is approximately 1 hour, before the solution should be reheated to 120 °C, after which the solution can be reused.

The spin coating is performed in two steps both at 500 rpm, to reach a final thickness of around 30 µm to 40 µm. The pouring of the hot polypropylene solution, onto the support substrate, is done at 250 rpm and then accelerated to 500 rpm for 60 s when the solution reaches the edge of the support substrate. After each spin coating, the samples are heat treated in an oven at 180 °C for 2 min., this is to ensure complete evaporation of the cyclohexane and to reduce the internal stress in polypropylene, which the spin coating has introduced.

Even though a spin coating technique is used, the surface of the samples are very rough, up to ±10 µm, and to ensure a

DOI 10.1109/TDEI.2015.004891

consistent surface morphology the samples are leveled in a press.

2.2 PRESS AND COOLING

To ensure a consistent surface morphology the samples are pressed at 10 bar and 180 °C for 5 min. On top of the sample that is to be pressed, a silver-coated silicon wafer is placed, the silver is used as a non-adherence surface. Around the sample and the silver-coated wafer, silicon rubber sheets are used to ensure an even distribution of the pressure. The thickness of the polypropylene after this treatment is approximately 30 µm.

After the samples have been pressed, they are exposed to one of three cooling methods, which eventually determines the size of the spherulites: 1) Slow cooling – cooled from 180 °C to room temperature in 5 min. 2) Medium cooling – cooled from 180 °C to room temperature in approximately 10 s. 3) Fast cooling – cooled in an ice bath, from 180 °C to 0 °C in approximately 1 s.

2.3 SPHERULITE SIZE

The size of the spherulites is determined by a combination of optical reflection microscopy, Scanning Electron Microscopy (SEM), and image processing and analysis using the program ImageJ 1.48v. For the samples, where the spherulites were visible by optical microscopy, five images were taken at different locations: center, north, south, east and west. Samples from each cooling method were also investigated in a FEI Quanta FEG 200 SEM, where enhanced sensitivity towards small spherulites was obtained. Before the SEM investigation the samples were exposed to a selective etch as described in [8–9]. This was done to enhance the contrast in the SEM between the amorphous and the crystalline areas. The spherulite density at the surface and the mean area of the spherulites were determined with ImageJ.

2.4 CRYSTALLINITY

The crystallinity of the samples was determined with a Differential Scanning Calorimeter (DSC) 4000 from Perkin Elmer. 10 mg to 18 mg of polypropylene was removed from the substrates for each analysis. The crystallinity stated in this work is an average of a minimum of five runs. The heating rate was 20 °C/min and the crystallinity was determined from the first cycle. This was done from the ratio of the melting peak to the heat of fusion for polypropylene (207 J/g [10]).

2.5 CHARGING AND SURFACE POTENTIAL

The samples were charged in a corona discharge setup for 2 min., the principle behind the setup is described in [11]. The distance from the needle to the grid is 3 cm and the distance from the grid to the sample is 3 mm. The grid is used as a common ground for the needle and the sample, and the potential from the needle to the grid is fixed at -10 kV using an EMCO high voltage component "Q101N". The potential from the grid to the sample can be controlled from 0 V to 2000 V using an EMCO USB high voltage power supply "USB20P". All samples are charged to -500 V and left at ambient conditions for a minimum of 12 hours before being used in any experiments. This was done because we are interested in the longtime stability of the electrets and we would like to exclude the short time decay from the experiments. There was no correlation between the size of the spherulites and the decay in the first 12 hours.

The surface potential has been measured with an electrostatic voltmeter located 1 mm to 2 mm above the surface of the samples. Two electrostatic voltmeters have been used which both were reading the same values: Isoprobe 244A with probe 1017AE and Trek 347 with probe 6000B-7C.

2.6 ISOTHERMAL VOLTAGE DECAY

The isothermal voltage decay experiments were conducted at 90 °C and at 120 °C, both for 25 hours. Each sample was measured five times in the 25 hour period and each time at five different locations similar to the areas, used for optical microscopy, where the size of the spherulites had been analyzed. At each measurement all samples were taken out of the oven and returned when all the measurements had been performed. For practical reasons the samples used for the 120 °C experiment had previously been used first for the 90 °C and then for the humidity experiment. This is acceptable because there is no phase transitions in polypropylene between room temperature and 120 °C. Furthermore the recrystallization temperature for isotactic polypropylene, coming from room temperature, is well above 120 °C [12] and the stress of the experiments are gradually increasing. The relative humidity for the isothermal experiment is expected to be below 2 %RH.

2.7 HUMIDITY VOLTAGE DECAY

The humidity induced voltage decay experiment was conducted at 50 °C and 90 %RH for 25 hours. The climate chamber used was a Vötsch VC 4060. Each sample was measured in the same way as the samples at the isothermal experiments. The samples used for the humidity experiment had previously been used in the isothermal 90 °C experiment.

2.8 THERMALLY STIMULATED VOLTAGE DISCHARGE

The thermally stimulated voltage discharge experiments were conducted using a programmable hotplate, EchoTherm Model HS60, and one of the electrostatic voltmeters mentioned in section 2.5; e.g. open circuit. The samples were placed on a 6 mm thick aluminum block, with a built in temperature probe in the center of the block. The signal from the temperature probe was fed back to the hotplate. The stack was placed on top of the hotplate, and the temperature was raised, with a heating rate of 3 °C/min, from room temperature to 200 °C. The surface potential was measured continuously throughout the experiments with the aluminum block as electrical ground.

3 RESULTS AND DISCUSSION

This section covers the result from the experiments described in section 2. Unless stated otherwise, each data point is based on an average from five different measuring points from five equivalent samples. The presented data has also been normalized at t=720 min., when the stressing of the samples began.

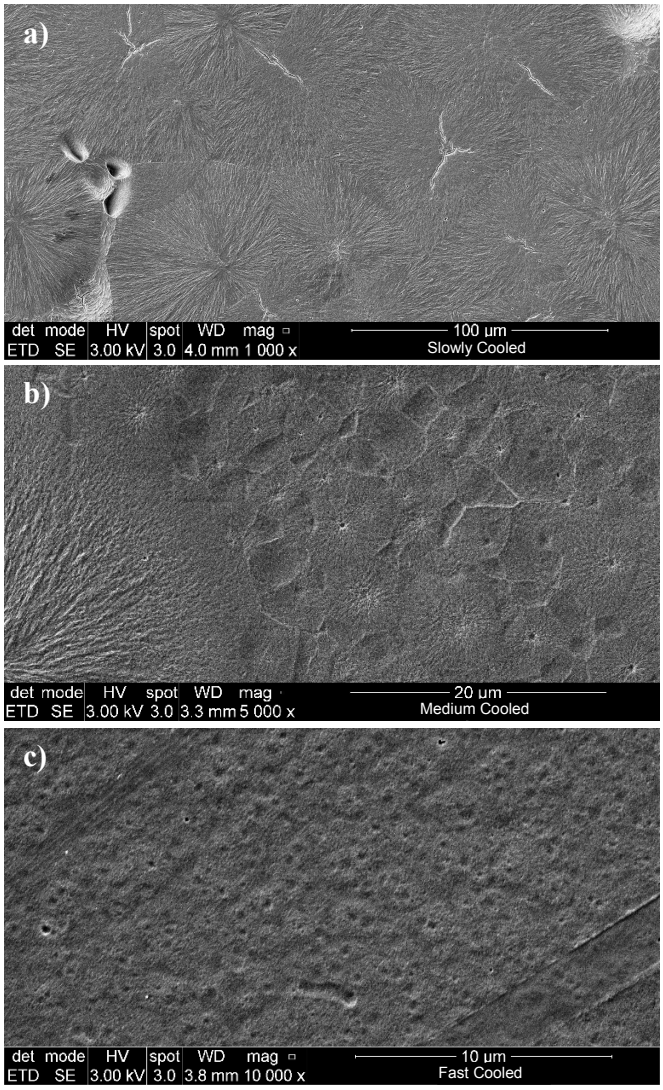

Figure 1 SEM Images of samples that all have been cooled at different rates, (a) slowly, (b) medium and (c) fast. The results from the data analysis is summarized in Table 1.

Table 1. Summary of the data analysis of the SEM images from the different types of samples ("Spherulite density" and "Mean spherulite area") and the degree of crystallinity from the DSC analysis ("Mean crystallinity").

	Slowly cooled	Medium cooled	Fast cooled
Spherulite density	10k-30k cm^{-2}	2M-11M cm^{-2}	32M-204M cm^{-2}
Mean spherulite area	2950 μm^2	23 μm^2	1 μm^2
Mean crystallinity	49 %	43 %	41 %

3.1 SPHERULITE SIZE

Figure 1a, 1b and 1c show SEM images from samples that have all been exposed to different cooling methods: slowly, medium and fast, respectively; as described in section 2.2. It is easy to see the difference in the size of the sperulites between Figure 1a and 1b, where the largest shperulites are seen in Figure 1a. A few of the large spherulites, on the samples that have been medium cooled, are still present, see e.g. the left corner in Figure 1b. In Figure 1c, the spherulites are harder to see, but the structures that look like craters are the center of the spherulites. The spherulites seen in Figure 1a and 1b could also be seen in the optical microscope whereas the spherulites visible in Figure 1c were too small to be observed.

Table 1 summarizes the results from the data analysis of the optical and SEM images from the different types of samples. The data for the slowly and medium cooled samples are based on a combination of both optical and SEM images, while the data for the fast cooled samples are only based on the SEM images. As seen, the density of the spherulites is increased 2-3 orders of magnitude from the slowly cooled to the medium cooled samples and additionally 1-2 orders of magnitude from the medium cooled to the fast cooled samples. The size of the spherulites also decreases drastically as the cooling rate goes up. From the slowly to the fast cooled sample the mean size of the spherulites decreases from 2950 μm^2 to 1 μm^2.

In Table 1, the crystallinity of the samples are also seen, and as expected, it is the slowly cooled samples that have the highest degree of crystallinity, which is 49 %. As the cooling rate goes up the degree of crystallinity goes down and for the fast cooled samples the crystallinity is 41 %.

As the radius of gyration for the polypropylene that is used is around 5 nm it is fair to assume that the formation of the spherulites is a bulk phenomenon; that is the formation of the spherulites takes place throughout the polypropylene film. It is therefore expected that the samples that have been cooled medium and fast have multiple layers of spherulites. For the samples that have been slowly cooled, only a single layer of spherulites is expected since the size of the spherulites, is larger than the thickness of the polypropylene film.

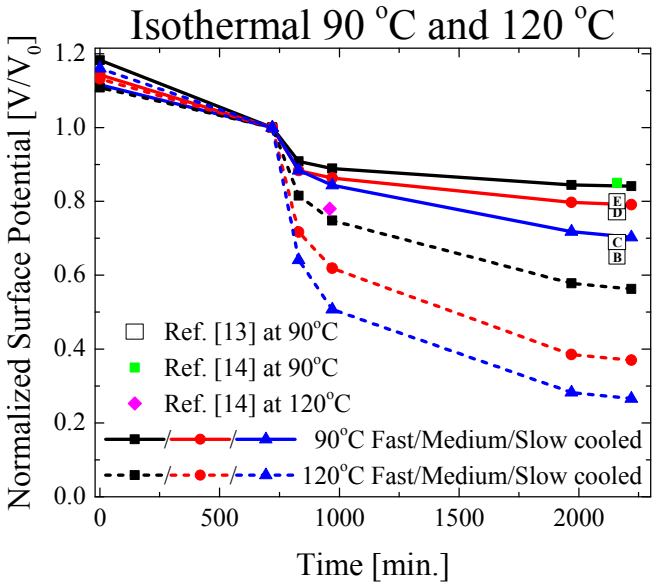

Figure 2. The normalized surface potential decay at isothermal conditions at 90 °C (solid lines) and 120 °C (dashed lines) for 25 hours. The data from [13] (letters) were cooled at temperature rates B=10 K/min, C=10 K/min, D=235 K/min and E=300 K/min. The data from [14] are for biaxially stretched isotactic polypropylene. The data has been normalized at t=720 min. when the stressing of the samples began.

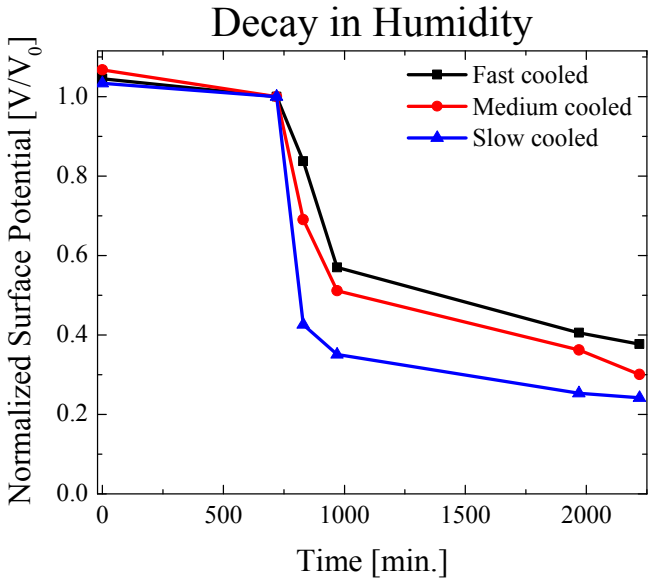

Figure 3. The normalized surface potential decay at 50 °C and 90 %RH. The trend of better charge retention for samples that have been exposed to the highest cooling rate can be seen again. The data has been normalized at t=12 min. when the stressing of the samples began.

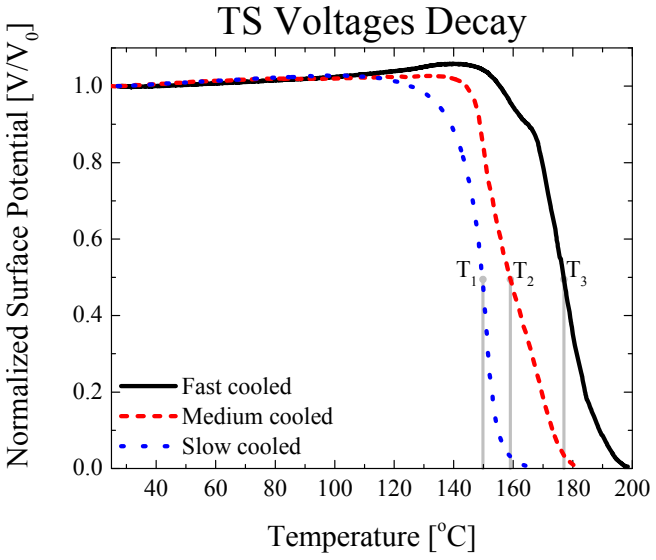

Figure 5. The normalized surface potential for the thermally stimulated voltage discharge experiments. It is seen that the charge retention is better for samples that have experienced a fast cooling form its liquid state, supporting the findings in Figure 2, 3 and 4. T_1, T_2 and T_3 indicate the critical charge release temperature, which is 150 °C, 159 °C and 177 °C respectively.

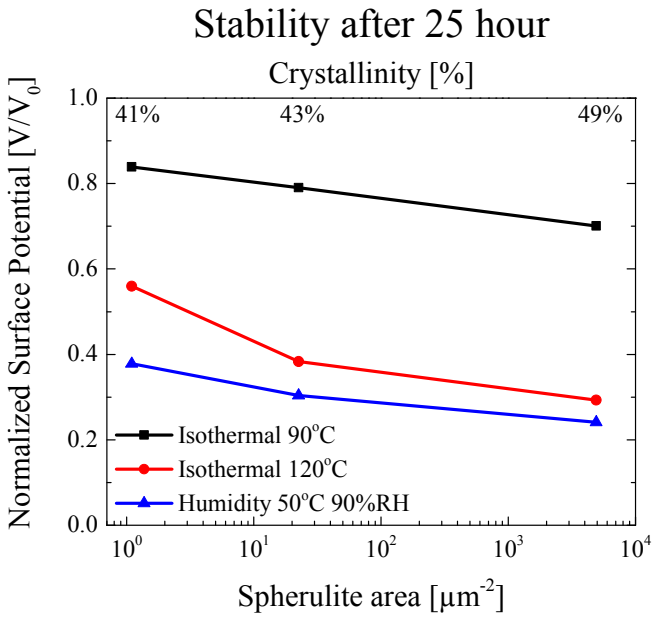

Figure 4. The normalized surface potential measured after 25 hours for the isothermal and humidity experiments, plotted against the mean spherulite area. The corresponding crystallinity for the different cooling methods is also displayed.

We note that the thermal treatment of the film that is part of the measurements (25 h at 90 °C; 25 h at 50 °C, 90 % RH; 25 h at 120 °C) does not lead to any change in the film morphology as observed in optical microscopy. We take this observation as an indication that all samples are partially crystalline and only differ in the reported difference in spherulite size and (to a small degree) in the degree of crystallinity.

3.2 THERMAL AND HUMIDITY STABILITY

Figure 2 shows the decay of the normalized surface potential at isothermal conditions at 90 °C (solid lines) and 120 °C (dashed lines) for 25 hours. The general trend is that the faster the samples have been cooled, the better the charge retention is. This effect is more prominent at 120 °C than at 41% 90 °C. The better charge retention at faster cooling rates correlates well with what others have reported. In [13] they used ~50 µm thick isotactic polypropylene samples that were compressed from a 1.1 mm thick injection molded sample. The letters in Figure 2 indicate different cooling rates (calculated within [13] from 260 °C to 110 °C): B=10 K/min, C=10 K/min, D=235 K/min and E=300 K/min.

Comparing our results with [14], where they have used biaxially stretched isotactic polypropylene with a thickness of ~50 µm, it is seen that the improvement in charge retention from quenching the samples is comparable with the charge retention gained from air voids within polypropylene. The cooling rate in [14] is, however, not stated.

Figure 3 shows the decay of the normalized surface potential at 50 °C and 90 %RH. The trend of better charge retention for samples that have been exposed to the highest cooling rate, can be seen again. However, the charge retention at 50 °C and 90 %RH is lower than at isothermal condition at 120 °C. This suggests that the exposure to water vapor is more critical for charge retention than temperature, when looking at what can be expected at normal ambient conditions.

In Figure 4, the normalized surface potential after 25 hours for the isothermal and humidity experiments is plotted against the mean spherulite area, listed in Table 1. The corresponding crystallinity for the different cooling methods is also

displayed. Here it is seen that there is a correlation between the area of the spherulites and the charge retention. Again, it is seen that the charge retention at 50 °C and 90 %RH is worse than at isothermal conditions at 120 °C. It is seen that the samples with the lowest crystallinity has the best stability.

Figure 5 shows the normalized surface potential for the thermally stimulated voltage discharge experiments. Here it is clearly seen that, the charge retention is better for samples that have been treated with the highest cooling rate, supporting the findings in Figure 2, Figure 3 and Figure 4. In Figure 5 the critical charge release temperature, for the different cooling methods, has been indicated as T_1, T_2 and T_3 which is at 150 °C, 159 °C and 177 °C respectively. We have defined the critical charge release temperature as the temperature where the initial surface potential has decayed to 50 % under a constant heat rate. What is seen is that the critical charge release temperature is increased from 150 °C for the slowly cooled samples to 177 °C for the fast cooled samples. What also is seen in Figure 5 is that the normalized surface potential increases to above 1.0 before it rapidly discharges. This can partially be explained as thermal expansion of polypropylene, however, it cannot explain the entire increment. The fact that the normalized surface potential increases to above 1.0 can be seen as the samples being very stable, until their individually critical charge release temperature is reached.

The obtained charge stability, observed with a high cooling rate, presented in Figure 2 to Figure 5, is a combined effect of the increased number of spherulites and the decrease in the size of the spherulites. The decrease in the crystallinity does not dominate the stability. In [1] it is demonstrated how the deep charge traps are located at the center of the spherulites and the shallow traps are located at the boundaries and the peripheral regions of the spherulites. The increased charge stability has happened in spite of the decrease in crystallinity. A decrease in crystallinity will counteract the combined effect of the increased number of spherulites and the decrease in the size of the spherulites. Even though it would be excepted that a decrease in crystallinity would have a negative effect on the charge stability, this is not seen due to the dominating effect from the increased number of spherulites and the decrease in the size of the spherulites.

4 CONCLUSIONS

In the presented work, we conclude that smaller and increased number of spherulites give better charge retention in polypropylene. We have demonstrated that there is a correlation between increased charge stability, with respect to temperature and humidity, and a combination of a decrease in the size of the spherulites and an increased number of spherulites.

The size of the spherulites has been controlled through cooling from polypropylenes liquid state to its solid state. The control through cooling was chosen to eliminate the influence from any nucleating agents. For the samples that have been cooled the fastest, the size of the spherulites were too small to be seen in an optical microscope and they were instead visualized using SEM. The mean area of the spherulites that have been cooled the fastest was 3 orders of magnitude smaller than the area of the spherulites that had been slowly cooled, going from 1 μm^2 to 2950 μm^2 respectively.

The crystallinity for the fast cooled samples was 41 % and 49 % for the slowly cooled samples. Even though it is excepted that a decrease in crystallinity will have a negative effect on the charge stability, this is not seen due to the dominating effect from the increased number of spherulites and the decrease in the size of the spherulites.

The fast cooled samples exhibited significantly improved charge stability in comparison with the slowly cooled samples. After 25 hours in the isothermal experiments at 90 °C the charge retention increased from 70 % of the initial surface potential in the slowly cooled samples to 84 % in the fast cooled samples. For the isothermal experiments at 120 °C the corresponding numbers are 26 % and 56 % for the slowly and fast cooled samples, respectively. Similarly for the humidity experiments the numbers are 24 % and 37 % for the slowly and fast cooled samples, respectively.

The effect of the higher cooling rate is also seen in the thermal stimulated voltage decay as a high cooling rate resulted in an increased critical charge release temperature, from 150 °C for the slowly cooled samples to 177 °C for the fast cooled samples.

This work has also shown that the preparation of electret samples is of utmost importance when looking at their charge stability. It is therefore extremely important to know these parameters and, how and why they affect the charge stability.

5 REFERENCES

[1] A. Yagishita, K. Ikezaki, and H. Yamanouchi, “Charge trapping sites in spherulitic polypropylene,” Japanese J. Appl. Physics, Part 1 Regul. Pap. Short Notes Rev. Pap., Vol. 38, No. 4A, pp. 2053 – 2058, 1999.

[2] D. Libster, A. Aserin, and N. Garti, “Advanced nucleating agents for polypropylene,” Polym. Adv. Technol., Vol. 18, no. 9, pp. 685–695, Sep. 2007.

[3] M. Dong, Z. Guo, Z. Su, and J. Yu, “Study of the crystallization behaviors of isotactic polypropylene with sodium benzoate as a specific versatile nucleating agent,” J. Polym. Sci. Part B Polym. Phys., Vol. 46, No. 12, pp. 1183–1192, 2008.

[4] G.-S. Jang, W.-J. Cho, and C.-S. Ha, “Crystallization behavior of polypropylene with or without sodium benzoate as a nucleating agent,” J. Polym. Sci. Part B Polym. Phys., Vol. 39, No. 10, pp. 1001–1016, May 2001.

[5] F. J. Padden and H. D. Keith, “Spherulitic Crystallization in Polypropylene,” J. Appl. Phys., Vol. 30, No. 10, pp. 1479–1484, 1959.

[6] J. Varga and J. Karger-Kocsis, “Rules of supermolecular structure formation in sheared isotactic polypropylene melts,” J. Polym. Sci. Part B Polym. Phys., Vol. 34, No. 4, pp. 657–670, 1996.

[7] D. Norton and A. Keller, “The spherulitic and lamellar morphology of melt-crystallized isotactic polypropylene,” Polymer (Guildf)., Vol. 26, pp. 704–716, 1985.

[8] M. Aboulfaraj, B. Ulrich, A. Dahoun, and C. G’Sell, “Spherulitic morphology of isotactic polypropylene investigated by scanning electron microscopy,” Polymer (Guildf)., Vol. 34, no. 23, pp. 4817–4825, 1993.

[9] J. Park, K. Eom, O. Kwon, and S. Woo, “Chemical Etching Technique for the Investigation of Melt-crystallized Isotactic Polypropylene Spherulite and Lamellar Morphology by Scanning Electron Microscopy,” Microsc. Microanal., Vol. 7, No. 3, pp. 276–286, 2002.

[10] [1] C. C. Ibeh, Thermoplastic materials : properties, manufacturing methods, and applications. New York: CRC Press, 2011.

[11] J. A. Giacometti and O. N. Oliveira, "Corona charging of polymers," IEEE Trans. Electr. Insul., Vol. 27, No. 5, pp. 924–943, 1992.
[12] M. Iijima and G. Strobl, "Isothermal crystallization and melting of isotactic polypropylene analyzed by time- and temperature-dependent small-angle X-ray scattering experiments," Macromolecules, Vol. 33, pp. 5204–5214, 2000.
[13] N. Mohmeyer, N. Behrendt, X. Zhang, P. Smith, V. Altstädt, G. M. Sessler, and H.-W. Schmidt, "Additives to improve the electret properties of isotactic polypropylene," Polymer (Guildf)., Vol. 48, No. 6, pp. 1612–1619, 2007.
[14] J. Hillenbrand, N. Behrendt, V. Altstädt, H.-W. Schmidt, and G. M. Sessler, "Electret properties of biaxially stretched polypropylene films containing various additives," J. Phys. D. Appl. Phys., Vol. 39, No. 3, pp. 535–540, 2006.

A. Thyssen was born in Toftlund, Denmark in 1986. He received the B.Sc. and M.Sc degrees from the Technical University of Denmark, Kgs. Lyngby, Denmark in 2010 and 2012. He is currently a Ph.D. student at the Technical University of Denmark at the department of Micro and Nanotechnology.

K. Almdal was born in Frederiksberg, Denmark in 1958. He received his M.Sc. and Ph.D. for the University of Copenhagen in 1985 and 1989. His research interests include polymer synthesis, polymer physics, polymer degradation and self-organization phenomena in particular in block copolymers. He is currently professor in polymers in micro- and nanotechnology at the Technical University of Denmark in Kgs. Lyngby. He is elected member of the Danish Academy of Natural Sciences and Danish Academy of Technical Science.

E. V. Thomsen was born in Aarhus, Denmark, in 1964. He received the M.Sc. degree in physics from Odense University, Odense, Denmark, and the Ph.D. degree in electrical engineering from the Technical University of Denmark (DTU),Kgs. Lyngby, in 1998. He has been affiliated with the Department for Micro and Nanotechnology, DTU, since 1992. He is group leader for the MEMS Applied Sensors Group. His current research and teaching interests include Electret based devices, MEMS multisensors; bio-medical devices; small scale energy systems, such as miniature fuel cells and energy harvesting devices; capacitive micromachined ultrasonic transducers; and piezoelectric MEMS. He teaches classes in solid-state electronics, microtechnology, and nano- and microfabrication. Dr. Thomsen received the AEG Electron Prize in 1995 and has received several teaching awards at DTU.

H.4 IEEE Sensors 2015

- A. Thyssen, K. Almdal and E. V. Thomsen *"Electret Stability Related to the Crystallinity in Polypropylene"*, Proceeding, IEEE Sensors 2015, 2015, pp. 1879-1882.

Electret Stability Related to the Crystallinity in Polypropylene

Anders Thyssen, Kristoffer Almdal and Erik Vilain Thomsen
Department of Micro- and Nanotechnology, Technical University of Denmark,
Kgs. Lyngby, Denmark
Anders.Thyssen@nanotech.dtu.dk

***Abstract*—Through mixing isotactic-polypropylene (i-PP) and atactic-polypropylene (a-PP), we have demonstrated the importance of the crystallinity in polypropylene as an electret material. A high degree of crystallinity in polypropylene, used as an electret, gives a better charge stability towards temperature and humidity changes. The semicrystalline i-PP significantly outperforms a-PP regarding charge stability. a-PP is an amorphous polymer. By mixing a-PP and i-PP the degree of crystallinity can be controlled, while all other sample preparation processes and characteristics can be identical. This is important since the performance of an electret material is sensitive to its previous process history.**

Keywords—electret; crystallinity; charge stability; humidity stability; spherulites; isotactic-polypropylene; atactic-polypropylene

I. INTRODUCTION

Electret materials are dielectrics with quasi-permanent electric charges or dipole polarization and they are used where one would like to utilize a permanent electrical field without any power supply. Polypropylene, in its isotactic and atactic form, is used as a model system for investigating the discharge mechanisms in polymer electret materials. The goal is to get an understanding of how to enhance the temperature and humidity stability for polypropylene and to be able to transfer this knowledge to other electret polymers. Polypropylene is chosen as a model system due to the limited charge lifetime compared to other much more stable electrets. Elevated temperature and controlled humidity conditions are used as accelerated aging conditions. This makes it possible to study the performance of polypropylene as an electret material much faster than other more stable electret polymers. In reference [1], [2] it has been revealed that the electrical charges in polymer electrets are associated with the crystalline spherulitesa, in particular their centres. In [3] we have demonstrated that the size of the spherulites are of great importance to the charge stability. The influence of the degree of crystallinity is, however, to be determined. Others have had success to increase the charge stability in polymer electrets through treatment with Titanium-Tetrachloride Vapor [4]. Electret materials can for example be used in small-scale vibrational energy harvesters, air filters or pre-polarized microphones; e.g. electret microphones [5], [6].

II. SAMPLE PREPARATION

This section covers the details regarding sample preparation and experimental procedures.

A. Support Structure and Spin Coating

All samples consist of a support structure and a spin coated layer of either isotactic polypropylene (i-PP), atactic-polypropylene (a-PP) or a mixture hereof. The i-PP has a weight average molecular weight of 250,000 g/mol, a number average molecular weight of 67,000 g/mol and came as beads. The weight average molecular weight for the a-PP was 12,000 g/mol and came as a waxy solid. The supplier for the i-PP was Sigma-Aldrich and the supplier for the a-PP was Goodfellow.

The support structures consist of a single side polished, 10 cm diameter, highly doped silicon wafer with a 100 nm thick layer of titanium on the front side. The titanium provides good electrical conductivity throughout the support structure and ensures the adhesion of polypropylene to the front side. A highly doped silicon wafer as support structure has been chosen due to its very low electrical resistivity, which is below 0.025 ohm·cm, and flatness.

The polypropylene is spin coated onto the support structure, from a polypropylene/cyclohexane solution. Four mixtures were used where the content of the polypropylene was changed as follows (by weight): 1) 100 % i-PP, 2) ⅔ i-PP and ⅓ a-PP, 3) ⅓ i-PP and ⅔ a-PP, and 4) 100 % a-PP. Prior to spin coating, mixture 1), 2) and 3) had been heated to 120 °C under pressure for at least 18 hours to ensure complete dissolution of the polypropylene beads. Before use, the solution is cooled to 78 °C. At this temperature the solution is metastable with respect to crystallization induced precipitation of the i-PP. The time window of use, at 78 °C, is approximately 1 hour. The 120 °C heat treatment can be repeated and the solution reused. Mixture 4) forms a homogenous solution at room temperature and, thus, did not need to be heated.

The spin coating process was tuned to the four different mixtures so that the final thickness became around 30 µm to 40 µm. After each spin coating, the samples are heat treated in an oven at 180 °C for 2 min., this is to ensure complete evaporation of the cyclohexane and to reduce the internal stress in polypropylene, which the spin coating has introduced.

B. Press and Cooling

To ensure a consistent surface morphology the samples were pressed at 10 bar and 180 °C for 5 min in a mechanical press. The sample to be pressed is covered by a silver-coated silicon wafer. The silver is a non-adherent surface. Around the sample and the silver-coated wafer, silicone rubber sheets are

used to ensure an even distribution of the pressure. The thickness of the polypropylene after this treatment is approximately 30 µm.

After the samples have been pressed, they are exposed to quenching in an ice bath, going from 180 °C to 0 °C in approximately 1 s. This is to ensure small size spherulites, which work done previously [3] concluded was very important to obtain a good charge stability.

C. Crystallinity

The crystallinity of the samples was determined with a Differential Scanning Calorimeter (DSC) 4000 from Perkin Elmer. 8 mg to 15 mg of polypropylene was removed from the substrates for each analysis. The crystallinity stated in this work is an average of a minimum of six runs. The heating rate was 20 °C/min and the crystallinity was calculated from the ratio of the melting peak, from the first cycles, to the heat of fusion for polypropylene (207 J/g [7]).

D. Charging and Surface Potential

The samples were charged in a corona discharge setup for 2 min. The principle behind the setup is described in [8]. The distance from the needle to the grid was 3 cm and the distance from the grid to the sample was 3 mm. The grid was used as a common ground for the needle and the sample, and the potential from the needle to the grid was fixed at –10 kV using an EMCO high voltage component "Q101N". The potential from the grid to the sample can be controlled from 0 V to 2000 V using an EMCO USB high voltage power supply "USB20P". All samples were charged to –500 V and left at ambient conditions for a minimum of 12 hours before being used in any experiments. This was done because we are interested in the longtime stability of the electrets and we would like to exclude the short time decay from the experiments.

The surface potential has been measured with an electrostatic voltmeter located 1 mm to 2 mm above the surface of the samples. The electrostatic voltmeter used was a: Trek 347 with probe 6000B-7C.

Samples used in the following voltage decay experiments were not recharged for new decay experiments. Some of the samples were however, used after the decay experiments to determine the degree of crystallinity; which was a destructive process.

E. Isothermal Voltage Decay

The isothermal voltage decay experiments were conducted at 90 °C and at 120 °C, both for 24 hours. Each sample was measured five times in the 24-hour period. Each measurement is performed by a robot that took 101 independent readings of the surface potential evenly distributed over the wafer, with a minimum distance to the edge of 10 mm. At each measurement, all samples were taken out of the oven and returned when all the measurements had been performed. The relative humidity for the isothermal experiment was below 2 %RH.

F. Humidity Voltage Decay

The humidity induced voltage decay experiment was conducted at 50 °C and 90 %RH for 24 hours. The climate chamber used was a Vötsch VC 4060. Each sample was measured in the same way as the samples at the isothermal experiments. The samples used for the humidity experiment were not reused for other experiments.

III. Results

This section covers the results from the experiments described in section II. Unless stated otherwise, each data point is based on an average from four equivalent samples, each with 101 different measuring points.

A. Thermal and Humid Charge Stability

In Fig. 1, the isothermal charge stability at 90 °C and 120 °C is seen. As the content of the a-PP is increased, the charge stability is substantially reduced. The fully amorphous samples that contain only a-PP were so unstable that they lost more than 250 V from the end of charging to the start of the first surface potential measurement. This transfer takes approximately 2 min.

In Fig. 2, the charge stability at 50 °C and 90 % relative humidity is seen. Again, it is seen that after 1440 min. the samples with the least amount of a-PP are the most stable and that the samples with 100 % a-PP drop most of their charges before the actual experiment begins.

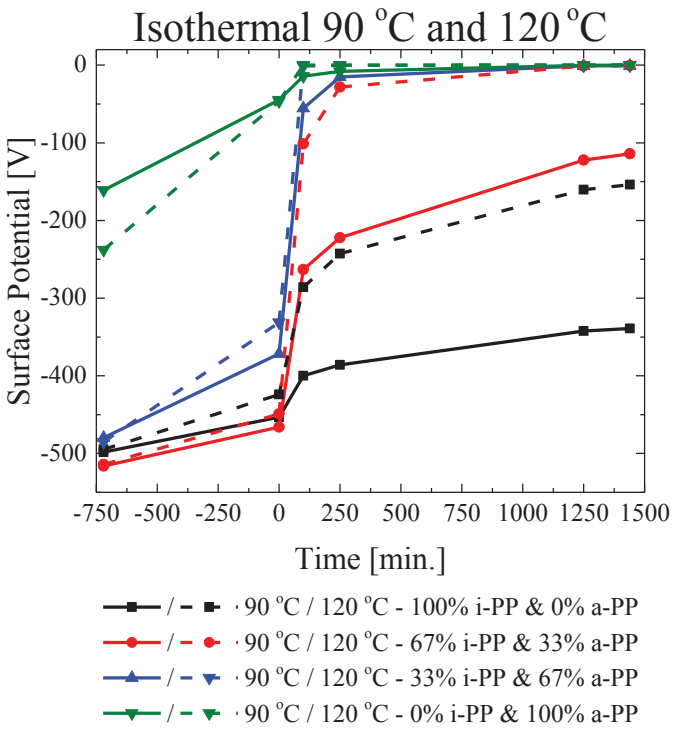

Fig. 1. The isothermal charge stability at 90 °C and 120 °C. At t=0 min. the temperature is changed from room temperature to the process temperature. As the content of the a-PP is increased, the charge stability is significantly reduced. The fully amorphous samples, the samples that only content a-PP, are so unstable that they loses more than 250 V from the end of charging to the start of the first surface potential measurement.

In Fig. 3 charge stability data for four samples that were kept at ambient conditions for a period of approximately 120 h is shown.

In Fig. 4 the charge stability data is replotted as a function of degree of crystallinity.

The changes seen at ambient conditions (Fig. 3) are augmented under accelerated conditions. Thus the small difference, seen in Fig. 3 between the three crystalline samples, are reflected in the faster and more dramatic changes at time=0 in Fig. 1 and Fig. 2. The '⅓ i-PP and ⅔ a-PP' sample in Fig. 3 (blue curve) is somewhat at odds with the interpretation from Fig. 1 and Fig. 2. This sample is characterized by 10 fold larger

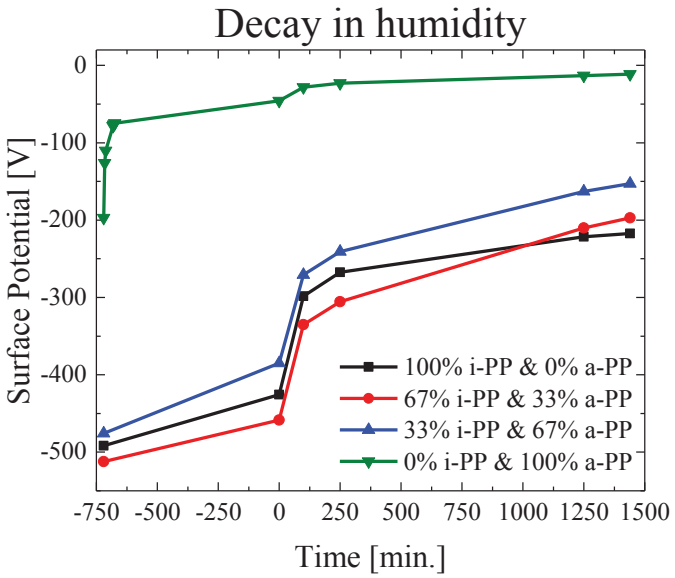

Fig. 2. The charge stability at 50 °C and 90 % relative humidity. At t=0 min. the conditions are changed from ambient to the process conditions. It is seen that after 1440 min. the samples with the least amount of a-PP are the most stable.

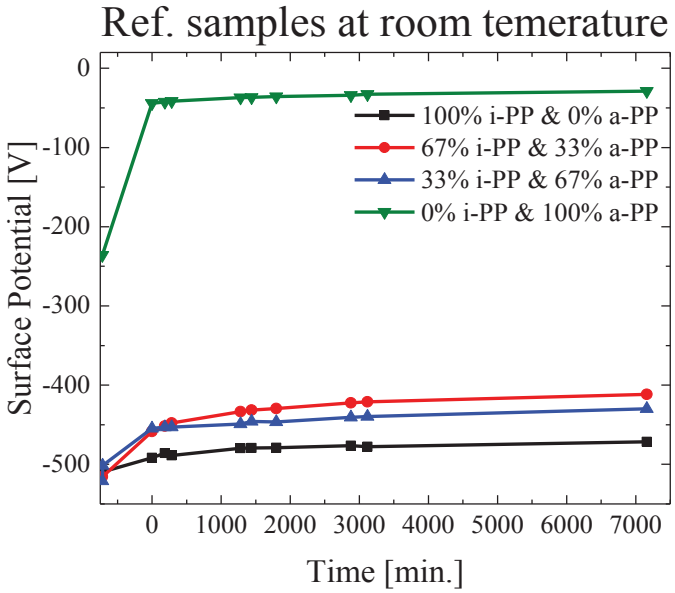

Fig. 3. The charge stability for four reference samples. The four samples had been stored at room temeprature. Comparring this figure with Fig. 1 and Fig. 2, it is easy to see the thermal effect on the charge stability.

variation in the surface potential which may account for the fact that this sample appears more stable in Fig. 3 than the more crystalline sample '⅔ i-PP and ⅓ a-PP' (red curve). Thus the charge stability trend at ambient conditions is reflected under accelerated conditions, namely that the samples containing the most i-PP have the best charge stability. This correlates well with the crystallinity of the samples.

B. Crystallinity

The crystallinity of the different types of samples have been calculated from DSC analysis and the results are listed in Table 1. What is seen is that the crystallinity decreases as the amount of i-PP is lowered. This is expected, as a-PP is an amorphous polymer. We note that the calculated crystallinity is 5 % for the samples only consisting of a-PP indicates that the used a-PP is not 100 % atactic as specified by the manufacturer.

Fig. 4 shows the surface potential after 24 hours as a function of the crystallinity of the samples. The solid lines represent data from Fig. 1 to Fig. 3 and the dashed lines represent data from previous work [3]. In Fig. 4, a clear

TABLE I. THE PERCENT'S IN THE SAMPLE COLUMN IS BY WEIGHT.

Sample Crystallinity	
Samples	***Crystallinity***
100 % i-PP	37 %
67 % i-PP & 33 % a-PP	31 %
33 % i-PP & 67 % a-PP	17 %
100 % a-PP	5 %

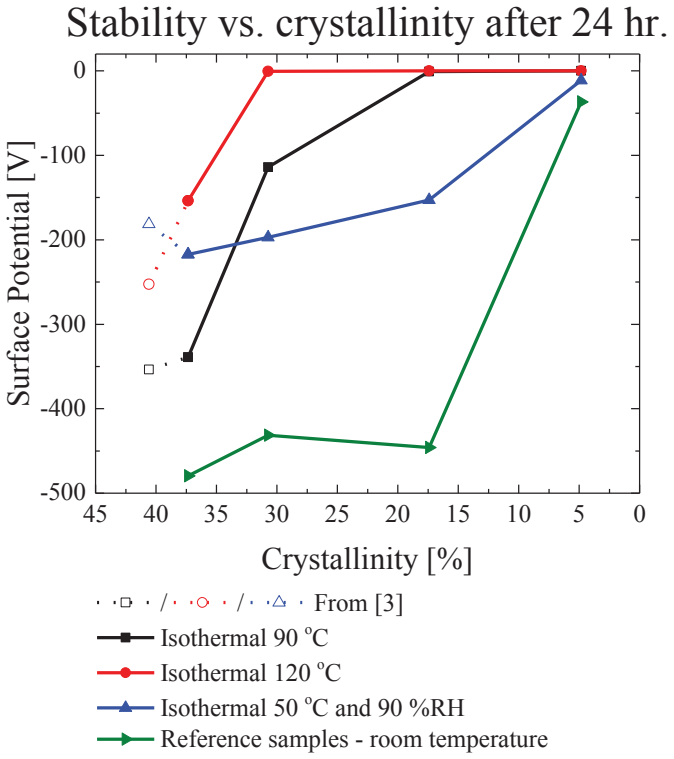

Fig. 4. Charge stability after 24 hours as a function of crystallinity for the different aging methods. Data from [3] included.

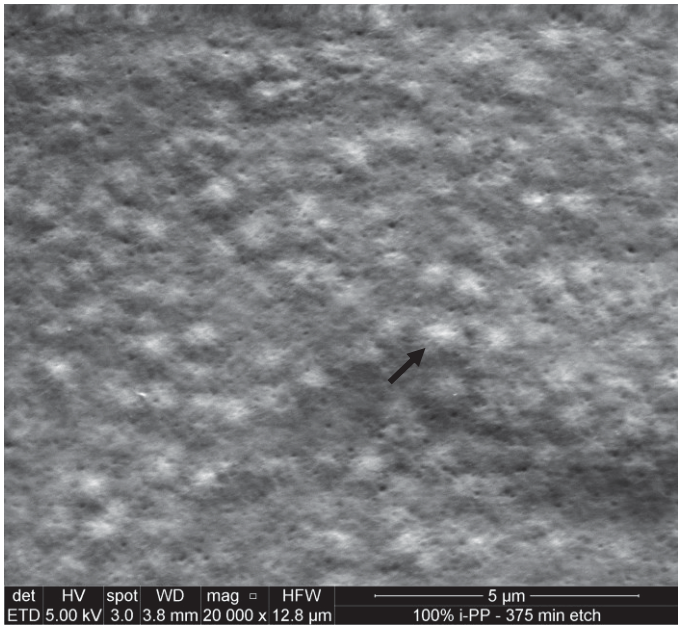

Fig. 5. SEM image of a sample that consist of 100 % i-PP. What appears as bumps (one is indicated by the black arrow) are sherulites at the surface of the sample, which all are smaller than 1 µm.

correlation is seen between increased charge stability and an increased degree of crystallinity. The higher the degree of crystallinity is the better the charge stability will be. However, since crystallite size plays an even bigger role than the crystallinity [3], increasing the crystallinity should not happen through increased spherulites size but through increased spherulites number.

The size of the spherulites in these set of experiments have been smaller than 1 µm, which have been confirmed by Scanning Electron Microscopy (SEM) on samples that prior to the SEM have been exposed to a selective etch as described in [9], [10]. A SEM image from a sample consisting of 100 % i-PP is seen in Fig. 5. The areas that appear as bumps are the spherulites. The black arrow in the middle of the image indicate one of these spherulites.

IV. Conclusion

On the basis of the presented work, we conclude that the best charge stability is achieved with a high degree of crystallinity. We have demonstrated this with respect to temperature and humidity.

The degree of crystallinity has been controlled by mixing a-PP in i-PP, while all other process parameter have been kept constant, as charge stability in electret materials is known to be sensitive to the process history. There were four types of samples with crystallinity of 37 %, 31 %, 17 % and 5 %.

The samples with highest crystallinity exhibited significantly better charge stability in comparison to the samples with lower crystallinity. All samples were charged to –500 V and after 12 hours of stabilization, the experiments began. For the samples with a high degree of crystallinity (37 %) the surface potential dropped 25 % (from –453 V to –339 V) after 24 hours at 90 °C. In contrast, for the samples with a low degree of crystallinity (5 %) the surface potential dropped 100 % (from –46 V to 0 V) after 24 hours at 90 °C. Thus, not only could the low degree of crystallinity samples not support a high surface potential: The surface potential that the low degree of crystallinity samples could support vanishes in less than 24 hours at 90 °C.

For the isothermal experiments at 120 °C, the corresponding numbers are a 64 % drop (from –424 V to –154 V) and a 100% drop (from –46 V to 0 V). Similarly, for the humidity experiments the numbers are a 49 % drop (from –425 V to –217 V) and a 76 % drop (from –46 V to 0 V). For the ambient condition samples the observation is a 3 % drop (from –492 V to –479 V) and a 17 % drop (from –44 V to –37 V).

We emphasize the importance of the small size of the spherulites [3]. The size of spherulites was characterized through visualization using SEM to be smaller than 1 µm.

References

[1] K. Ikezaki, A. Yagishita, and H. Yamanouchi, “Charge trapping sites in spherulitic polypropylene,” in *Proceedings of 8th International Symposium on Electrets (ISE 8)*, 1994, pp. 428–433.

[2] A. Yagishita, K. Ikezaki, and H. Yamanouchi, “Charge trapping sites in spherulitic polypropylene,” *Japanese J. Appl. Physics, Part 1 Regul. Pap. Short Notes Rev. Pap.*, vol. 38, no. 4A, pp. 2053 – 2058, 1999.

[3] A. Thyssen, K. Almdal, and E. V. Thomsen, “Electret Stability Related to Spherulites in Polypropylene,” *IEEE Trans. Dielectr. Electr. Insul.*, no. in press.

[4] D. Rychkov, R. Gerhard, V. Ivanov, and A. Rychkov, “Enhanced electret charge stability on polyethylene films treated with titanium-tetrachloride vapor,” *IEEE Trans. Dielectr. Electr. Insul.*, vol. 19, no. 4, pp. 1305–1311, Aug. 2012.

[5] R. Kressmann, G. M. Sessler, and P. Gunther, “Space-charge electrets,” *IEEE Trans. Dielectr. Electr. Insul.*, vol. 3, no. 5, pp. 607 –623, Oct. 1996.

[6] A. Crovetto, F. Wang, and O. Hansen, “An electret-based energy harvesting device with a wafer-level fabrication process,” *J. Micromechanics Microengineering*, vol. 23, no. 11, p. 114010, 2013.

[7] C. C. Ibeh, *Thermoplastic materials : properties, manufacturing methods, and applications*. New York: CRC Press, 2011.

[8] J. A. Giacometti and O. N. Oliveira, “Corona charging of polymers,” *IEEE Trans. Electr. Insul.*, vol. 27, no. 5, pp. 924–943, 1992.

[9] M. Aboulfaraj, B. Ulrich, A. Dahoun, and C. G’Sell, “Spherulitic morphology of isotactic polypropylene investigated by scanning electron microscopy,” *Polymer (Guildf).*, vol. 34, no. 23, pp. 4817–4825, Jan. 1993.

[10] J. Park, K. Eom, O. Kwon, and S. Woo, “Chemical Etching Technique for the Investigation of Melt-crystallized Isotactic Polypropylene Spherulite and Lamellar Morphology by Scanning Electron Microscopy,” *Microsc. Microanal.*, vol. 7, no. 03, pp. 276–286, Feb. 2002.

H.5 Transactions on Dielectrics and Electrical Insulation 2016

- A. Thyssen, K. Almdal and E. V. Thomsen, *"Electret Stability Related to the Crystallinity in Polypropylene"*, IEEE Transactions on Dielectrics and Electrical Insulation, Submitted Jannuar-2016, *Status: under submission.*

Published by:
DTU Nanotech
Department of Micro- and Nanotechnology
Technical University of Denmark
Ørsteds Plads, building 345C
DK-2800 Kgs. Lyngby